

Contact and Length Dependent Effects in  
Single-Molecule Electronics

by

Thomas Hines

A Dissertation Presented in Partial Fulfillment  
of the Requirements for the Degree  
Doctor of Philosophy

Approved July 2013 by the  
Graduate Supervisory Committee:

Nongjian Tao, Co-Chair  
Jian Li, Co- Chair  
Vladimiro Mujica  
David Allee

ARIZONA STATE UNIVERSITY

August 2013

## ABSTRACT

Understanding charge transport in single molecules covalently bonded to electrodes is a fundamental goal in the field of molecular electronics. In the past decade, it has become possible to measure charge transport on the single-molecule level using the STM break junction method. Measurements on the single-molecule level shed light on charge transport phenomena which would otherwise be obfuscated by ensemble measurements of groups of molecules. This thesis will discuss three projects carried out using STM break junction.

In the first project, the transition between two different charge transport mechanisms is reported in a set of molecular wires. The shortest wires show highly length dependent and temperature invariant conductance behavior, whereas the longer wires show weakly length dependent and temperature dependent behavior. This trend is consistent with a model whereby conduction occurs by coherent tunneling in the shortest wires and by incoherent hopping in the longer wires. Measurements are supported with calculations and the evolution of the molecular junction during the pulling process is investigated.

The second project reports controlling the formation of single-molecule junctions by means of electrochemically reducing two axial-diazonium terminal groups on a molecule, thereby producing direct Au-C covalent bonds *in-situ* between the molecule and gold electrodes. Step length analysis shows that the molecular junction is significantly more stable, and can be pulled over a longer distance than a comparable

junction created with amine anchoring bonds. The stability of the junction is explained by the calculated lower binding energy associated with the direct Au-C bond compared with the Au-N bond.

Finally, the third project investigates the role that molecular conformation plays in the conductance of oligothiophene single-molecule junctions. Ethyl substituted oligothiophenes were measured and found to exhibit temperature dependent conductance and transition voltage for molecules with between two and six repeat units. While the molecule with only one repeat unit shows temperature invariant behavior. Density functional theory calculations show that at higher temperatures the oligomers with multiple repeat units assume a more planar conformation, which increases the conjugation length and decreases the effective energy barrier of the junction.

## ACKNOWLEDGEMENTS

I have received a great deal of mentoring and guidance throughout my graduate career and writing this thesis. I would like to begin by thanking my co-advisors Nongjian Tao and Jian Li. Professors Tao and Li have offered me motivation, insight, knowledge, and patience. I also express thanks to the other members of my committee including Vladimiro Mujica and David Allee.

I would also like to express thanks to collaborators who synthesized the molecules measured in this thesis. Klaus Mullen of the Max Planck Institute oversaw the synthesis of the molecular wires used in Chapter 2. Additionally, Zhou Gang at Fudan University has been very helpful in synthesizing the molecules measured in Chapter 4, and has also provided us with many molecules that we have yet to investigate.

I am also thankful to those who have provided calculations and simulations to supplement the experimental measurements I have taken. Jianwei Zhao performed Hartree-Fock calculations for the molecular wires used in Chapter 2. Additionally, Hisao Nakamura and Yoshihiro Asai performed density functional theory and non-equilibrium Green's function calculations for the diazonium and amine terminated molecules measured in Chapter 3. And finally, Julio Palma Anda performed density functional theory calculations for the oligothophenes measured in Chapter 4.

I would also like to thank Rolf Schuster and Raphael Rosch at the Karlsruhe Institute of Technology, for hosting a visit on my behalf to their lab. I performed many

variants of a room temperature inelastic electron tunneling spectroscopy measurement during my stay, and learned a great deal in the process.

I am also very thankful to past and present members of the Molecular Electronics group at Arizona State University for the many fruitful discussions. Specifically, I would like to thank Dr. Joshua Hihath, Dr. Fang Chen, Dr. Ismael Diez Perez, Dr. Jilin Xia, Dr. Shaoyin Guo, Dr. Julio Palma Anda, Mr. Chris Bruot, Mr. Limin Xiang, and Ms. Yueqi Li. I would also like to thank visiting members including Dr. Artem Mischenko, Dr. Juan Artes Vivancos and Dr. Raphael Rosch.

I am also very thankful to agencies which have helped fund my work at Arizona State, including the National Science Foundation and the Department of Energy. I am thankful that the public has had the trust to make an investment in me and investment in science.

Finally, I would like to express thanks to my family, including my mother, father, brother and sister for offering love and support.

## TABLE OF CONTENTS

LIST OF TABLES.....	viii
LIST OF FIGURES.....	ix
CHAPTERS	
1 INTRODUCTION.....	1
1.1 Introduction and Motivation for Molecular Electronics.....	1
1.2 A Brief History of Molecular Electronics.....	4
1.3 Charge Transport Models.....	8
1.3.1 Mesoscopic Transport.....	8
1.3.2 The Landauer Formula.....	10
1.3.3 Coherent Transport: Non-Resonant Tunneling.....	13
1.3.4 Incoherent Transport: Sequential Hopping.....	17
1.3.5 Inelastic Coherent Transport: The Cotunneling Model.....	21
1.3.6 Current-Voltage Behavior: The Simmons Model.....	24
1.4 Contacts in Molecular Electronics.....	28
1.5 Summary.....	32
2 TRANSITION FROM TUNNELING TO HOPPING IN SINGLE-MOLECULE JUNCTIONS BY LENGTH AND TEMPERATURE DEPENDENCE.....	33
2.1 Introduction.....	33
2.2 Methods.....	36
2.2.1 Chemicals.....	36
2.2.2 Sample Preparation.....	36
2.2.3 Electrical Measurements.....	37

2.3	Experimental Results.....	39
2.3.1	Conductance of the Molecules.....	40
2.3.2	Length Dependence.....	43
2.3.3	Temperature Dependence.....	44
2.4	Transition from Tunneling to Hopping.....	48
2.5	The Role of Coupling between Repeat Units.....	48
2.6	Molecular Junction Formation.....	51
2.7	Conclusions.....	57
3	CONTROLLING FORMATION OF A SINGLE-MOLECULE JUNCTION BY ELECTROCHEMICAL REDUCTION OF DIAZONIUM TERMINAL GROUPS.....	59
3.1	Introduction.....	59
3.2	Methods.....	61
3.2.1	Sample Preparation.....	61
3.2.2	Electrical Measurements.....	62
3.2.3	Data Processing.....	63
3.3	Experimental Results.....	64
3.4	Control Experiments with an Amine Terminated Molecule.....	68
3.5	Supporting Calculations.....	71
3.6	Summary.....	76
4	THERMALLY INDUCED CONFORMATION CHANGES IN OLIGOTHIOPHENE SINGLE-MOLECULE JUNCTIONS.....	77
4.1	Introduction.....	77
4.2	Methods.....	77

3.2.1	Chemicals.....	79
3.2.2	Sample Preparation.....	79
3.2.2	Electrical Measurements.....	80
3.2.3	Data Processing.....	81
4.3	Conductance vs. Length.....	82
4.4	Conductance vs. Temperature.....	85
4.5	Transition Voltage Spectroscopy Statistics.....	87
4.6	Discussion of Experimental Results.....	94
4.7	Comparing Change in Conductance with Change in TVS.....	96
4.8	Density Functional Theory and Statistical Mechanics Calculations.....	98
4.9	Summary.....	102
5	CONCLUSION AND OUTLOOK.....	103
	REFERENCES.....	105



## LIST OF TABLES

Table	Page
2.1 Biases Used in Measurements.....	42
3.1 Calculated Parameters for Diazonium and Amine Molecules.....	74
3.2 Orbital Mappings for Diazonium and Amine Molecules.....	75
4.1 Calculating Expected Transition Voltage Change I.....	97
4.2 Calculating Expected Transition Voltage Change II.....	97
4.3 Population Densities of Thiophene Conformations.....	102

## LIST OF FIGURES

Figure	Page
1.1 Examples of STM Break Junction Measurements.....	7
1.2 Example of Quantum Point Contact Measurements.....	12
1.3 Energy Diagram for Donor-Bridge-Acceptor System.....	14
1.4 Charge Transfer Rate vs. Length in a Donor-Bridge-Acceptor System.....	21
1.5 Transition Voltage Spectroscopy and Energy Diagram Explanation.....	26
1.6 Correlation of Transition Voltage with Energy Barrier.....	28
1.7 Correlation of Contact Resistance with Electrode Work Function.....	31
2.1 Schematics of Molecular Wires Studied.....	35
2.2 Conductance Histograms for Different Lengths.....	40
2.3 Conductance Dependence on Bias.....	42
2.4 Conductance as a Function of Wire Length.....	44
2.5 Conductance as a Function of Temperature.....	46
2.6 Calculated Structure of Molecules.....	50
2.7 Energy Gaps of Molecules.....	51
2.8 Conductance Step Analysis.....	54
2.9 Molecular Junction Evolution.....	57
3.1 Cyclic Voltammogram for Diazonium Molecule.....	64
3.2 Conductance Histograms for Diazonium Molecule.....	66
3.3 Yield Enhancement of Junction Formation.....	67
3.4 Comparison of Diazonium and Amine Molecules.....	70

4.1	Conductance Histograms of Oligothiophenes.....	83
4.2	Conductance as a Function of Temperature.....	86
4.3	Building of Transition Voltage Spectroscopy Statistics.....	88
4.4	TVS as a Function of Oligomer Length.....	90
4.5	TVS as a Function of Temperature.....	93
4.6	Energy Diagram for Rotational Angle in Thiophene.....	99
4.7	Calculated Thiophene Conformations.....	101

# 1. INTRODUCTION

## 1.1 Introduction and Motivation for Molecular Electronics

The ability to measure, control and understand charge transport through a single molecule covalently bonded to metallic electrodes is of paramount importance in the field of molecular electronics. Although the field is still in its nascent stages, the development of functional devices made from single molecules or small numbers of molecules could have enormous impacts in many fields. First, molecular based electronics could act as a new foundation by which micro- and nanoelectronic devices are fabricated by replacing the current complimentary metal-oxide-semiconductor (CMOS) fabrication platform.(1-3) Such a paradigm shift in micro and nanoelectronic fabrication techniques could help extend or accelerate the trend whereby the density of devices in microelectronic components increases exponentially, which is commonly known as Moore's "Law". Secondly, molecular based electronics could allow the development of a plethora of chemical and biological sensors based on the principle of electrically detecting molecular binding events of analytes with a known molecular signature.(4-8) And finally, understanding charge transport in single molecules could help us understand charge transport in many biological systems, a phenomenon which is generally poorly understood.(4, 9)

The use of a single molecule as a functional electronic device was first proposed by Aviram and Ratner in 1974.(10) In their seminal paper, the authors described a donor-molecule-acceptor system that could achieve electronic rectification. Since then, numerous advancements have been made in the field in both experiment(11-14) and

theory.(15-29) Numerous experimental techniques have been developed to measure charge transport through molecules directly linked to electrodes. These include electromigrated junctions,(30-32) mercury contact experiments,(33-36) cross wire techniques,(37-40) conducting atomic force microscope(41-44) and scanning tunneling microscope(45-49) based techniques, as well as other microfabrication based techniques.(50-52) While these experiments provide tremendous insight into how charge propagates at the nanoscale, they are limited to measuring a small number of molecules in a monolayer where ensemble measurements obfuscate the individual behavior of a single molecule.(53, 54) Only recently have techniques such as mechanically controlled break junction(55-57) and scanning tunneling microscope break junction(58-61) been developed whereby it is possible to measure the conductance of a single molecule. These techniques will be discussed in greater detail in section 1.2.

Despite the advances made in the field of molecular electronics, there are still many obstacles which the field must overcome before devices made from single molecules or small numbers of molecules become widely implemented. Particularly relevant is developing a greater understanding of charge transport in order to close the gap between theoretical simulations and experimental results.(62, 63) For example, due to inherent shortcomings associated with density functional theory,(64-66) conductance values calculated by DFT-NEGF are often far greater than values obtained experimentally(67-69), often times by more than an order of magnitude. Additionally, there are mismatches in simulated and measured current-voltage behavior(70, 71),

whereby first principles simulations often fail to reproduce the convex nature of current-voltage characteristics as measured through experiments.

There are also many technical challenges which must be resolved before molecules can be used as functional devices. It is particularly important to be able to control the contact geometry between a molecule and its electrodes because atomic scale variations in contact geometry can have profound impacts on a junction's electrical characteristics.<sup>(72-75)</sup> Furthermore, the local environment plays a key role in how a molecular junction behaves, and therefore must be controlled. We will see in Chapters 2 and 4 that temperature plays a role in conductance behavior;<sup>(52, 76-79)</sup> however other factors than can play a role include solvent molecules,<sup>(80)</sup> pH<sup>(81, 82)</sup> and ion concentration.<sup>(7, 83)</sup> Finally, it is critically important to be able to reliably wire molecules together to form functional device architectures. This task will likely require the use of self-assembly techniques, and may require integration of these techniques with conventional microfabrication techniques.<sup>(74)</sup>

While there are many challenges and issues that remain to be addressed in the field of molecular electronics, the field has shown remarkable progress, and developing a deeper understanding of electrical transport through single molecules has played a key role in this development. To that end, this report will discuss several projects which have demonstrated a deeper understanding of how charge transport occurs through single molecules. First, it will present a study on the length and temperature dependent transition between two charge transport mechanisms in a series of molecular wires. It will then discuss the ability to electrochemically control the formation of a molecular

junction and will present of comparison vis-à-vis the same junction formed by conventional linkers. Next, an interesting temperature dependent tunneling mechanism will be discussed in oligothiophenes whereby increasing the temperature induces a more planar conformation in the molecule which reduces the energy barrier of the junction and increases conductance. Finally, a summary of experimental work and research outlook will be discussed.

## **1.2 A Brief History of Molecular Electronics**

Most journal articles on molecular electronics cite the seminal paper by Aviram and Ratner<sup>(10)</sup> in 1974 describing a molecular rectifier as the birth of the field. While the importance of Aviram and Ratner's work cannot be overlooked, there were in fact other noteworthy milestones that deserve mention as well. For example, the advent of molecular monolayers was a key step in the early stages of the field in the late 1960's and early 1970's. Particularly important was the Langmuir-Blodgett film, which provided the first means of sandwiching molecules between metal electrodes and measuring the resultant conductivity. Hans Kuhn and co-workers used this approach to measure the conductivity of fatty acids sandwiched between Aluminum and Mercury electrodes.<sup>(84)</sup> Their results showed an exponential decay in conductivity as the length of the molecules increased, which has been confirmed numerous times and is attributed to a non-resonant tunneling mechanism.

Ari Aviram and Mark Ratner published the first article which considered a molecule as a single electronic device.<sup>(10)</sup> Their work described a molecular rectifier made of a donor-bridge-acceptor molecule. Such a molecule could take advantage of the

electronic structure that resulted from a functional unit rich in electrons and another functional unit poor in electrons. This same layout has allowed for rectification in solid state systems, via the use of a PN junction. While largely cited today, Aviram and Ratner's article did not attract a great deal of attention in 1974, due to the inability to measure a single molecule at the time.

Molecular electronics took a great step forward with the invention of the Scanning Tunneling Microscope (STM) by Gerd Binnig and Heinrich Rohrer in 1981.(85, 86) The STM has acted as the basis for numerous investigation techniques, including STM-Break Junction, which has been used in the studies presented in this thesis. However as early as 1985, the STM was providing insights into the electrical conductivity of multilayers and monolayers. In 1985, Fujihira and co-workers demonstrated a Langmuir-Blodgett monolayer photodiode using STM.(87) And later in 1997, Robert Metzger and co-workers confirmed the Aviram and Ratner rectification mechanism in a monolayer of gamma-hexadecyl-quinolinium tricyanoquinomethanide using STM.(88) Works by Fujihira and Metzger were both ground breaking in that they demonstrated unimolecular reactions, meaning that they occurred within single molecules; however the measurements themselves were not made at the single molecule level.

In 1997 Mark Reed and James Tour published the first study which claimed to measure electron transport at the single molecule level.(55) The authors utilized a mechanically controlled break junction (MCBJ) in which gold electrodes were covered in a monolayer of benzenedithiol. A piezoelectric actuator was employed to bring the two electrodes together until the onset of a measurable current, which was attributed to



transport through a metal-molecule-metal junction. The results reported by Reed and Tour have since been questioned due to the unambiguous nature of the measurements.

The scanning tunneling microscope break junction technique (STM-BJ) was the first technique to provide unambiguous measurements of a single-molecule junction. The technique was pioneered by Bingxian Xu and co-workers in 2003.<sup>(58)</sup> This technique is similar to MCBJ, in that a piezoelectric actuator is employed to control the separation between two electrodes with atomic precision. Unlike Tour and Reeds report though, Xu incorporated a clever trick whereby the electrodes were repeatedly brought into and out of contact, which allowed for the formation and breaking of many single-molecule junctions, and the subsequent analysis of statistics for molecular junctions, as illustrated in Figure 1.1 The accumulation of statistics has proven to be a valuable analysis tool in molecular electronics due to the many factors which can affect the conductance of a single-molecule junction, including contact geometry,<sup>(63, 89)</sup> conformations and defects,<sup>(90)</sup> and molecule-electrode coupling.<sup>(63, 91, 92)</sup>

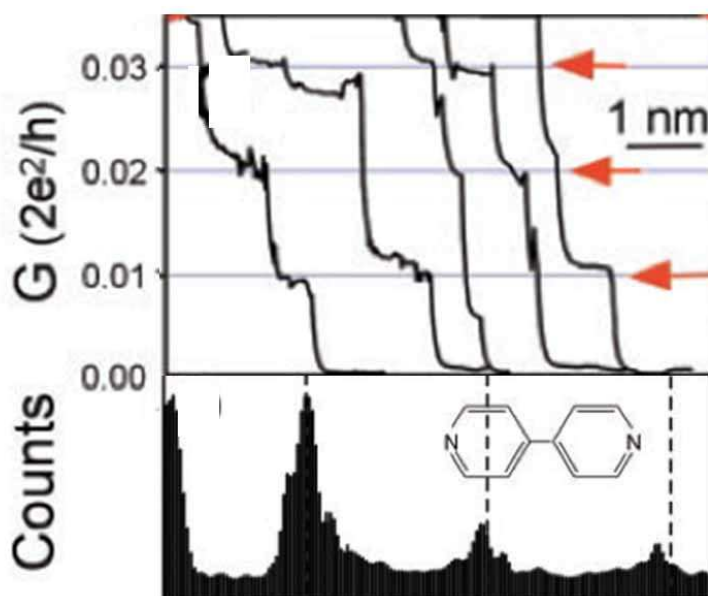


**Figure 1.1:** Measurements taken with STM break junction taken from reference (58). The decay curves on top recorded during the tip pulling process can be compiled into conductance histograms on the bottom. The rapid accumulation of measurements is one the key strengths of STM break junction

Since the first unambiguous demonstration of single-molecule conductance measurement, numerous effects have been reported, including switching,(93-95) rectification,(96, 97) negative differential resistance,(98, 99) orbital gating,(100) electrochemical gating,(101) thermal effects,(102) quantum interference,(103) thermoelectricity,(104) electron-phonon coupling,(8, 105, 106) and spin effects.(107) If properly implemented, these effects could prove to be valuable in making circuits with single molecules acting as individual devices. Of course, in order to truly understand the

origin of these effects, a more detailed description of the electron transport process is needed.

### 1.3 Charge Transport Models

Generally speaking, charge transport in single molecule electronics is not well understood; however some models can be applied to help explain experimental findings in the field. Those models will be discussed here. First, a discussion of what happens as length scales decrease and Ohm's Law no longer becomes relevant will be presented. Secondly, a derivation and justification for the Landauer Formula will be discussed. Then a discussion of the non-resonant tunneling mechanism, whereby an electron can traverse a bridge of molecular states will be presented, followed by a discussion of the hopping mechanism, whereby an electron can be thermally activated across molecular states will be discussed. Then an intermediate mechanism known as the co-tunneling model will be discussed. And finally, current-voltage characteristics will be discussed with respect to the Simmons Model.

#### 1.3.1 Mesoscopic Transport

The Ohmic description of conductance describes electron flow as response to an applied field according to the following:

$$j_i = \sigma_{ij} E_j \quad (1.3.1)$$

Where  $j_i$  represents the current density,  $\sigma_{ij}$  represents the sample conductivity and  $E_j$  represents the applied electrical field. Under this formalism, the conductivity results from scattering events an electron experiences with impurities and lattice defects. Thus, as a sample grows shorter in the direction of current flow, fewer scattering events will

occur and the resulting conductance will increase. If we were to extrapolate this reciprocal relationship between conductance and length to an infinitely small sample, one would expect an infinitely large conductance; however experiments show us that this is not the case.

In order to understand, electron transport at the mesoscopic scale, it is important to first consider a few length scales determined by the scattering events in this region. The first characteristic length of importance is the mean free path,  $L_m$ , which characterizes the average distance a charge carrier can travel between scattering events. It is important to keep in mind that elastic scattering events may cause a phase shift in an electron's coherency; however the wave itself is still coherent. Coherency can only be lost due to inelastic scattering events, which are separated by a distance referred to as the phase-relaxation length, or coherency length of an electron, which is represented as  $L_\phi$ .

Based on the characteristic lengths described above, one can break down transport into three general regimes: Classical, Diffusive and Ballistic. Classical transport applies to length scales much greater than the phase-relaxation length and is described by Ohm's Law. But as we showed earlier this transport regime is not appropriate for very small length scales. Diffusive transport applies to length scales greater than the mean free path, but less than the phase-relaxation length, these length scales are still greater than those which are applicable to single-molecule electronics. For the length scales we are dealing with, we need to consider transport in the ballistic regime, which applies to lengths less than the mean free path of an electron. The best method to understand transport in this regime is to consider the Landauer Formula, which is described below.

### 1.3.2 Landauer Formula

As discussed in the previous section, the Ohmic description of conductance breaks down when considering small constrictions that are shorter than the mean free path of an electron. In order to describe conductance at these length scales, the Landauer Formula is needed. The Landauer Formula was first introduced by Rolf Landauer(19, 108) with additions later made by Markus Buttiker,(15) and it described conductance as a transmission process, rather than a reaction to applied electric field. In this framework, transmission results from the scattering and reflection events a charge carrier encounters while traversing a constriction.

The Landauer Formula can be derived in its simplest form by considering a small constriction of length  $L$  connected to two leads. In this case, the constriction is taken to be a single chain of metallic atoms which is assumed to have a single conduction mode that is completely open. The density of states in this 1-dimensional constriction is given by:

$$n(\kappa)d\kappa = 2\left(\frac{1}{L}\right)\left(\frac{L}{2\pi}\right)d\kappa \quad (1.3.2)$$

Where the factor of two is added to account for electron spin. Assuming free electron like behavior, the derivative of the dispersion relation with respect to  $\kappa$  yields the group velocity, which is given by:

$$v = \frac{h\kappa}{2\pi m} \quad (1.3.3)$$

Where  $h$  is Plank's constant and  $m$  is the electron mass. We can then express the current by:

$$I = nev \quad (1.3.4)$$

Where  $n$  is the number of charge carriers,  $e$  is the electron charge and  $v$  is the group velocity of the charge carrier. In this case, the number of charge carriers is found by multiplying the density of states of each electrode by its respective Fermi function, integrating over all possible states, and taking the difference:

$$I = e \int_0^{\infty} n(\kappa) f_1(\kappa) v(\kappa) d\kappa - e \int_0^{\infty} n(\kappa) f_2(\kappa) v(\kappa) d\kappa \quad (1.3.5)$$

By plugging equations 1.3.1 and 1.3.2 into equation 1.3.4, one obtains:

$$I = e \frac{1}{\pi} \frac{h\kappa}{2\pi n} \left( \int_0^{\infty} f_1(\kappa) d\kappa - \int_0^{\infty} f_2(\kappa) d\kappa \right) \quad (1.3.6)$$

Converting the integration from momentum space to energy space gives:

$$I = e \frac{1}{\pi} \frac{h\kappa}{2\pi n} \left( \frac{2\pi}{h} \frac{2\pi n}{h\kappa} \int_{-\infty}^{\infty} f_1(E) \frac{d\kappa}{dE} dE - \frac{2\pi}{h} \frac{2\pi n}{h\kappa} \int_{-\infty}^{\infty} f_2(E) \frac{d\kappa}{dE} dE \right) \quad (1.3.7)$$

Which simplifies to:

$$I = \frac{2e}{h} \left( \int_{-\infty}^{\infty} f_1(E) dE - \int_{-\infty}^{\infty} f_2(E) dE \right) \quad (1.3.8)$$

However, if we assume zero temperature,  $f_1$  and  $f_2$  become two step functions, and can be replaced by the electrochemical potentials of each lead. This simplifies the situation to:

$$I = \frac{2e}{h} (\mu_1 - \mu_2) \quad (1.3.9)$$

And if we define the voltage as  $V = (\mu_1 - \mu_2)/e$ , the expression further simplifies to:

$$I = \frac{2e^2}{h}V \quad (1.3.10)$$

Where  $2e^2/h$  represents the quantum of conductance ( $G_0 = 77.5 \mu\text{S}$ ), that is the conductance of a single conductance channel that is completely open. Quantized conductance can be observed in an STM-break junction system quite easily when a quantum point contact is formed between the gold substrate and tip. When the contact first forms, it is usually thick enough to contain several channels; however pulling results in a stepwise decrease in conductance in integer multiples of the conductance quantum as the number of channels is reduced with the width of the constriction, illustrated in Figure 1.2. The final step in the conductance trace represents the conductance of a single channel.

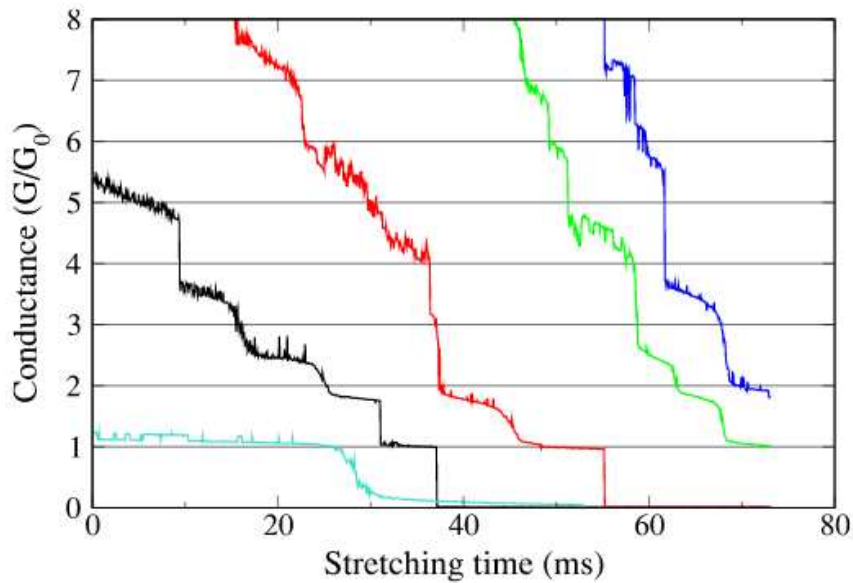


**Figure 1.2:** Examples of quantum point contacts formed with gold. Flat regions in the conductance trace are clearly visible at  $1 G_0$ , corresponding to formation of a contact with one channel that is completely open. Figure taken from Klein et al.(109)

In order to adapt the Landauer Formula for use in molecular electronics, we must account for the fact that there can be multiple conductance channels, and they usually have transmission probabilities far below 100%, meaning each channel is not completely open. In this case, the conductance can then be found by summing the transmission over all available modes using the following expression:

$$G = \frac{2e^2}{h} \sum_{i,j} T_{ij}(E_F) \quad (1.3.11)$$

It should be noted, that the Landauer Formula is generally only valid for low biases. High bias conditions will be discussed in section 1.3.6.

### *1.3.3 Coherent Transport: Non-Resonant Tunneling*

The Landauer Formula is useful in understanding general principles behind transmission through molecules; however a more detailed model must be employed to understand the factors which affect transmission through a molecular bridge. We will thus consider a non-resonant tunneling model (otherwise known as a superexchange model), whereby we have a donor-bridge-acceptor system consisting of  $N+2$  electronic states ( $N$  states on the bridge, plus the donor and acceptor). The energy levels of the  $N$  sites will be energetically distant from the energy levels of the donor and acceptor. We will use a tight binding approach whereby electronic states are localized in space and strong coupling results between adjacent bridge states, but coupling between non-adjacent bridge states is non-existent. Additionally, we will assume that that the



transmission time is less than the nuclear relaxation time of the states on the bridge, so that traversing charge carriers do not actually reside on the bridge. These factors will ensure that transport through the donor-bridge-acceptor system is coherent.

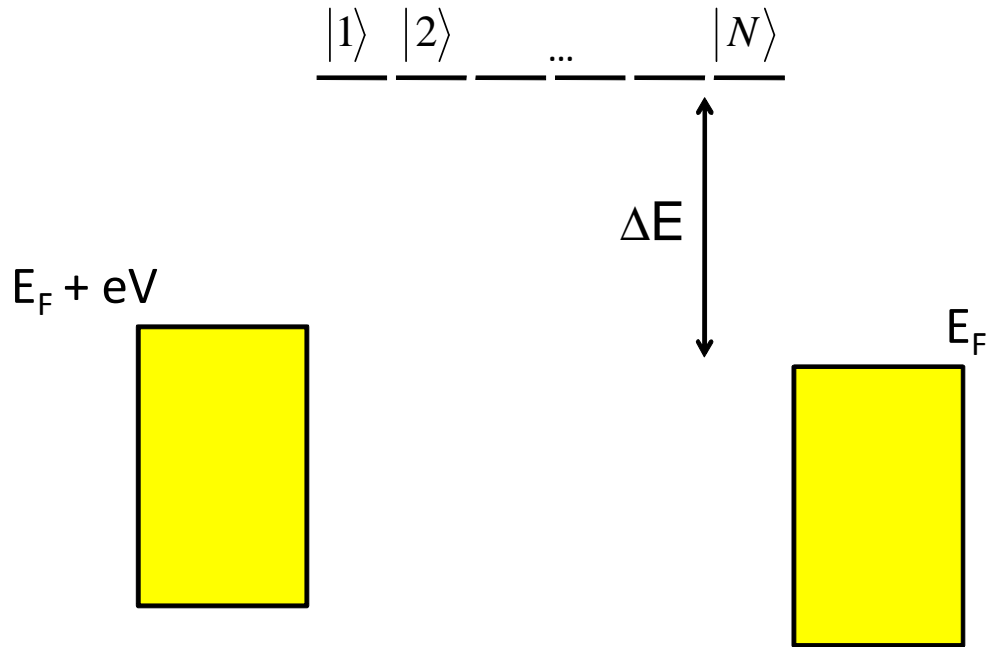


**Figure 1.3:** Energy diagram for the donor-bridge-acceptor system described in the non-resonant tunneling model. In this system a series of discrete states are localized on the bridge such that there is a large energetic difference between them and the electrochemical potentials of the donor and acceptor. The result is that a traversing electron tunnels through the bridge.

In this description of electron transport, we first recall Fermi's Golden Rule, which describes the transfer rate between states  $i$  and  $f$ , represented as:

$$k_{et} = \frac{4\pi^2}{h} |T_{f \leftarrow i}(E)|^2 \rho(E_F) \quad (1.3.12)$$

Where  $\rho(E_F)$  represents the thermally averaged, Franck-Condon weighted density of states. However in the case of our system in which we consider a molecule connected to leads with an applied voltage, we replace the Franck-Condon density of states with the Fermi functions of each electrode, which we represent as:

$$k_{et} = \frac{4\pi^2}{h} \sum_{i,f} f(E_i)(1-f(E_f)) |T_{f \leftarrow i}(E)|^2 \delta(E_i - E_f) \quad (1.3.13)$$

Where  $T_{f \leftarrow i}$  represents the coupling between donor and acceptor states such that:

$$T_{f \leftarrow i}(E) = \langle i | T(E) | f \rangle \quad (1.3.14)$$

Here, the T operator is defined as:

$$T(E) = V + VG(E)V \quad (1.3.15)$$

Where G is the Green's function of the bridge defined as:

$$G(E) = \frac{1}{E - H + \left(\frac{i\Gamma}{2}\right)} \quad (1.3.16)$$

And  $\Gamma$  represents the inverse lifetime matrix of bridge levels. However for our Donor-Bridge-Acceptor system, we are assuming only nearest neighbor coupling whereby  $|D\rangle$  only couples to  $|1\rangle$  and  $|N\rangle$  only couples to  $|A\rangle$ . Additionally, we assume that there is no through space transfer in our system, which causes the coupling between donor and acceptor term in 1.3.12 to drop out. Invoking this condition reduces the T operator to

$$T_{A \leftarrow D}(E) = V_{D1} G_{1N}(E) V_{NA} \quad (1.3.17)$$

Now it becomes necessary to describe the Green's Function in greater detail. If we assume that a small bias is applied to the bridge system relative to the difference in energies between donor and bridge sites, we can invoke the weak coupling limit in the tight binding approximation and express the Green's Function as:

$$G_{1N}(E) = \frac{1}{E - E_N} \prod_{n=1}^{N-1} \frac{V_{n,n+1}}{E - E_n} \quad (1.3.18)$$

And if we assume that the energy levels of the bridge are identical,  $E_n$  and  $V_{n,n+1}$  become constants, which simplifies the Green's Function to

$$G_{1N}(E) = \frac{1}{E - E_B} \left( \frac{V_B}{E_B - E} \right)^{N-1} \quad (1.3.19)$$

And defining  $V = E - E_b$  produces:

$$G_{1N}(E) = \frac{1}{V_B} \left( \frac{V_B}{E_B - E} \right)^N \quad (1.3.20)$$

Now we can recall Fermi's Golden Rule introduced in 1.3.12, and represent the  $T$  operator as:

$$\sum_{i,f} T_{f \leftarrow i}(E) = \sum_{D,A} |T_{A \leftarrow D}| \delta(E - E_D) \delta(E - E_A) \quad (1.3.21)$$

And plugging the expression for  $T_{A \leftarrow D}$  (1.3.17) into the expression for  $T_{i \leftarrow f}$  (1.3.21), we see the transmission is directly proportional to the square of the Green's Function, such that

$$\sum_{i,f} T_{f \leftarrow i}(E) \propto \left( \frac{V_{D1} V_{NA}}{V_B} \right)^2 \left( \frac{V_B}{E_B - E} \right)^{2N} \quad (1.3.22)$$

Rearranging we get:

$$\sum_{i,f} T_{f \leftarrow i}(E) \propto \left( \frac{V_{D1} V_{NA}}{V_B} \right)^2 \left( \frac{E_B - E}{V_B} \right)^{-2N} \quad (1.3.23)$$

And taking the natural log of an exponent, we can further rearrange to yield:

$$\sum_{i,f} T_{f \leftarrow i}(E) \propto \left( \frac{V_{D1} V_{NA}}{V_B} \right)^2 \exp \left[ \frac{-2}{a} \ln \left( \frac{E_B - E}{V_B} \right) Na \right] \quad (1.3.24)$$

Where  $a$  is the length of each bridge state and  $d=Na$  is the length of the entire bridge. One can see from this relation that the transmission, and in turn the conductance, is exponentially dependent on the length of the bridge, where the decay constant  $\beta$  is defined as:

$$\beta = \frac{2}{a} \ln \left( \frac{E_B - E}{V_B} \right) \quad (1.3.25)$$

This form fits with a non-resonant tunneling model, also referred to as a superexchange model. Here,  $\beta$  is an indirect measure of the energy barrier a charge carrier encounters as it tunnels through the bridge states. Typical values for  $\beta$  are approximately 1 Angstrom<sup>-1</sup> for saturated alkane systems and 0.2 to 0.6 Angstrom<sup>-1</sup> for conjugated systems. These values are much lower than for through solvent tunneling, which typically has a  $\beta$  value closer to 2 Angstrom<sup>-1</sup>.

#### 1.3.4 Incoherent Transport: Sequential Hopping

In contrast to the non-resonant tunneling mechanism presented in section 1.3.3, there exists an incoherent mechanism in the weak coupling limit whereby charge carriers are thermally populated onto states within the molecular bridge and hop from site to site across the bridge. This mechanism is appropriately named the hopping mechanism. The hopping mechanism begins to occur when the electron traversal time is greater than the

nuclear relaxation time of the molecular states, which ensures that an electron has enough time to reside on a site within the bridge. In contrast to the exponential length dependence of the electron transfer rate found with the superexchange mechanism, the hopping mechanism only produces weakly length dependent electron transfer behavior.

We begin our description of the hopping mechanism by considering the single channel Landauer Formula(20) derived in section 1.3.2:

$$G = \frac{2e^2}{h} T(E_F) \quad (1.3.26)$$

This can be represented in an equivalent form relating the steady state transition rate  $k_{ss}$  to the Transmission  $T$  according to the following:

$$k_{ss}(E) = \frac{h\kappa}{2\pi m L} T(E) \quad (1.3.27)$$

Where  $h\kappa/2\pi m$  is the incident momentum of a charge carrier and  $L$  is the normalization length in the metal. Considering we can define the density of initial states with respect to the momentum as:

$$\rho_i = \frac{4\pi L m}{h^2 \kappa} \quad (1.3.28)$$

We can relate conductance  $G$  to the transfer rate  $k_{ss}$  by:

$$G = e^2 k_{ss}(E_F) \rho_i(E_F) \quad (1.3.29)$$

Where  $k_{ss}$  represents the contribution of not only the coherent component  $k_{ss}^{tun}$ , but also the incoherent component  $k_{ss}^{hop}$ :

$$k_{ss} = k_{ss}^{tun} + k_{ss}^{hop} \quad (1.3.30)$$

From the previous section, we know that  $k_{ss}^{tun}$  will be exponential with respect to bridge length. We make the assumption that electrons that tunnel through the bridge do so elastically or quasi-elastically. With this in mind, we can assume no change in energy for the charge carriers traversing the bridge and represent the tunneling current for a given applied voltage  $V$  as:

$$j^{tun} = e \int \rho_i(E) k_{ss}^{tun}(E) (f(E + eV)(1 - f(E)) - f(E)(1 - f(E + eV))) dE \quad (1.3.31)$$

Integrating over  $E$  and dividing by voltage yields:

$$g^{tun} \approx e^2 \rho_i(E_F) k_{ss}^{tun}(E_F) \quad (1.3.32)$$

When we consider the hopping component of conductance, we must account for the fact that transport in this regime is inelastic, so that charge carriers that enter the bridge with an energy  $E_f$ , subsequently leave the bridge with an energy  $E_f + \Delta E$ . Taking this into account, we represent the hopping component to current as:

$$j^{hop} = e \int \rho_i(E) k_{ss}^{hop}(E) (f(E + eV)(1 - f(E_F + \Delta E)) - f(E)(1 - f(E_F + \Delta E + eV))) dE \quad (1.3.33)$$

However in the limit of small bias and low temperature ( $kT < \Delta E$ ), the Fermi distributions in the leads simplifies to:

$$f(E + eV)(1 - f(E_F + \Delta E)) \approx f(E + eV) \quad (1.3.34)$$

$$f(E)(1 - f(E_F + \Delta E + eV)) \approx f(E) \quad (1.3.35)$$

And as a result the hopping component of the conductance can be expressed as:

$$G \approx e^2 k_{ss}^{hop}(E_F) \rho(E_F) \quad (1.3.36)$$

This expression shows us two things: first that the Landauer Formula is still valid in the low bias limit, and second that the conductance due to hopping(1.3.36) has the same rate

dependence as that due to tunneling(1.3.29), except for the differing rate constants and densities of states.

It is important to consider that in the hopping mechanism, the charge transfer rate constant depends on thermally populating charge carriers into bridge states, and is thus a thermally activated process which follows an Arrhenius relation. This stands in contrast to the tunneling mechanism, which is of course temperature independent. Likewise, the hopping mechanism follows a weakly length dependent behavior. Taking these two factors together, we can say that the hopping rate constant scales as:

$$k_{ss}^{hop} \propto \frac{e^{-E_A/kT}}{\alpha_1 + \alpha_2 N} \quad (1.3.37)$$

Where  $\alpha_1$  represents the inverse rate for traversal between donor and acceptor and  $\alpha_2$  represents the inverse rate to hop between bridge sites.

The transition between tunneling and hopping mechanisms is of great interest and will be discussed in greater detail in Chapter 2. Oligomeric series of molecules have proven to be popular test beds for measuring the transition between charge transport mechanisms, due to the ability to systematically vary the length of the molecule studied and the temperature at which the measurement is made. A model of charge transfer rate vs. length for two different temperatures is reproduced from Segal et al.(20) in Figure 1.4. The figure clearly illustrates both length and temperature dependence of the transfer rate. However, specifics regarding the transfer rate behavior, including tunneling decay constant, hopping length dependence, transition length and activation energy for hopping are system dependent, and therefore must be measured experimentally.

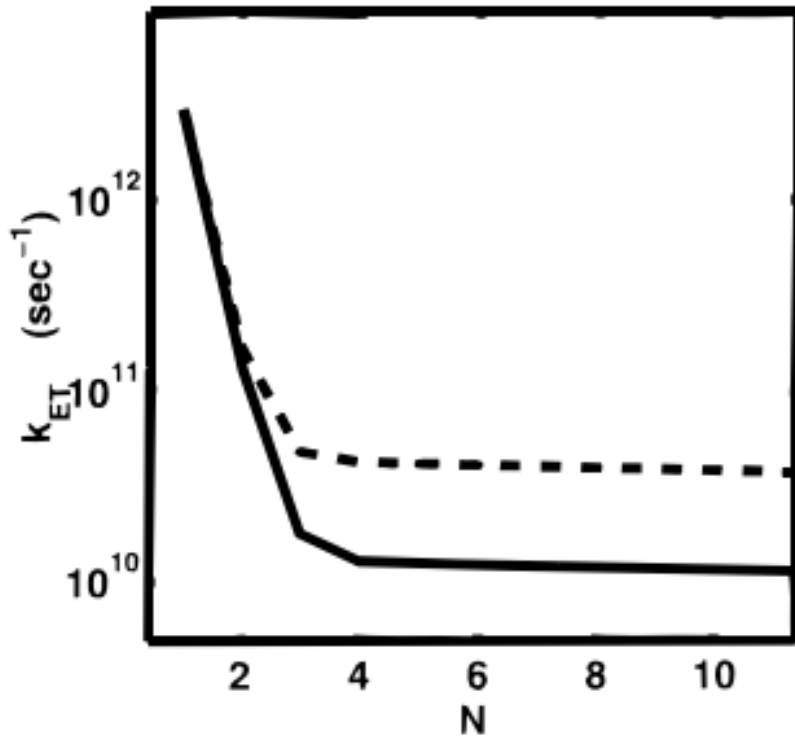


**Figure 1.4:** Charge transfer rate for a donor-bridge-acceptor system with  $N$  sites at 250 K (bold) and 350 K (dotted). Figure reproduced from Segal et al.(20)

### 1.3.5 Coherent Inelastic Transport: The Cotunneling Model

Thus far descriptions of coherent elastic transport via the Superexchange mechanism and incoherent inelastic transport via the Hopping mechanism have been presented. There is however an intermediate mechanism in the weak coupling regime known as the cotunneling mechanism.(110) The cotunneling mechanism results from an electronic transition in the molecular bridge which is mediated by the self energies of the electrodes. The electronic transition is most commonly achieved by application of a large bias or an electrochemical potential; however it can also occur in the weak coupling limit by heating processes in the junction, which is most commonly seen among quantum dots



that exhibit coulomb blockade.(111) The cotunneling process does not occur at the expense of coherent tunneling, but rather occurs in conjunction with elastic tunneling, whereby electrons traverse the bridge along different potential energy surfaces. The cotunneling mechanism has been used to explain switching in molecular wires,(50, 94) and the dissociation of acetylene by an STM tip.(112)

The mathematical description presented herein will not attempt to derive the cotunneling model step for step: for that the reader is referred to the original description published by Hansen et al.(110) In this section only the highlights of the model will be presented which are most important for understanding the mechanism. We begin by reiterating that the total current through the junction is the sum of an elastic component (tunneling) and an inelastic component (cotunneling).

$$I(t) = I_e(t) + I_i(t) \quad (1.3.38)$$

The current is calculated using a scattering approach, in which the transition rate is approximated using a generalized form of Fermi's Golden Rule.

$$k_{fi} = \frac{4\pi^2}{h} |T_{fi}|^2 \delta(E_i - E_f) \quad (1.3.39)$$

The current then is simply given by

$$I = -ek_{fi} \quad (1.3.40)$$

The transition matrix for the scattering processes occurring in the junction is given by

$$T(E) = V + VG^{ret}(E)V \quad (1.3.41)$$

Where G is the retarded Green's Function of the full Hamiltonian given by

$$G^{ret}(E) = \frac{1}{E - H + i\eta} \quad (1.3.42)$$

In our model though, there is a perturbation to the molecule which changes the charge, meaning that the Green's Function can be expanded as a Dyson's Equation

$$G = G_0 + G_0 \Sigma G \quad (1.3.43)$$

Where  $G$  and  $G_0$  are the Green's Functions corresponding to the unperturbed and perturbed Hamiltonians respectively. Additionally the self energy is defined as

$$\Sigma = VG_0V \quad (1.3.44)$$

When only the first order expansion of the Green's Function is considered, the transition matrix reduces to

$$T(E) = \Sigma^{ret}(E) \quad (1.3.45)$$

And the generalized Fermi's Golden Rule becomes

$$k_{fi} = \frac{4\pi^2}{h} |\Sigma^{ret}|^2 \delta(E_i - E_f) \quad (1.3.46)$$

This equation has important implications because it relates the electron transport through the bridge to the energy transfer required for a chemical reaction, which in our case is the charging of the molecular bridge.

A complex analysis of tunneling rates can be invoked to calculate the tunneling rates for both the cotunneling and tunneling processes. When this is done, one finds the inelastic cotunneling is given by

$$k_{fi} = \frac{\Gamma^L \Gamma^R}{h} \frac{eV - \Delta E}{(A - W)(B - W) + \frac{eV}{2} \Delta E - \frac{e^2 V^2}{4}} \quad (1.3.47)$$

Where  $A$  and  $B$  are the ionization potentials of states a and b given by  $A=E_{n-1}-E_a$  and  $B=E_{n-1}-E_b$  and  $W$  is the work function of the electrodes and  $\Delta E = E_b - E_a$ . We can obtain the transition rate for the elastic component by setting  $E_a = E_b$ , which gives

$$k_{fi} = \frac{\Gamma^L \Gamma^R}{h} \frac{eV}{(A-W)^2 - \frac{e^2 V^2}{4}} \quad (1.3.48)$$

A comparison of the two tunneling rates shows that the elastic tunneling does not depend on a voltage threshold  $\Delta V$ , whereas the inelastic cotunneling process does depend on a voltage threshold  $\Delta V$ . This is a defining feature of the cotunneling mechanism and is responsible for many effects observed experimentally, including conductance switching in molecular wires.(50, 94)

### 1.3.6 Current-Voltage Behavior: The Simmons Model

The current-voltage behavior of molecular junctions is inherently non-linear in nature above small applied biases. This non-linearity is very difficult to reproduce from first principles; however an approximation known as the Simmons Model(113) has proven quite effective in describing experimental results. The Simmons Model is derived from the WKB approximation, and describes the current-voltage behavior by the following equation:

$$I = \frac{eA}{h^2 d^2} \left( \left( \phi - \frac{eV}{2} \right) \exp \left( -\frac{4\pi d \sqrt{2m_e}}{h} \sqrt{\phi - \frac{eV}{2}} \right) - \left( \phi + \frac{eV}{2} \right) \exp \left( -\frac{4\pi d \sqrt{2m_e}}{h} \sqrt{\phi + \frac{eV}{2}} \right) \right) \quad (1.3.49)$$

Where  $A$  is the junction area,  $d$  is the barrier length,  $m_e$  is the effective mass of the electron,  $e$  is the electron charge and  $\phi$  is the tunneling barrier height, approximated as the energy offset between the electrochemical potential of the electrode and the nearest

molecular orbital ( $E_F - E_{HOMO}$ ). It should also be noted that this equation was derived for a scenario in which the electrochemical potential of the donor and acceptor electrode are offset by  $eV/2$  and  $-eV/2$  from the Fermi level respectively.

The Simmons model is useful in illustrating two distinct tunneling regimes: the low bias tunneling regime (regime I), and the high bias field emission regime (regime II). In the low bias regime ( $eV_{bias} < \phi$ ), the energy barrier is approximated as a trapezoid (Figure 1.5a), and the model simplifies to:

$$I \propto V \exp\left(-\frac{4\pi d \sqrt{2m_e \phi}}{h}\right) \quad (1.3.50)$$

We see that in this regime there is an approximately linear relationship between voltage and current. As higher biases are applied though,  $eV$  approaches the energy barrier in the junction, and as a result the barrier becomes triangular (Figure 1.5b). In this case the current-voltage behavior can be approximated as:

$$I \propto V^2 \exp\left(-\frac{8\pi d \sqrt{2m_e \phi^3}}{3heV}\right) \quad (1.3.51)$$

Tunneling in this regime is also known as Fowler-Nordheim tunneling or field emission.

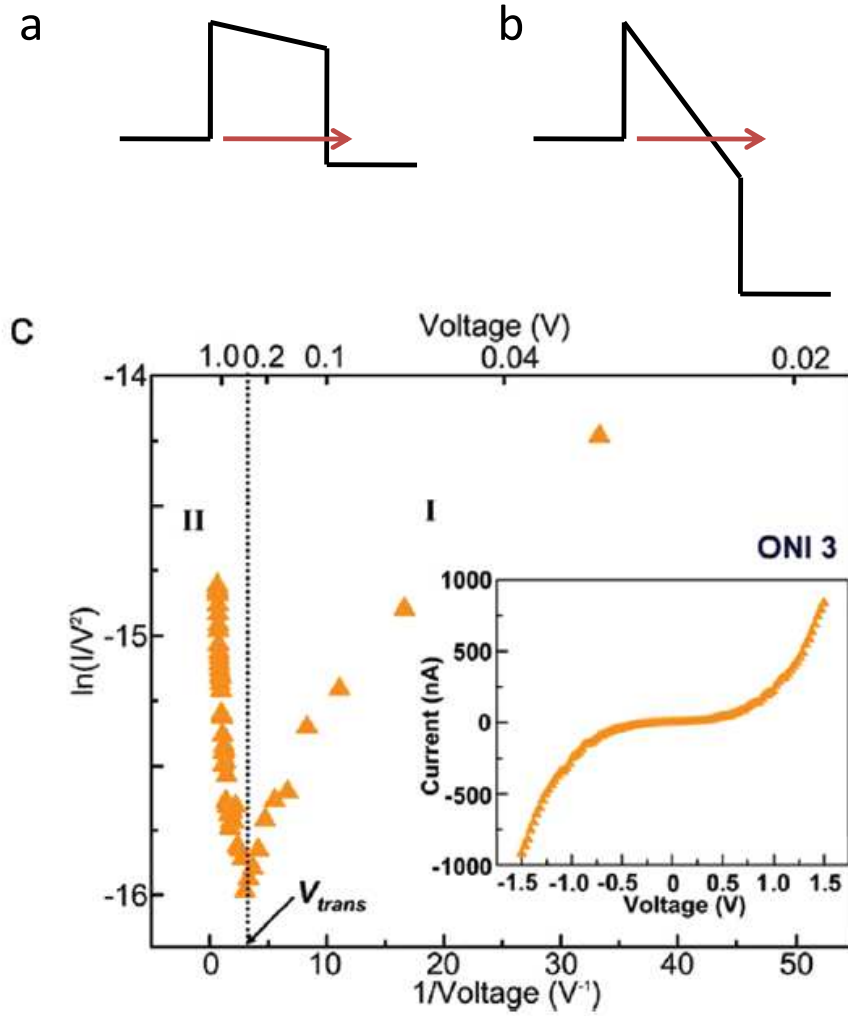


**Figure 1.5:** Illustration of a trapezoidal energy barrier consistent with low bias tunneling (a) and a triangular energy barrier consistent with high bias field emission (b). A Fowler-Nordheim plot reproduced from Frisbie et al.(114) and illustrating the two tunneling regimes is presented in (c).

The transition between low bias tunneling and high bias field emission can be illustrated with the use of a Fowler-Nordheim plot whereby  $\ln(I/V^2)$  is plotted against  $1/V$ .

Such a plot can also be referred to as a transition voltage spectroscopy (TVS) plot. The relevance of this plot can be illustrated by linearizing expression 1.3.51 such that

$$\ln\left(\frac{I}{V^2}\right) \propto -\frac{8\pi d\sqrt{2m_e\phi}}{3he}\left(\frac{1}{V}\right) \quad (1.3.52)$$

An example of a Fowler-Nordheim plot reproduced from Frisbie et. al.(114) is given in Figure 1.5c. One can see that the two tunneling regimes are indicated by two distinctly different slopes in the plot. One can see by inspection of equation 1.3.52 that the slope of the line in the field emission regime (regime II) is determined by the barrier height  $\phi$ . Another useful measure of the barrier height is obtained by finding the voltage associated with the minimum of the Fowler-Nordheim plot, which represents the voltage at which the energy barrier transitions from trapezoidal in shape to triangular in shape, otherwise known as the transition voltage. Beebe et al. performed transition voltage spectroscopy on a series of conjugated molecules and compared their measured transition voltages to the relative energy barriers measured through ultraviolet photoelectron spectroscopy (UPS).(115) The results, which are reproduced in Figure 1.6, show that transition voltage scales directly with  $E_F-E_{HOMO}$ , and is therefore a relative measure of the energy barrier of the molecular junction.

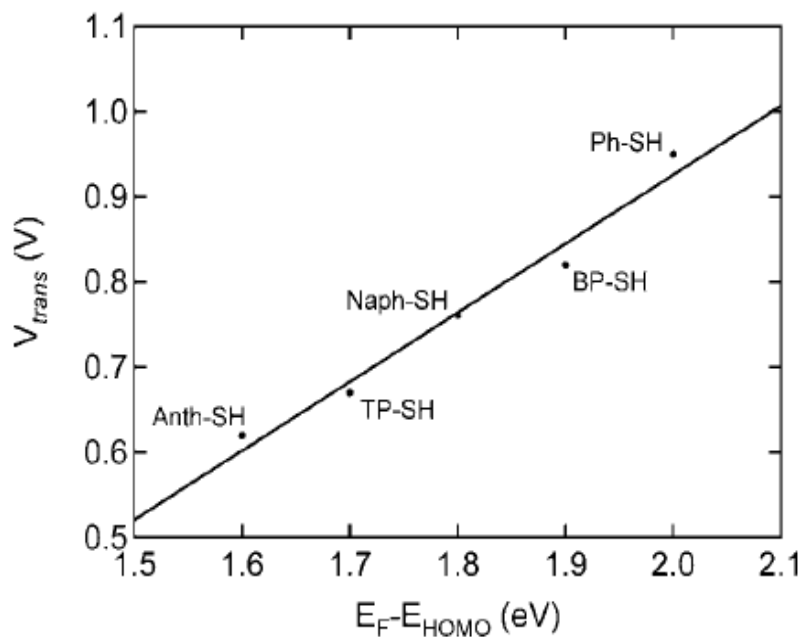


**Figure 1.6:** Correlation of transition voltage measured by transition voltage spectroscopy with molecular energy barrier measured by ultraviolet photoelectron spectroscopy reproduced from Beebe et al.(115) Results showed that the two measurements scale linearly.

#### 1.4 Contacts in Molecular Electronics

Investigations into the effects of molecule electrode bonding have become increasingly popular in the literature recently, in part because single-molecule measurements allow one to measure effects that would otherwise be obfuscated by ensemble measurements of large groups of molecules. The most common anchoring groups used in molecular electronics include thiol,(116, 117) amino,(61, 118) and pyridyl

groups.(58, 119, 120) However other anchoring groups reported in the literature include isocyano,(121) cyano,(122, 123) isothiocyanato,(124) methylselenide,(125) methylthiol,(125) fused thiophene,(125) demethylphosphine,(125) carboxylic acid,(116) dithiocarboxylic acid,(126) nitro,(123) and fullerenes.(127-130) Different anchoring groups have different strengths; however ideally a contact should offer good coupling to the electrodes, well defined contact geometry, and low fluctuations during the pulling process leading to well defined conductance values.

One notorious problem with contacts in molecular electronics is that they can produce variation both during the junction pulling process and from junction to junction. However, two breakthroughs have been able to shed light on why this is the case. The first was reported by Li et al. who investigate the effects of contact geometry on the conductance of alkanedithiol junctions.(131) The authors reported that alkanedithiols bonded in a hollow configuration geometry, whereby the thiol anchoring group was coordinated to three gold atoms, produced a conductance five times greater than when the thiol group was bonded in a top configuration in which the thiol anchoring group was coordinated to a single gold atom. This conclusion was supported by the fact that high conductance junctions frequently switched to low conductance junctions during the pulling process, which is consistent with the evolution of the anchoring group being pulled from hollow to top geometry. A second breakthrough in molecular electronics was reported by Venkataraman et al. by forming molecular junctions by amine linkers.(61) In this report, the authors compared alkane molecular junctions formed with amine anchoring groups to the same junctions formed with thiol and isonitrile groups.



The results showed that conductance histograms for amine terminated molecules had a better defined conductance peak. This result was attributed to the high angular flexibility and stable electronic coupling associated with the lone pair of electrons donated from the amine group to the gold contact.

The role that different electrodes play in the behavior of molecular junctions was first investigated by Frisbie and colleagues.<sup>(132)</sup> Frisbie performed AFM contact measurements of current-voltage characteristics in alkanedithiol and alkanethiol self assembled monolayers. However, by changing the tip and substrate coating independently between Au, Pt, and Ag, he was able to investigate the role that electrode work function plays in the junction. The results showed that contact resistance decreases approximately exponentially with the work function of the electrode material, as shown in Figure 1.7 reproduced from the original manuscript below. This result is consistent with a model whereby conduction proceeds via a non-resonant tunneling mechanism through the HOMO level of the molecule in the junction. In this description, the contact resistance scales with the exponential of the difference between the Fermi level of the contacts and the frontier orbital in the molecule. Furthermore, the authors showed that contact resistance decreases by almost two orders of magnitude with thiol bonds at either end of the junction, as compared to a thiol bond at a single end of the junction.

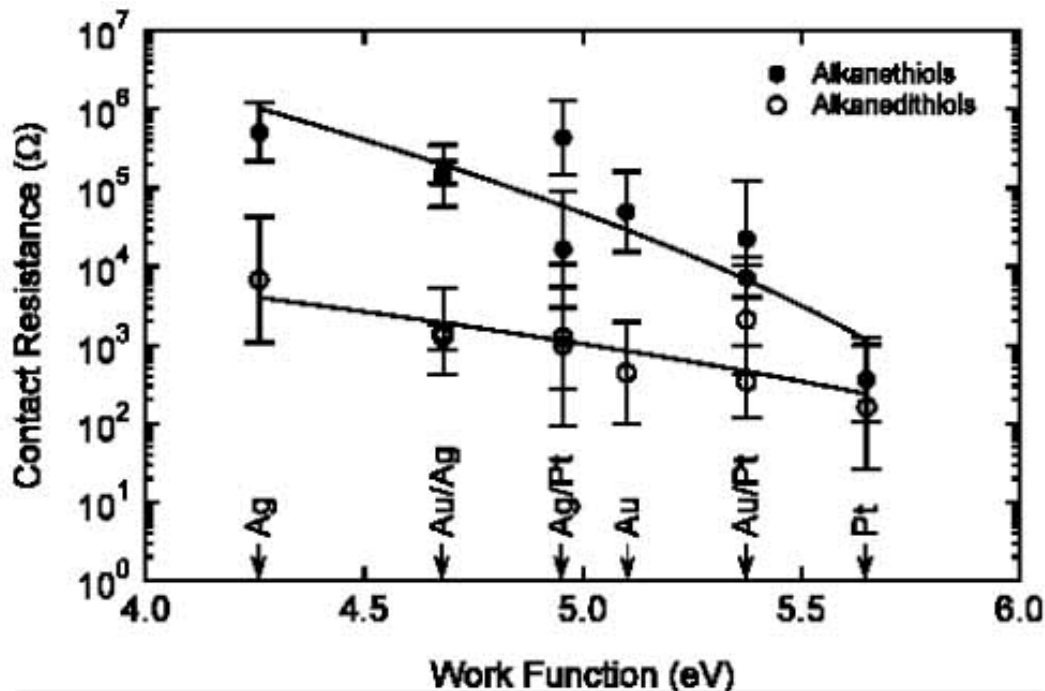


**Figure 1.7:** Contact resistance as a function of electrode work function reproduced from reference (132). The results are consistent with a model whereby conduction occurs by non-resonant tunneling through the HOMO of the molecule.

A recent trend in molecular electronics has been to form molecular junctions by directly graphing the carbon backbone of the molecule to the gold electrodes using Au-C covalent bonds. This was first demonstrated at the single molecule level by cleaving trimethyl-tin groups from an alkane backbone *in situ*;(133) however it has also been demonstrated by cleaving trimethyl-silyl groups.(134) The first reports based on this method showed significantly lower contact resistance owing to the higher metal-molecule coupling of Au-C bonds compared to metal-thiolate bonds. In fact, in a report by Chen et al. resonant tunneling is measured in methylene junctions formed by Au-C bonds.(135) However the hybridization state of the anchoring carbon atom plays a key role in the

behavior of junctions formed by Au-C bonds,(136) and as a result coupling is not always enhanced vis-à-vis metal-thiolate bonds. We will see that this is the case in Chapters 3 and 4, which will discuss the formation of Au-C bonds by electrochemical reduction of diazonium terminal groups, and cleaving iodine terminal groups *in situ*.

## **1.5 Summary**

The developing field of molecular electronics spans many disciplines from chemistry, physics and surface science, to electrical engineering. All of the theoretical and technical factors that affect measurements at the single molecule level cannot be summarized in a single chapter. Nor can all of the milestones that have been reported in the field. However the experimental background and theoretical framework presented should provide context in understanding the projects discussed in the next chapters.

## 2. TRANSITION FROM TUNNELING TO HOPPING IN SINGLE MOLECULE JUNCTIONS BY MEASURING LENGTH AND TEMPERATURE DEPENDENCE

### 2.1 Introduction

Understanding charge transport in a single molecule bridged between two electrodes is paramount to the goal of creating devices from single molecules, and directly relevant to electron transfer phenomena in many chemical and biological systems.(1, 2) Two distinct charge transport mechanisms have been extensively discussed in literature: coherent transport via tunneling or superexchange, and incoherent thermally activated hopping. Coherent tunneling or superexchange dominates through short molecules and the conductance is given by(137)

$$G = G_c e^{-\beta L} \quad (2.1)$$

where  $G_c$  is the contact conductance,  $\beta$  is the tunneling decay constant, and  $L$  is the length of the molecule. In addition to the exponential decay of the conductance with molecular length, this coherent process is characterized by temperature independence. Incoherent hopping is believed to be responsible for charge transport along long molecular wires, and the conductance follows an Arrhenius relation given by

$$G \propto \exp\left(\frac{-E_A}{k_B T}\right) \quad (2.2)$$

where  $E_A$  represents the hopping activation energy. Charge hopping is also characterized as a weakly length dependent process which gives rise to conductance that varies as the inverse of molecular length.

Wire-like molecules made of repeating units are ideal for understanding charge transport mechanisms because they allow one to study both coherent and incoherent transport, as well as the transition between the two by systematically changing the wire length. The transition from tunneling to hopping was observed by measuring photo-induced charge transfer kinetics in donor-bridge-acceptor systems with modulated molecular length(138) and in DNA molecules.(139) Theoretical works by various groups(12, 20, 23, 140-143) have provided additional insights into the experimental results and charge transport mechanisms in general.

Few conductance measurements of molecules with modulated length bridged between electrodes have been carried out. Xu et al. reported a hopping-like charge transport mechanism based on length dependence measurements in DNA molecules containing GC base pairs.(144) However, further work did not observe a strong temperature dependence in these DNA molecules due to the narrow temperature window accessible for the experiment.(145) Frisbie and colleagues first reported on the transition from tunneling to hopping by means of direct resistive measurements as a function of molecular length, temperature and applied bias in junctions made out of hundreds of molecules using conducting probe atomic force microscopy (CP-AFM).(77) The experiment was carried out in molecular thin films in which short range intermolecular interactions prevent these results from being directly correlated with the behavior of a

single molecule.(146) Wang and colleagues first reported on the mechanism transition at the single molecule level by characterizing the distance dependence of molecular conductance using scanning tunneling microscopy (STM) break junction and CP-AFM;(147) however, the results were reported only in light of length dependence, not temperature dependence, which is necessary to be completely certain that a transition from tunneling to hopping has occurred.(148)

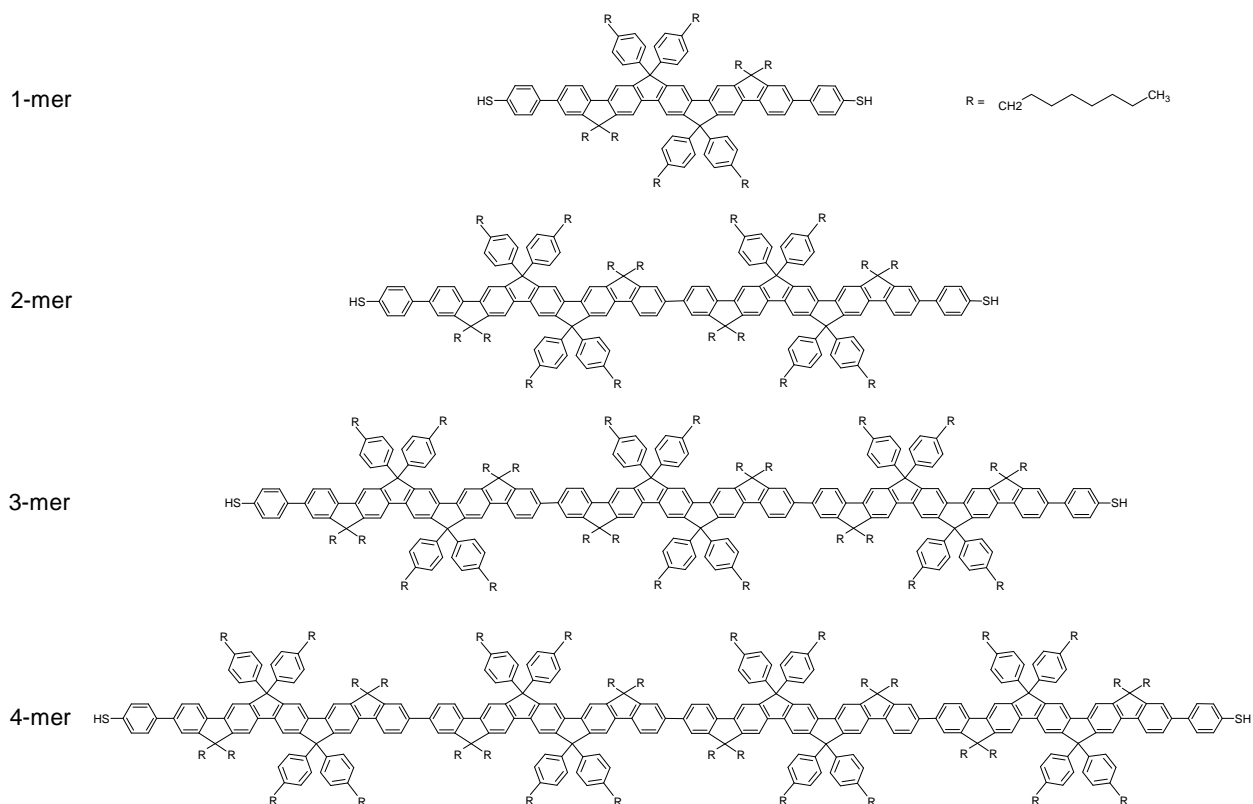


**Figure 2.1:** Molecular structure of the wires used in this study. The lengths measure 3.1 nm, 5.2 nm, 7.3 nm, and 9.4 nm for the 1, 2, 3, and 4-mer wire respectively.

Here, we report results that support a transition between tunneling and hopping in single molecule junctions by carrying out both length and temperature dependent measurements of conductance. The family of molecules investigated consisted of four molecular wires ranging from 3.1 to 9.4 nm in length, shown in Figure 1. To the best of our knowledge, the last molecule in this family represents the longest molecular wire studied by direct conductance measurements with the molecule covalently bound to both electrodes. At elevated temperatures one can observe higher conductance in the longer wires that conduct via hopping than in the shorter wires that conduct via tunneling. The formation and evolution during pulling of these long molecular wire junctions with the STM break junction method was studied by analyzing the individual transient current decay curves.

## **2.2 Methods**

### *2.2.1 Chemicals*

The molecular wires used in this study were synthesized at the Max-Planck Institute for Polymer Research.

### *2.2.2 Sample preparation*

Gold substrates were prepared by thermally evaporating 130 nm of 99.9995% Alfa Aesar gold onto freshly cleaved mica slides in a UHV chamber ( $\sim 5 \times 10^{-8}$  Torr), and annealing for 3 hours at 360° C to ensure a flat Au (111) surface. Each substrate was flame annealed with hydrogen for approximately 45 seconds before being placed in the STM cell with pure mesitylene. STM tips were prepared by cutting 0.25 mm 99.998%

gold wire from Alfa Aesar. Before adding molecules, the sample substrate was imaged in the STM to ensure that there was a clean surface that was free of contamination and that sharp terrace ledges were clearly visible, which is indicative of a sharp tip. Once the surface was experimentally confirmed to be free of contamination, the cell was taken out of the STM chamber and a solution of approximately 100  $\mu\text{M}$  of the protected molecules in mesitylene was added drop-wise to the cell. The acetyl protecting group was self-cleaved when the molecules were added to the STM cell because steps corresponding to formation of a molecular bridge were immediately observable when break junction measurements were carried out.

### *2.2.3 Electrical Measurements*

The STM break junction method was employed to repeatedly form molecular junctions between gold electrodes.<sup>(58)</sup> The current was modulated using a homemade LabVIEW program with two feedback setpoints. The setpoints were defined as 10 nA and 1 pA with a bin size of 0.7 pA for the 1-mer wire and 1 nA and 0.1 pA with a bin size of 0.07 pA for the 2, 3 and 4-mer wires. The upper setpoints used for either amplifier were not high enough to form a metallic contact between electrodes; however a molecular junction was still able to form. The LabVIEW program was used to engage the tip towards the surface until the upper setpoint current was reached. When this occurred, the tip was retracted. In the absence of molecules, a pure exponential decay in the current with respect to tip-sample distance is observed. However, when molecules are present, a molecular bridge occasionally forms, which produces a plateau in the transient decay curve corresponding to the approximate current through the molecule.



The retraction of the probe continues until it reaches a distance of two to five nanometers beyond the distance corresponding to the low setpoint current. The additional ramping beyond the minimum setpoint current was added to make sure that the molecular junction had been completely broken. When the probe has finished retracting the tapping cycle is repeated so that thousands of decay curves can be recorded.

The STM setup consisted of a Molecular Imaging STM head controlled by a Digital Instruments IIIa signal access module integrated with a homemade LabVIEW feedback program. A single stage 1 nA/V amplifier was used to measure the 1-mer wire, and an additional 10X second stage was employed to produce an overall gain of 0.1 nA/V for the 2, 3, and 4-mer wires. Sample temperature was controlled using a Peltier stage for the 1-mer wire and a resistive heating stage for the 2, 3 and 4-mer wires. For each temperature setting, the system was allowed to stabilize for approximately twenty to thirty minutes before measurements were taken to minimize thermally induced drift.

Approximately 5,000 to 15,000 decay curves were collected for each molecule at each temperature setting. Typically, more curves needed to be measured for longer molecules because step yield was relatively low at these lengths. Of the recorded curves, approximately 200-400 decay curves showing step like features for each measurement setting were selected manually to construct a conductance histogram. Curves with step like features were easily identified due to the long length of steps, typically close to a nanometer or more, and the generally clean drop in the step that results from breaking the molecular junction. A full discussion of the selection criteria is given in Section 2 of the supporting information. Experiments were repeated at two to three different temperatures

for each molecular wire to ensure reproducibility of results. Peaks in the histograms were used to determine the conductance of the single molecule junctions. The median and full width half maximum (FWHM) of peaks were found by fitting each conductance peak to a Gaussian distribution.

Step length data was extracted from transient decay curves showing step like features. The ramping rate of the tip was fixed at 20 nm/sec for all experiments in order to avoid ramping rate changes from affecting the stability of the junction.<sup>(149)</sup> When performing tapping experiments, noise from the use of high bias frequently caused dips in the current below the predetermined minimum setpoint current. To prevent the tip from prematurely ramping toward the surface before the junction had been completely broken, the piezoelectric actuator was assigned to ramp an additional two to five nanometers after the minimum setpoint current had been reached. Further distances were used for the longer molecular wires. Step length was determined by measuring the distance between a predetermined high and low current in each transient decay curve that showed current plateaus corresponding to formation of a molecular junction. Thus, both conductance and step length histograms were compiled from the same set of decay curves with current plateaus. Typically, the high current was chosen to be approximately three times the value of the median step height, while the low current was chosen to be about 10% of the median step height. Each transient decay curve was processed through a 1000 Hz low pass filter to minimize the presence of noise spikes, which can interfere with step length measurement.

### **2.3 Experimental Results**

### 2.3.1 Conductance of the Molecules

Figures 2a-d show conductance histograms for the four molecules at 40° C. This temperature was chosen to compare all four wires because the yield of forming molecular junctions at lower temperatures is prohibitively low for the 3 and 4-mer wires. The yield increases with temperature, an interesting observation that we will discuss later. The conductance is  $9.8 \times 10^{-6} G_0$  for the 1-mer wire with a length of 3.1 nm, where  $G_0$  is the conductance quantum defined as  $2e^2/h$  ( $e$  is the electron charge and  $h$  the Planck constant). The value drops to  $4.6 \times 10^{-8} G_0$ , more than 200 times, for the 4-mer wire with a length of 9.4 nm. To the best of our knowledge the 4-mer wire represents the longest molecule that has been measured with the STM break junction method. The shapes of the peaks in histograms vary from experiment to experiment; however experiments taken at the same conditions show reproducible peak locations. The distribution of values observed in conductance histograms is attributed to the statistical nature of the break junction system which can give rise to different molecule electrode contact geometries(63, 150, 151) and molecular configurations.(151)

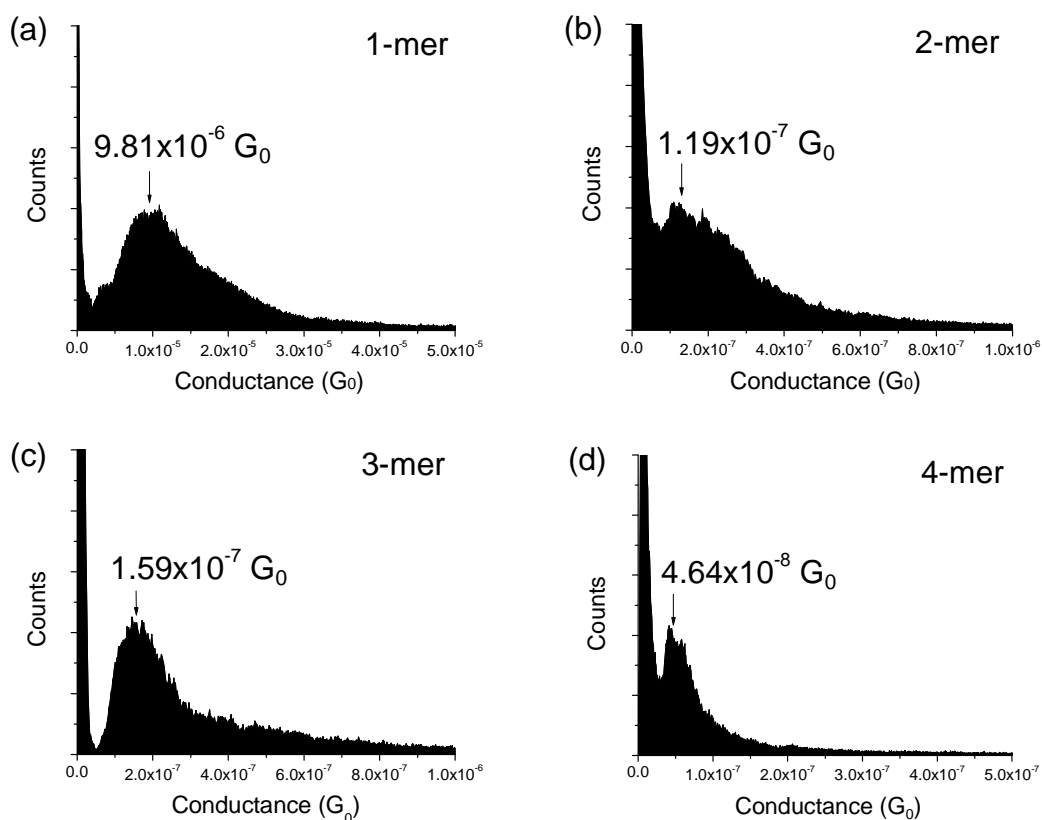


**Figure 2.2:** Conductance histograms of each molecular wire at 40° C. This temperature represents the lowest in which all four wires could be measured.

In order to measure molecular conductance, relatively large bias voltages between 200 to 1200 mV had to be employed to produce conductance steps that could be differentiated from the background. These bias values are listed in Table 2.1, and most are at or below 400mV. However, for the 3 and 4-mer, biases of 800 and 1200 mV had to be used to measure conductance at lower temperatures. Ideally, low biases are used because at higher biases the current voltage behavior becomes non-linear in nature.<sup>(115,</sup>

152) Thus, it is relevant to consider whether conductance measurements taken at higher biases still fall within the linear regime of the molecules. Figure 2.3 shows that conductance histograms for the 4-mer wire taken at 40 degrees Celsius at three different biases all show similar conductance peaks. This suggests that despite the high bias, conductance still falls within the linear regime. We can be certain that measurements taken with the shorter 1, 2 and 3-mer wires were also in the linear regime of conductance due to the larger energy gaps of the molecules (Figure 2.7), and lower applied biases that were used compared to the 4-mer wire.

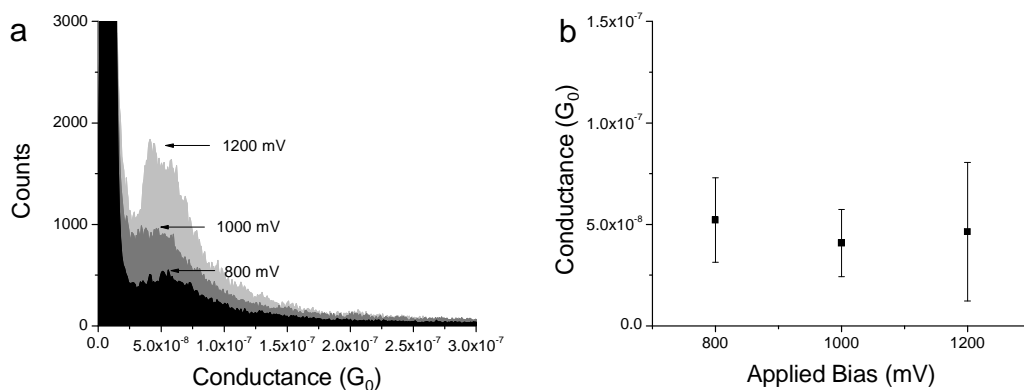


**Figure 2.3** Conductance of the 4-mer wire at 40 degrees Celsius as a function of bias. Even though relatively large biases were applied, there is very little change in conductance due to the wider energy gap of the molecule.

Temperature	1-mer	2-mer	3-mer	4-mer
0° C	200 mV	-	-	-
10° C	200 mV	-	-	-
20° C	200 mV	-	-	-

25° C	-	400 mV	800 mV	-
30° C	200 mV	-	-	-
40° C	200 mV	400 mV	400 mV	1200 mV
45° C	-	-	-	800 mV
50° C	200 mV	400 mV	400 mV	400 mV
55° C	-	-	-	400 mV
60° C	-	400 mV	400 mV	-

**Table 2.1** Biases used during STM break junction experiments.

### 2.3.2 Length dependence

A semi-log plot of conductance as a function of molecular wire length with error bars given by the FWHM of the conductance histograms is given in Figure 2.4. Note that all except the 4-mer wire data were obtained at 25°C. For the 1 and 2-mer wire, the conductance is highly length dependent, and an exponential fit of the curve gives a tunneling decay constant of  $2.06 \pm 0.09 \text{ nm}^{-1}$ , which is similar to the decay constant measured for other conjugated molecular wires(77, 114, 147, 153, 154), albeit with differing molecular structures. The conductance becomes weakly length dependent for the 3-mer and 4-mer wires. This trend suggests that electron transfer occurs via a non-resonant tunneling process in the 1 and 2-mer wires, and transitions to a charge hopping mechanism for the 3 and 4-mer wires. However, this statement cannot be verified by length dependence alone(148), and as a result the conductance values of the molecular wires were measured at different temperatures.

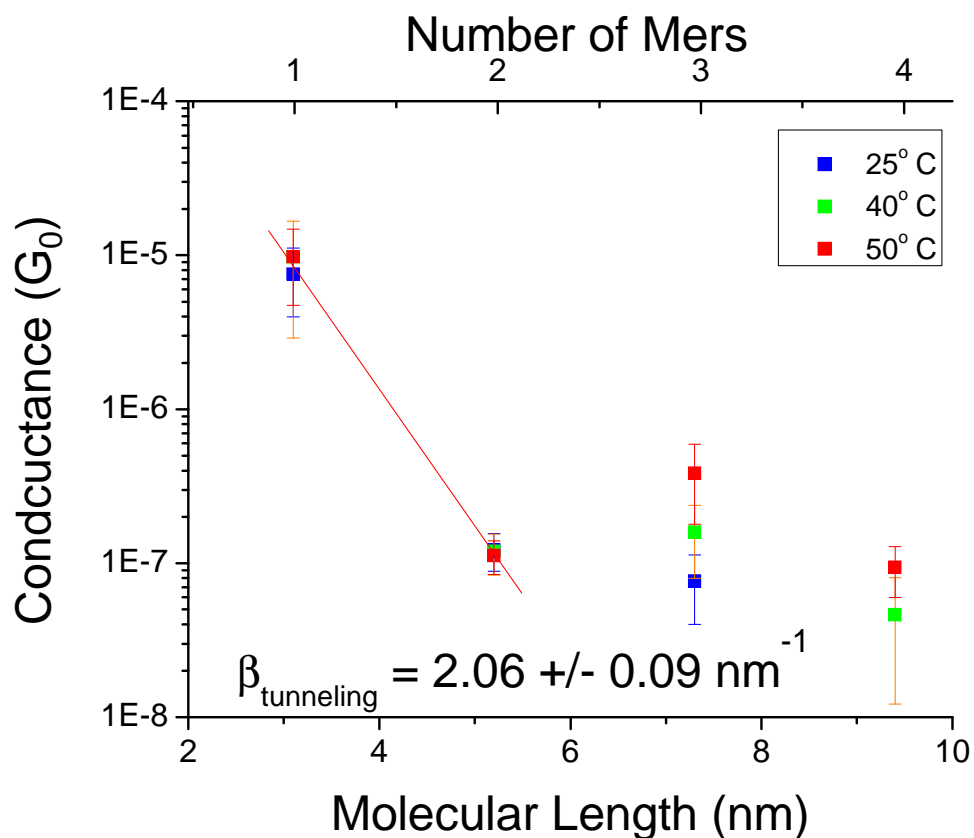


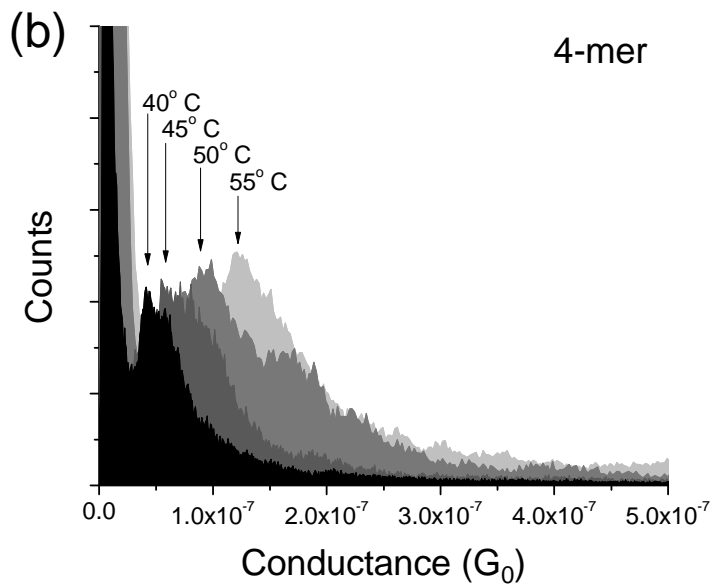
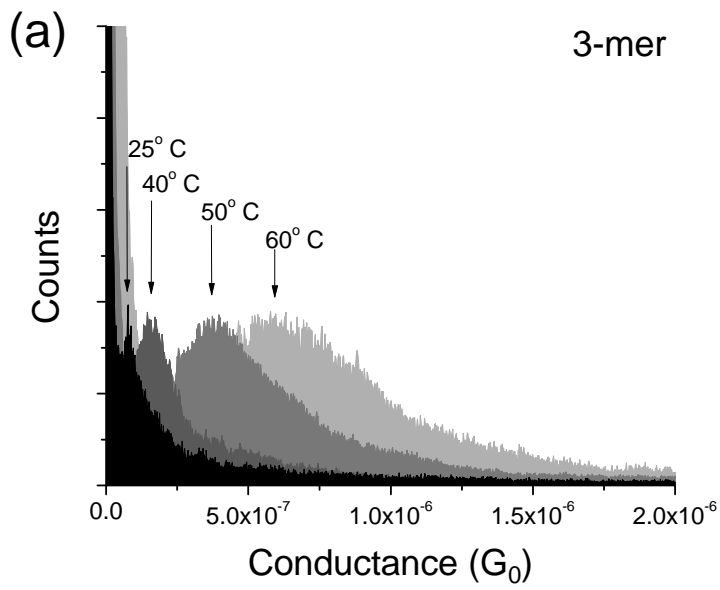
**Figure 2.4:** Measured conductance as a function of wire length at  $T = 25^\circ \text{C}$ ,  $40^\circ \text{C}$  and  $50^\circ \text{C}$ . Conductance was invariant of temperature in the 1 and 2-mer wires, and varied systematically with temperature for the 3 and 4-mer wires. Red lines are included as a guide to the eye.

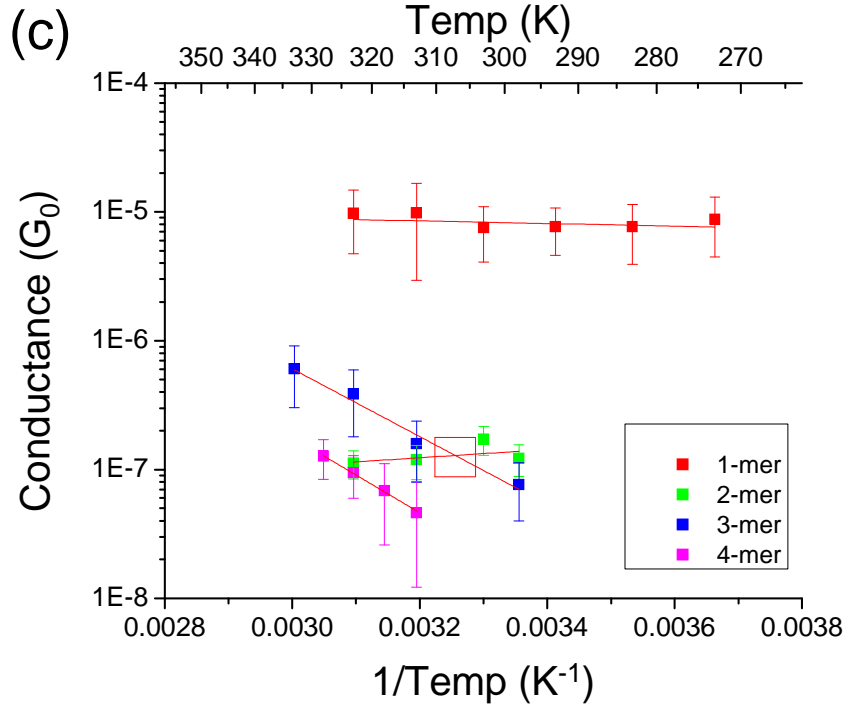
### 2.3.3 Temperature dependence

Figure 4c shows that the conductance of the 1 and 2-mer wires is independent of temperature, while Figures 4a and b show that the conductance of the 3 and 4-mer wires varies systematically with temperature. This trend supports the hypothesis that charge

transport occurs by tunneling in the shortest two molecules and by thermally activated hopping in the longer molecules. The transition occurs between the 2 and 3-mer wires for this molecular family, which represents a length of between 5.2 nm and 7.3 nm. Elsewhere, transitions in other conjugated systems have been approximately 2.5 nm(*138*), 2.75 nm(*147*), 4 nm(*77, 114*), and from 5.6 nm to 6.8 nm(*153*). Thus, compared to other systems, our set of molecular wires displays long range tunneling behavior.







**Figure 2.5:** (a,b) Conductance histograms for the 3-mer wire (a) and 4-mer wire (b) measured at different temperatures. (c) Arrhenius plot of conductance for the 1, 2, 3 and 4-mer wires. The conductance values measured for the 3 and 4-mer wires show a systematic dependence on temperature suggesting that charge transport occurs via a thermally activated hopping process. The red square marks the transition where the conductance of the 3-mer wire intersects the conductance of the 2-mer wire.

Charge hopping activation energies for the 3 and 4-mer wire were found by fitting Arrhenius curves to Figure 2.5c. The activation energies for the 3 and 4-mer wires were measured to be 0.52 eV and 0.58 eV with  $r^2$  values of 0.947 and 0.997 respectively.

These values are reasonably consistent with measurements on molecular wires carried out using conducting probe AFM(77) and electrochemical impedance spectroscopy.(155)

#### **2.4 Transition from tunneling to hopping.**

The transition from tunneling to hopping conduction mechanisms leads to a peculiar length dependent conductance for the 2-mer and 3-mer wires. At low temperatures, the shorter 2-mer wire is more conductive than the longer 3-mer wire. However, the 3-mer wire conductance increases with temperature while the 2-mer wire conductance remains temperature invariant. Consequently, the longer 3-mer wire becomes even more conductive than the shorter 2-mer wire when temperature is above 40°C. The crossover point is marked by a red square in Figure 4c. Wasielewski and colleagues observed a similar behavior in the study of photoexcited electron transport in donor-bridge-acceptor molecular wires.(138, 156) The authors attributed this phenomenon in context of the donor and bridge energy levels, and cite the decreasing energy mismatch between the lowest unoccupied molecular orbitals of the donor and bridge as bridge length increases as being responsible for the higher electron transfer rate in the hopping regime.(138) Thus the phenomenon Wasielewski et al. observed was only made possible by the fact that the molecular energy gap changes significantly with bridge length. This phenomenon does not apply to our system of wires for reasons discussed in the next section.

#### **2.5 The Role of Coupling Between Repeat Units**

Whenever studying a series of molecular wires, it is important to consider whether the role of coupling between units on the bridge. If the repeating units are coupled together, the energy barrier created by the orbital closest to the Fermi level can decrease, thereby affecting the conductance vs. length characteristics of the molecular system. To address this question, electronic structure calculations were carried out for simplified structures of the molecules 1, 2 and 3 by H. Liu, Z.-S. Wang, and J. Zhao at the Key Laboratory of Analytical Chemistry for Life Science at Nanjing University. Calculations for molecule 4 were not carried out because it was prohibitively large for meaningful results to be acquired.

In order to perform electronic structure calculations, the molecular structures were simplified to remove the side alkyl chains from the molecular backbone and thiols from the terminal end of the molecules. The resulting geometric structures were then optimized using Gaussian 03 software at the HF/6-31G(d) level. After the optimization, two thiols were re-connected to the resulting structure.

Calculate structures are presented in Figure 2.6. One can see that the repeat units are locked in place by fluorene groups, and that rotation can only occur between either two repeat units or between one repeat unit and the terminal end of the molecule. This is illustrated in Figure 2.5 where arrows indicate where the molecules are free to rotate. Calculations show that the resulting dihedral twist between repeat units are all very close to either 45 or -45 degrees. This angle is enough to impede substantial coupling between repeat units.

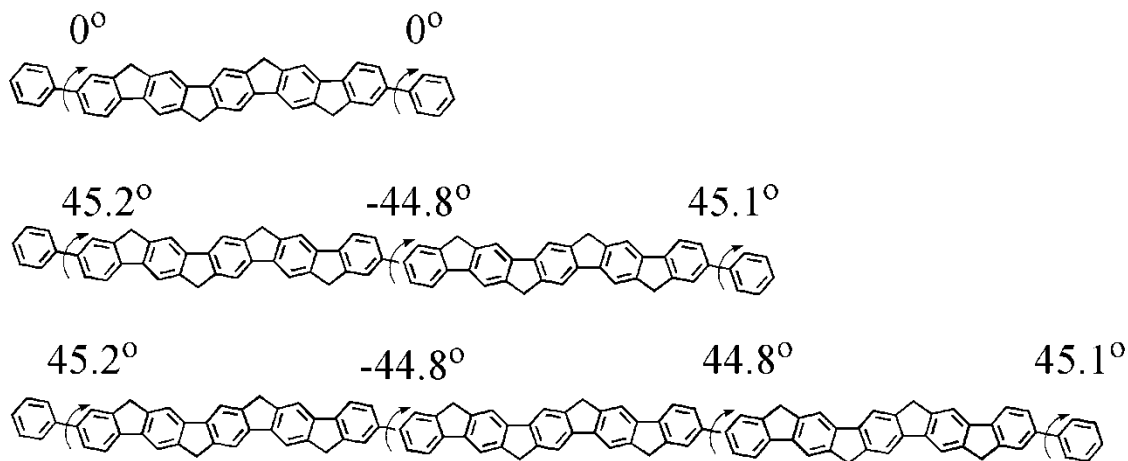


**Figure 2.6:** Calculated dihedral angles between repeating units in Molecules 1, 2 and 3. The angle between repeating units prevents significant coupling between units.

Ultraviolet-visible spectroscopy (UV-Vis) data can also be a useful tool in evaluating the electronic structure of the molecules, because the absorption peak in the spectrum is a measure of the HOMO-LUMO gap in the molecule and scales with the energy barrier in the junction. UV-Vis data for the four molecules used in this study are presented in Figure 2.6. From the data, it is clear that the HOMO-LUMO gap is fairly constant across all four molecules. In fact, the absorption peak only shifts from 413 nm for molecule 1 to 433 nm for molecule 4, which suggests that coupling between repeating units does not play a significant role in this series of molecules.

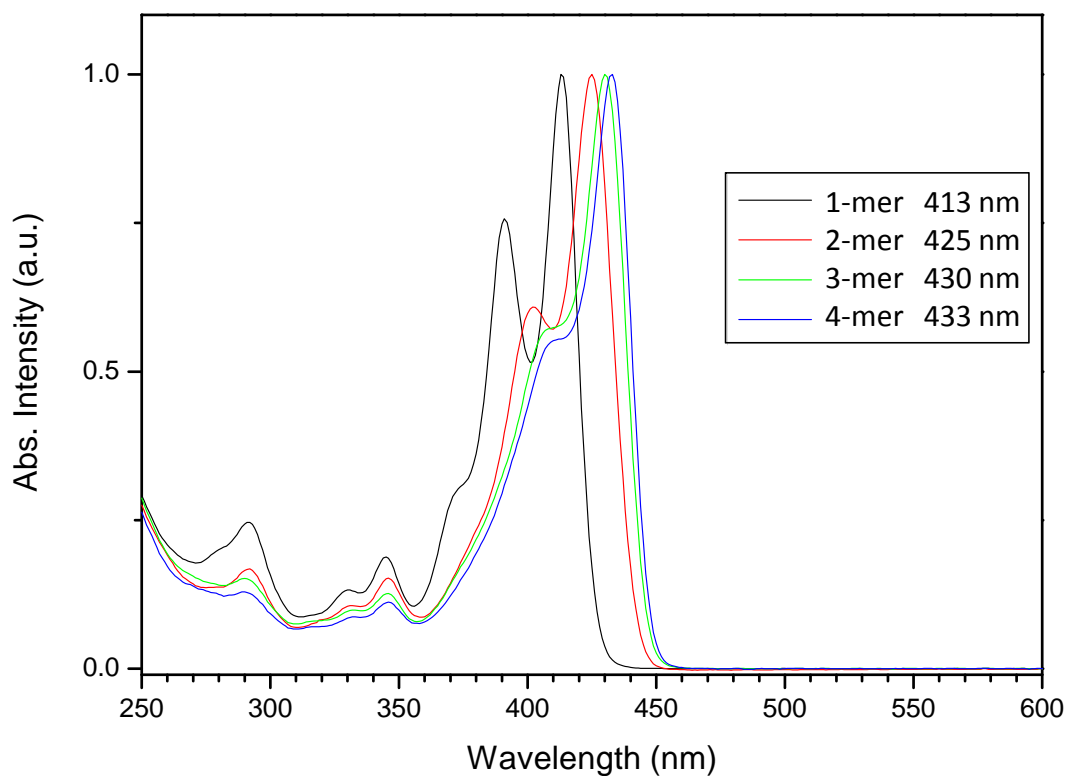


**Figure 2.7** Ultraviolet-Visible Spectroscopy data for the wires used in this study. The absorbance peaks are relatively consistent for all four molecules which suggests the HOMO-LUMO gap does not change significantly in this system.

In summary, the data presented in Figure 2.6 and 2.7 both support the conclusion that there is minimal coupling between repeating units in the series of molecules studied. This suggests that the energy barrier of the junction remains relatively constant across all four molecules, and that the conductance vs. length behavior observed in this system is in fact due to a transition from a tunneling mechanism to a hopping mechanism.

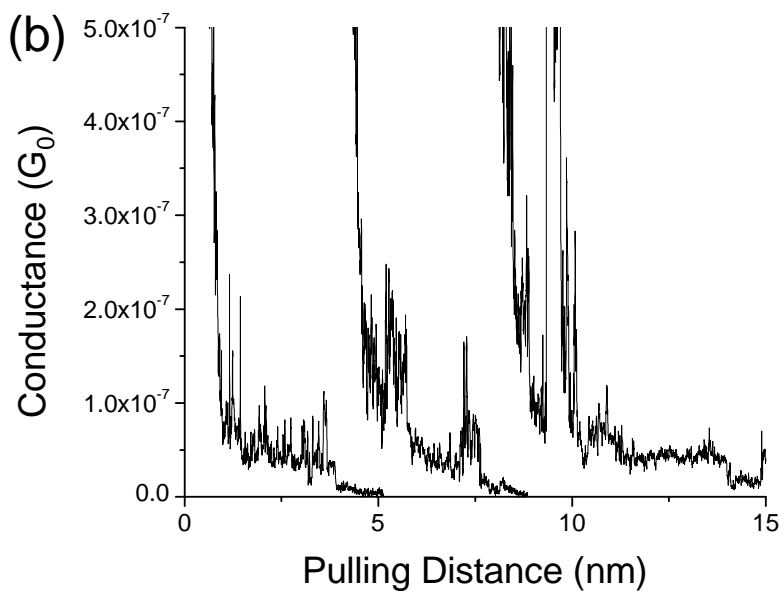
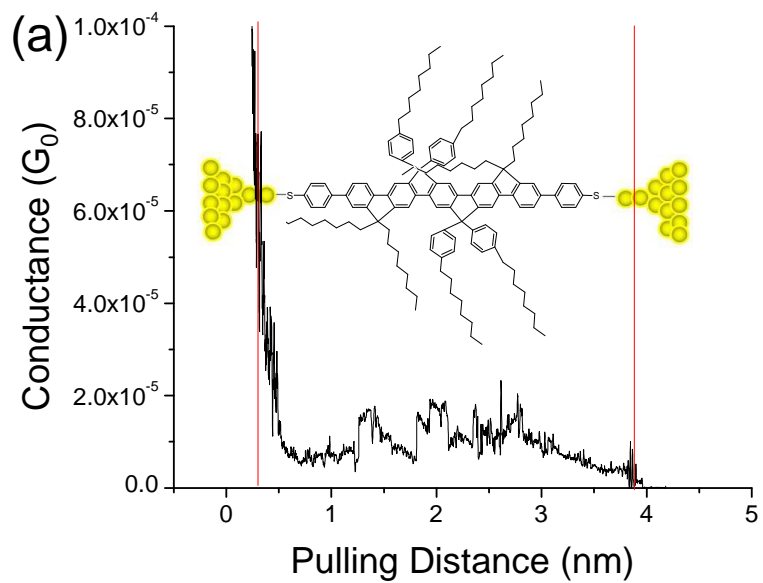
## 2.6 Molecular junction formation.

The yield of forming molecular junctions in the present system increases with temperature and decreases with molecular length. The temperature dependence results from the thermal activation required to form a S-Au bond between the STM tip and the terminal thiol group of the molecule. The molecular length dependence of junction yield results from the relative difficulty in forming a well ordered SAM with longer molecules. In decay curves where a junction is formed, the steps are frequently defined by fluctuations in current as the tip retracts (see Figure 5b). This phenomenon has also been observed in other system(157), which has been attributed to the formation and breakdown of the molecule-electrode contacts. In the present system, the sliding of the molecules on the electrode surfaces during pulling may also contribute to the fluctuations. This phenomenon is discussed in more detail later. Another observation worth noting here is the large step length, the length a molecular junction can be stretched before breakdown. In the case of alkanedithiols, an extensively studied molecular system, the typical step length is a fraction of a nanometer. The step length in the present system can be as large as several nanometers – comparable to the length of the molecules.

Step length information was extracted from transient decay curves collected at 40°C. Examples of steps collected for the 4-mer wire are given in Figure 2.8b. This temperature was the lowest in which all four molecular wires could be measured. Length histograms presented in Figure 2.8c show the step length distributions for all four of the molecular wires. The figure shows a progressive decrease in the median step length as molecular wire length is increased. This trend is accompanied by a corresponding increase in step length spread as wire length is increased. Across all wires studied, there

were examples of steps approaching the theoretical length of the molecule, measured from sulfur atom to sulfur atom. In fact, in the 3 and 4-mer wires, there were examples of steps exceeding 5 nm in length. The tail end of the step length histogram for the 1-mer wire exceeds the theoretical length of the molecule by as much as 0.75 nm, illustrated in Figure 2.8a. However, the theoretical length does not include the formation of Au-S bonds at either end of the junction, each of which measure 0.245 nm in length. When these bonds are accounted for, the longest step is only about 0.26 nm longer than the theoretical length of the junction. This length extension can be explained by the formation of a gold atom chain at either end of the junction. This concept is illustrated in Figure 2.8a. Previous studies have suggested that such a chain can form at each end of the contacts<sup>(90, 158, 159)</sup> and can reach several atoms in length at room temperature.<sup>(90)</sup> Given that the atomic distance between gold atoms is approximately 0.236 nm, a gold chain of only a single atom at either end of the junction could easily explain the observed steps that exceed the theoretical length of the 1-mer wire.





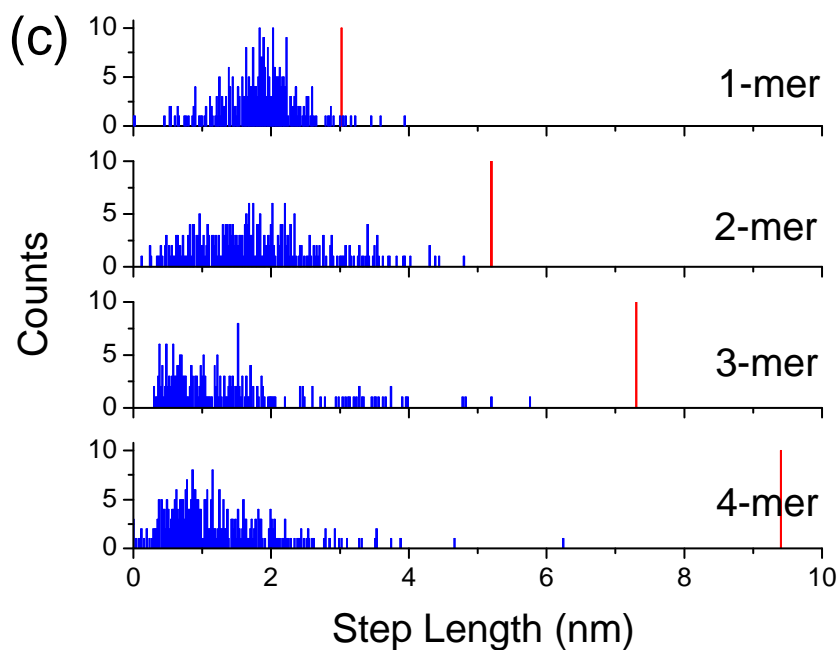


**Figure 2.8:** (a) Schematic illustration of 1-mer pulling which can form steps slightly longer than the molecular length when formation of gold chains at the electrodes is accounted for. The measured length of the step is illustrated by vertical red lines. (b) Transient decay curves of the 4-mer wire, where step length can exceed five nanometers in length. (c) Histograms of measured step lengths for all four wires at 40° C. The red lines denote the lengths of the molecular wires.

The histograms shown in Figure 2.8c all show a median step length significantly less than the theoretical length of the molecule. We propose a “sliding model”, illustrated in Figure 2.8, to explain the evolution of the molecular junction. The sliding model we describe here is similar to those proposed previously.<sup>(49, 160)</sup> In this model, the

molecules are inhibited from standing upright on the surface due to their length; however their alkyl side chains also prevent them from lying flat on the surface of the substrate. As a result, the molecules form a monolayer at an angle to the substrate when the molecular junction first forms. The retraction of the tip serves to pull the molecule in the junction into an upright position by sliding the Au-S bond on the surface so that it is positioned under the apex of the tip. The fluctuations shown in the decay curves in Figures 2.8a and 2.8b can be partially attributed to the Au-S bond sliding along the surface of the substrate as the tip retracts. Sliding is more difficult for longer molecules which inherently contain more degrees of freedom and are more likely to couple to the substrate. These factors may explain why median step length in Figure 2.8c decreases for longer molecules. While local heating in molecular junctions is known to affect junction stability(161), it is unlikely to have affected the junction stability of the longer molecules because heating is the result of current through the molecule and applied bias, and in our system of molecular wires current decreases substantially with molecular length even as bias is increased.

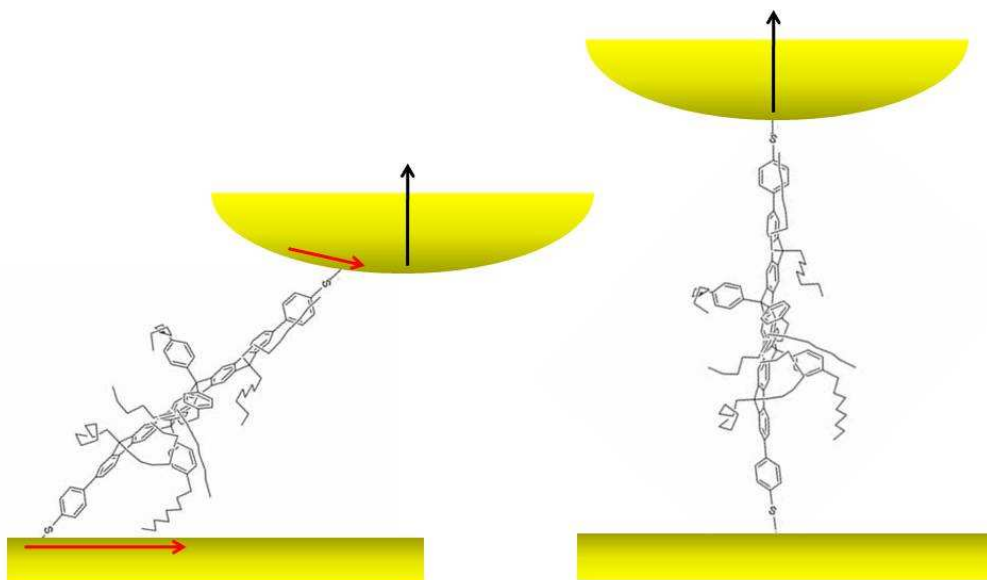


**Figure 2.9:** Schematic illustration of proposed molecular junction evolution. As the tip retracts, the molecule slides along the surface of the substrate so that it is pulled upright.

## 2.7 Conclusion

The STM break junction technique was used to study the electrical properties of a family of molecular wires from 3.1 to 9.4 nm in length. Results showed highly length dependent and temperature invariant behavior in the shortest two wires, and weakly length dependent and temperature variant behavior in the longer two wires. This data is consistent with a model whereby conduction is dominated by a coherent tunneling process in the shortest two wires and transitions to an incoherent hopping process in the

longer two wires. To the best of our knowledge, the last wire in the series represents the longest molecule measured by formation of a single molecule junction. We found that the transition in charge transport behavior occurs between wires measuring 5.2 nm and 7.3 nm in length, which represents relatively long range tunneling. For the wires that conduct via hopping, the activation energy was measured to be between 0.52 eV and 0.58 eV. At elevated temperatures, charge hopping in the 3-mer wire can yield a higher conductance than by non-resonant tunneling in the 2-mer wire. Analysis of the step length distribution showed that most steps were significantly shorter than the length of the molecule being measured. We feel that this phenomenon is best explained by sliding of the Au-thiol bond across the substrate as the probe is retracted until either the bond stochastically breaks, or the junction is mechanically broken.

### 3. CONTROLLING FORMATION OF A SINGLE MOLECULE JUNCTION BY ELECTROCHEMICAL REDUCTION OF DIAZONIUM TERMINAL GROUPS

#### 3.1 Introduction

The anchoring of a molecule to a metal surface is a key factor that affects both charge transport and stability in single-molecule junctions.<sup>(1)</sup> Anchoring is usually achieved by using one of several linker groups that covalently bond the molecule to the electrodes. Thiols<sup>(58, 116)</sup> and amines<sup>(61, 116)</sup> have been characterized extensively in the literature; while other reported linkers include pyridine,<sup>(158)</sup> isocyanide,<sup>(162)</sup> nitrile,<sup>(122)</sup> carbodithiolate,<sup>(126)</sup> and carboxyl<sup>(116)</sup> groups. Additionally molecular junctions formed by direct Au-C covalent bonds were reported by cleaving trimethyltin terminal groups,<sup>(133, 135)</sup> trimethyl silyl groups,<sup>(134)</sup> and by bonding fullerenes directly to gold.<sup>(127, 130)</sup> However, in all of these cases the energetics of bond formation is invariant to the surrounding environment. Thus, the only way to control formation and rupture of the junction is by mechanically manipulating electrodes, either through a mechanically controlled break junction<sup>(55, 163)</sup> or scanning tunneling microscope (STM) break junction<sup>(58)</sup>.

An alternative approach of binding molecules to electrodes utilizes the electrochemical reduction of a diazonium ion placed at the terminal end of a linear molecule.<sup>(164)</sup> This process allows control over the binding energetics of deposition via manipulation of an externally controlled electrochemical gate. Upon reduction, the terminal diazonium ion is cleaved from backbone of the molecule creating an aryl radical.

The radical then reacts with a carbon or metal electrode by forming a direct covalent bond with uninterrupted pi conjugation.<sup>(164-170)</sup> The nature of this bond has been verified using Raman<sup>(171, 172)</sup> and XPS.<sup>(171, 173)</sup> McCreery et al. have employed this process to graft 1000's of molecules to carbon electrodes so that they may be used as active components in hybrid devices fabricated by using conventional CMOS techniques.<sup>(174-178)</sup> This diazonium reduction process produced a more compact and robust organic layer than was achievable using conventional covalent linker groups, which reduced diffusion of metallic species from top coats deposited by thermal evaporation.<sup>(175)</sup>

Here we apply the electrochemical reduction of diazonium groups to the STM break junction process, thereby allowing electrochemical control over the formation of a stable single molecule junction. We use a biphenyl molecule with ortho placed methoxy groups and axially placed diazonium terminal groups on either end. Calculations presented in Table S1 show that the methoxy groups do not have a significant effect on either the assembly process or the conductance of the molecule. The structure of this molecule differs from molecules used in hybrid devices because in this case the diazonium ions are placed at both ends of the molecule. As a result, setting the electrochemical potential to the reduction potential of the diazonium ion induces formation of a metal-molecule-metal junction directly connected by Au-C bonds. By mechanically breaking the junction, the formation and breaking process may be repeated a finite number of times. Furthermore, we show that the molecule electrode coupling

created by the direct Au-C bonding produces a significantly more robust junction than in the same molecule connected using amine linkers.

## 3.2 Methods

### 3.2.1. Sample Preparation

Gold substrates were prepared by thermally evaporating 130 nm of 99.9995% Alfa Aesar gold onto freshly cleaved mica slides in a UHV chamber ( $\sim 5 \times 10^{-8}$  Torr), and annealing for 3 hours at 300° C to ensure a flat Au (111) surface. A solution of anhydrous acetonitrile with 25 mM tetrabutylammonium hexafluorophosphate (TBAPF<sub>6</sub>) was flushed with nitrogen gas to remove any dissolved oxygen prior to preparation of the substrate. The substrate was then flame annealed with hydrogen for approximately 45 seconds before being placed in the STM and filled with acetonitrile and TBAPF<sub>6</sub> solution. The working electrode was prepared by cutting and wrapping a small piece of 0.25 mm platinum/iridium (80%/20%) wire in a tight coil and flame annealing and quenching the coil several times. Upon the last cycle, the coil was flame annealed, allowed to cool in air for a few seconds, and then inserted into the STM cell. The reference electrode was prepared by cutting a small piece of 0.25 mm silver wire, flame annealing one end to form a small ball free of any oxide layer and immediately inserting it into the STM cell. STM tips were prepared by cutting 0.25 mm 99.998% gold wire from Alfa Aesar. Before adding molecules, the sample substrate was imaged in the STM to ensure that there was a clean surface that was free of contamination and that sharp terrace ledges were clearly visible, which is indicative of a sharp tip. Once the surface was experimentally



confirmed to be free of contamination, the cell was taken out of the STM chamber and a solution of approximately 2 mM of 2,2'-dimethoxybiphenyl-4,4'-bis(diazonium) zinc tetrachloride (Sigma-Aldrich, 95% and referred to as **bp1** from this point forward) was added dropwise to the STM cell at 0 mV applied electrochemical potential (vs. Ag/AgCl).

### *3.2.2 Electrical Measurements*

The STM used to carry out experiments was equipped with a bi-potentiostat that allowed electrochemical control of the diazonium reaction. First, cyclic voltammograms were recorded in order to characterize the redox reactions of the **bp1** molecule. Next, molecular junctions were formed using the scanning tunneling microscope (STM) break junction technique.<sup>(58)</sup> This process entailed repeatedly bringing a gold STM tip into and out of contact with the gold substrate with the sample-tip bias fixed at 20 mV and electrochemical potential applied to both electrodes. When the tip was retracted in the absence of molecules binding to the electrodes, a clean exponential decay in the current was recorded within the conductance range below  $G_0$ . However when a molecular bridge was formed a plateau was recorded in the current decay curve, which corresponded to the approximate current measured through a single molecule junction. Due to the irreversible nature of the diazonium electrochemical reduction, conductance traces were recorded starting 0 mV applied potential (vs. Ag/AgCl) and the electrochemical potential was successively decreased in intervals of 100 mV until reaching the potential of the diazonium reduction reaction. The experiment was carried out on four separate occasions.

### 3.2.3 Data Processing

Conductance histograms were compiled by applying the same automated selection criteria to each set of recorded decay curves. In this process, traces showing counts exceeding a defined threshold at conductance values within a given interval range were added to the conductance histogram. This selection process made peaks in the conductance histograms more prominent above the tunneling background and also allowed a quantitative measure of the yield of molecular junction formation in all of the conductance traces. This process also allowed all decay curves showing steps to be saved to a separate directory so that the pulling distance of each molecular junction could be measured.

Pulling distance histograms were compiled by processing all decay curves which had been identified as showing molecular steps while processing conductance histograms. An automated LabVIEW program identified the point in the decay curve where the conductance dropped below approximately 5x the average conductance of the molecule (corresponding approximately to where the molecular step began) and the point where the conductance drops below one fifth the average conductance of the molecular junction (corresponding to the point where the junction ruptures). The distance between these two points was measured to show the distance over which the junction had been pulled. It should be noted that it is difficult to measure precisely at which point a junction forms and ruptures; however as long as the same criteria are applied to each molecule measured, the measured pulling distance can give a very good relative comparison over which two different molecular junctions can be pulled.

### 3.3 Experimental Results

The cyclic voltamogram shown in Figure 3.1 displays successive scans in green (1<sup>st</sup> cycle) and red (2<sup>nd</sup> cycle) showing a prominent reduction peak at approximately -650 mV vs. Ag/AgCl. As illustrated in the inset schematic, this potential corresponds to the reduction of the diazonium linker groups, and deposition of the **bp1** molecule directly onto the gold electrode via a Au-C covalent bond.<sup>(165, 168)</sup> Also noteworthy is the lack of any corresponding oxidation peak, and the surface passivation observed by the peak intensity decrease in successive cycles, showing that the reaction is irreversible and the backbone of the molecule is electrochemically inactive.

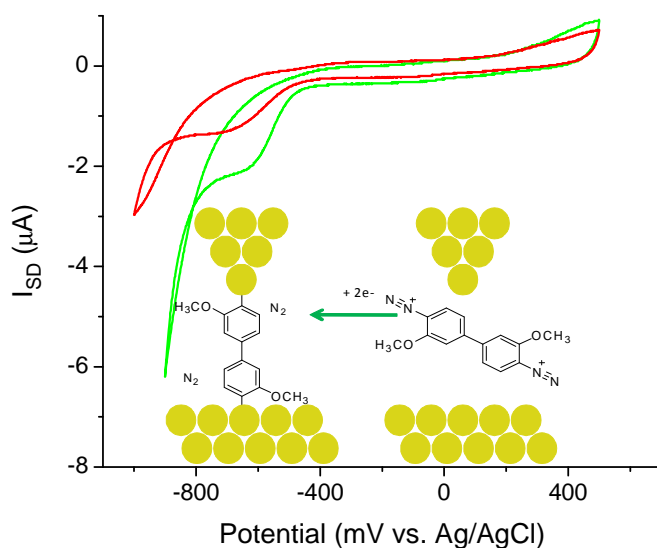


**Figure 3.1:** Cyclic voltamogram of the **bp1** molecule used in experiments. The diazonium terminal groups were irreversibly reduced at approximately -650 mV vs. Ag/AgCl.

The conductance histograms in Figure 2 show that between 0 and -200 mV vs. Ag/AgCl, a conductance peak is not noticeable above the tunneling background. This is attributed to the relatively low yield of molecular junction formation at these electrochemical potentials compared to the inevitable “false counts” that result from employing automated selection criteria. However, when the electrochemical potential is decreased to -300 mV vs. Ag/AgCl and below, conductance histograms show a prominent peak centered at approximately  $2.3 \times 10^{-3} G_0$ .

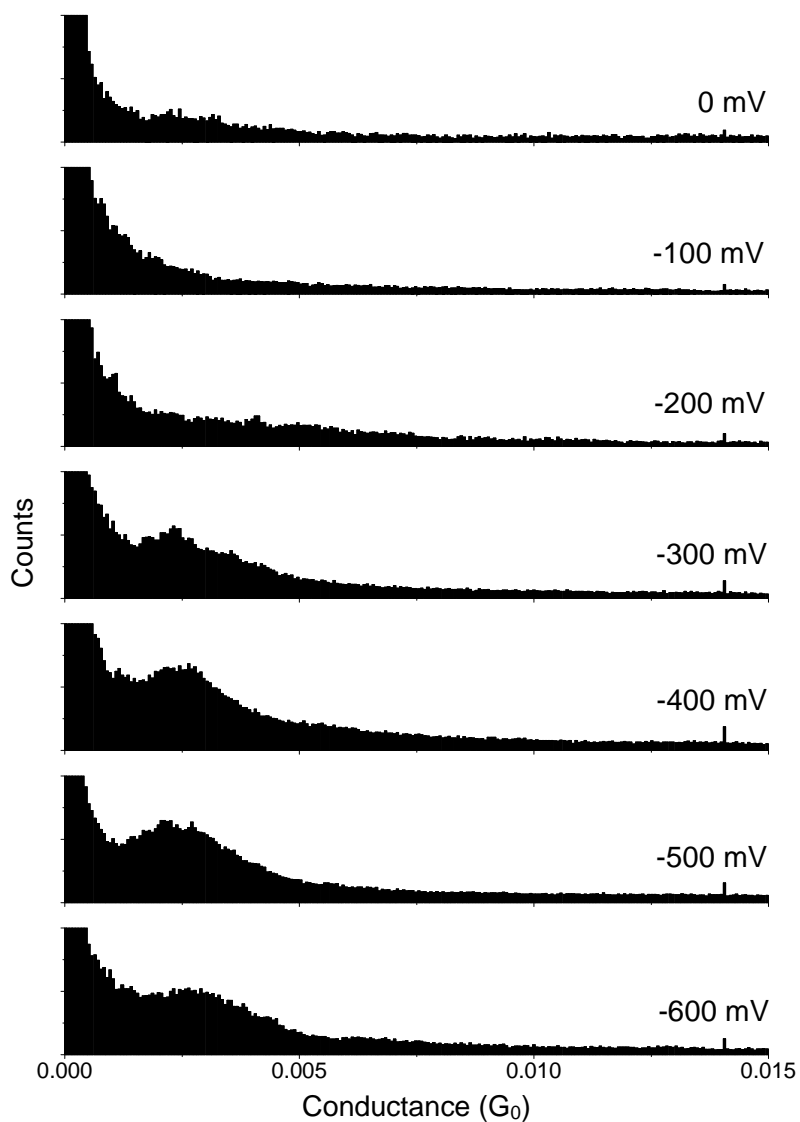


**Figure 3.2:** Conductance histograms in linear scale taken at electrochemical potentials ranging from 0 mV to -600 mV vs. Ag/AgCl. Conductance peaks appeared at -300mV and below, indicating that single-molecule junction formation occurs near the reduction potential of the diazonium groups.

A plot of measured conductance of **bp1** as a function of applied electrochemical potential vs. Ag/AgCl is presented in Figure 3.3a. Median and standard deviation of conductance were found by fitting each peak presented in Figure 3.2 to a Gaussian distribution. Those histograms that did not show any prominent peaks were not fitted and thus are not represented in Figure 3.3a. It is evident that once the two-diazonium linker groups are reduced to form a molecular junction, the measured conductance is relatively invariant to the applied electrochemical potential. This is supported by the fact that the CV shown in Figure 3.1 does not show any electrochemical activity associated with the biphenyl backbone of the molecule.

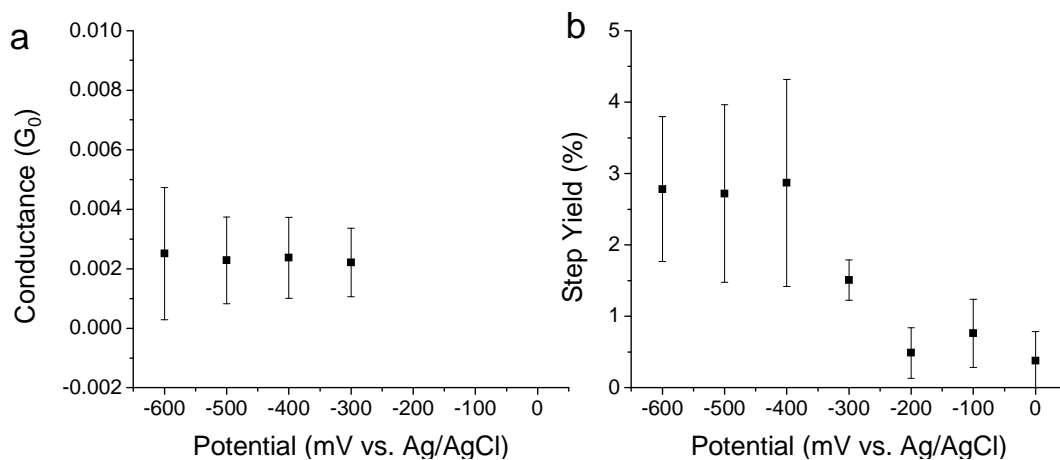


**Figure 3.3:** (a) Conductance peaks extracted from Figure 3.2 as a function of applied electrochemical potential. (b) Relative yield of forming a molecular junction as a function of applied electrochemical potential.

The yield of molecular junction formation for **bp1** was found by applying the same automated selection criteria to each set of conductance decay curves collected at different electrochemical potentials. Yield is defined as the number of transient decay curves showing steps divided by the total number of decay curves collected. Thus, the yield serves as a measure of the tendency of a molecular junction to form. Figure 3.3b shows the weighted mean yield of molecular junction formation, along with standard deviation, recorded across four different experiments. For applied electrochemical potentials between 0 and -200 mV vs. Ag/AgCl the data shows relatively low single-molecule junction formation, on average below 1%, which correlates with the lack of any apparent peaks in the corresponding conductance histograms. However when the applied electrochemical potential is set to -300 mV and below, step yield noticeably increases to between 1% and 5%. This trend shows a direct correlation between the applied electrochemical potential and the formation of single-molecule junctions, which supports the conclusion that the molecular junction is forming by electrochemical reduction of the diazonium terminal groups.

### 3.4 Control Experiments with an Amine Terminated Molecule

In order to determine the role that the Au-C covalent bond plays in the conductance and stability of the molecular junction, STM break junction measurements were also performed on 3,3'-dimethoxybenzidine (Sigma-Aldrich, and referred to as **bp2** from this point forward). **Bp2** has the same backbone structure with ortho placed methoxy groups as **bp1** but has axially placed amine linkers instead of diazonium terminal groups (see inset of Figure 3.4b for schematic). Thus, the **bp2** molecule acted as

a control to the measurements taken with **bp1**. Previous reports of molecular junctions created by direct Au-C bonds by Venkataraman et al. reported up to a 100x increase in conductance compared to analogous molecular junctions bound by covalent amine bonds.<sup>(133, 135)</sup> Conductance traces for **bp2** were recorded under the same bias conditions and in the same electrolyte as **bp1**; however the electrochemical potential was fixed at 0mV vs. Ag/AgCl because neither the backbone nor the amine linker groups of **bp2** are electrochemically active within the electrochemical working range. The conductance histogram for **bp2** (Figure 3.4b) shows a median conductance of  $1.4 \times 10^{-3} G_0$ , meaning that the **bp1** junction is only 60% more conductive than **bp2** (Figure 3.4a). Thus we see that despite previous reports of significantly higher conductance due to direct Au-C bonds, the measured conductances of the diazonium terminated **bp1** and amine terminated **bp2** molecules are fairly similar.



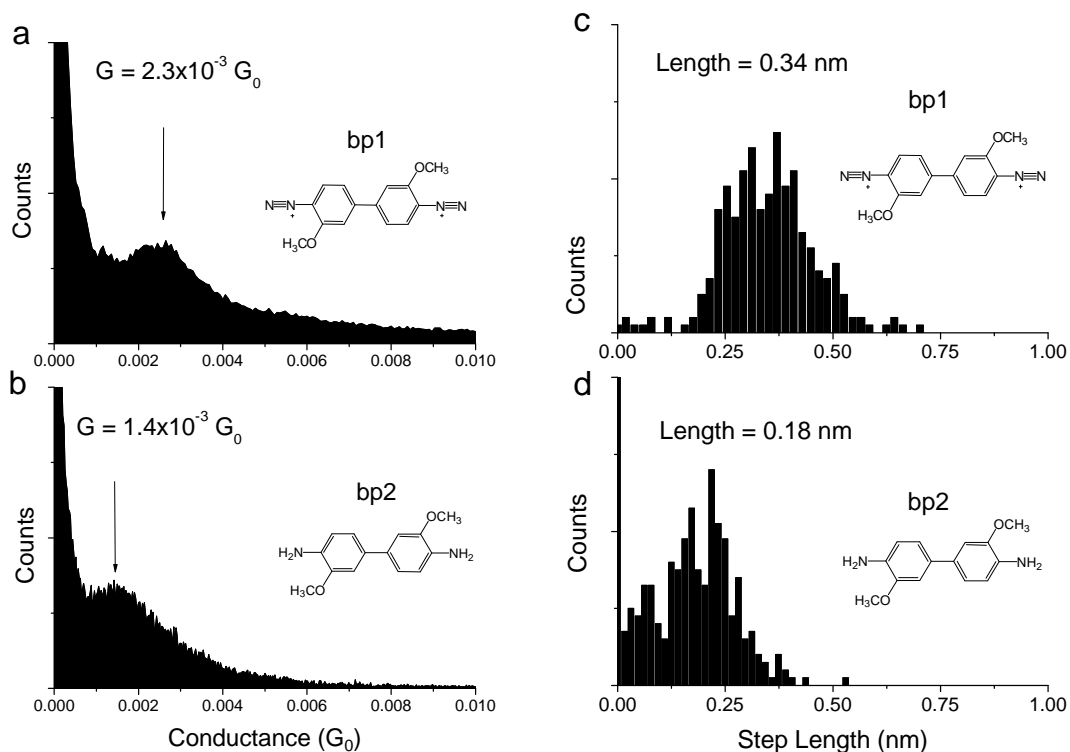


**Figure 3.4:** Side by Side Comparison of **bp1** and **bp2**. The conductance of **bp1** (3.4a) is only 60% greater than that of **bp2** (3.4b). However the **bp1** junction can be pulled (3.4c) nearly twice as far as that of **bp2** (3.4d).

The stretching distance of molecular junctions created with **bp1** and **bp2** was measured and plotted as step length histograms in Figure 3.4c and 3.4d. Gaussian distributions were fitted to both histograms and show that the median pulling length for **bp1** is 0.34nm, while for **bp2** it is much shorter, only 0.18nm. This is the case despite the fact that the **bp1** junction measures 1.13 nm from Au apex to Au apex, compared to

1.34 nm for the **bp2** junction, which is longer because it contains intermediate amines between the phenyl rings and gold contacts. The longer pulling distance associated with the **bp1** junction can be attributed to the direct Au-C bond, which created a stronger bond with the gold electrode than the amine bond used in the **bp2** junction.

### 3.5 Supporting Calculations.

In order to complement the measured conductance and step length data for both molecules, density functional theory (DFT) and non-equilibrium Green's function (NEGF) transmission calculations were performed by H. Nakamura, T. Shimazaki, and Y. Asai at the Nanosystems Research Institute at the National Institute of Advanced Industrial Science and Technology in Japan. The DFT calculations were carried out using SIESTA package(179), while the transport calculations were performed by the HiRUNE subroutines,(180) which is in-house code interfaced with SIESTA. Parameters calculated include molecule-electrode adsorption energy, conductance, highest occupied molecular orbital (HOMO) energy, and coupling energies between the HOMO and electrode. The adsorption energy,  $E_{ads}$ , is defined as

$$E_{ads} = E_{tot} - (E_{mol} + E_{ele} + E_{mol-ele}) \quad (3.1)$$

where  $E_{tot}$ ,  $E_{mol}$ ,  $E_{ele}$  are the energy of the entire molecular junction, the bridge molecule, the right-side electrode, respectively. The last term  $E_{mol+ele}$  is the energy of adsorbed molecule and the left-side electrode. We define the conductance as the transmission at the Fermi Level,  $T(E_f)$ , which is arrived at using DFT-NEGF:

$$g = g_0 T(E_f) = g_0 \text{Tr} \left[ \Gamma_L(E_f) G^r(E_f) \Gamma_R(E_f) G^a(E_f) \right] \quad (3.2)$$

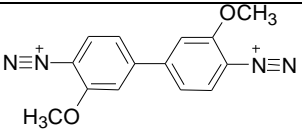
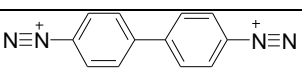
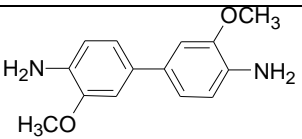
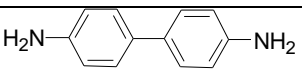
where  $G^{r/a}$  is retarded (advanced) Green's function and  $\Gamma_{L/R}$  is defined by the retarded and advanced self-energy terms of left (right) electrode as  $\Gamma_{L/R} = i(\Sigma_{L/R}^r - \Sigma_{L/R}^a)$ . The constant  $g_0$  is the quantum of conductance defined as  $2e^2/h$  ( $e$  is the electron charge and  $h$  the Planck constant).

Calculations are summarized in Table 3.1. Optimized junction geometries for both molecules showed that **bp1** had a much lower binding energy to the gold electrode than **bp2**, specifically -2.695 eV for **bp1** compared with -0.252 eV for **bp2**. This trend fits well with the step length histograms given in Figure 3.4, because the more stable binding energetics of the Au-C bonding in **bp1** will give rise to a junction that can be pulled over a longer distance compared to the **bp2** counterpart. The calculations also show that the coupling of the conducting pi-orbital to the contacts is far lower for **bp1** (0.057 eV) compared to **bp2** (0.095 eV). We believe that this difference accounts for the fact that there is a relatively small difference in measured conductance between **bp1** and **bp2** compared to other side by side comparisons of Au-C and Au-N bonding schemes. Venkataraman et al. reported large differences – up to 100x - in conductance values between Au-C bonds and Au-N bonds in sigma dominated alkanes(133) and pi dominated xylylenes.(135) In both of these systems the direct Au-C bond resulted in strong coupling between the electrodes and the conducting orbital; however in the case of our system, the Au-C bond of **bp1** results in relatively weak coupling between the electrode and pi-orbital compared to that seen in **bp2**. This is also illustrated by the fact

that the HOMO orbital overlap with the electrode (illustrated in Table 3.2) is far greater for **bp2** than for **bp1**. Additionally, calculated conductance values confirm that **bp1** has only marginally higher conductance than **bp2**. In fact, the values in table 3.1 show that the calculated conductance of **bp1** ( $1.6 \times 10^{-2} G_0$ ) is only 60% greater than **bp2** ( $1.0 \times 10^{-2} G_0$ ), which is the same ratio observed between measured values for **bp1** and **bp2**. Since DFT often underestimates the energy gap of the highest occupied molecular orbital (HOMO) and lowest unoccupied molecular orbital (LUMO), it is difficult to compare the absolute values of calculated and observed conductance.<sup>25</sup> However the calculations are useful in illustrating a qualitative comparison between anchoring and conductance, which complements experimental measurements well.

The methoxy groups in **bp1** likely play a role in stabilizing the diazonium ion; however in doing so it is important to consider whether they affect the conductance of the junction. In order to evaluate this question, the same parameters that were calculated for **bp1** and **bp2** were also calculated for their analogs without ortho-placed methoxy groups. These results are also presented in Table 3.1. One can see that methoxy groups have nearly no affect on the calculated binding energies of the junction. That is the difference in binding energies between **bp1** and its analog without methoxy groups (-2.695 eV to -2.631 eV) is negligible compared to the difference between **bp1** and **bp2** (-2.695 eV to 0.252 eV). The calculations also show that the presence of the methoxy groups slightly increases the conductance and HOMO-electrode coupling in the **bp1** junction. This observation, while interesting, does not have implications for the conclusion that in our

experiments we did not observe substantially higher coupling energies or conductance values associated with the junctions formed with direct Au-C bonds.

	$E_{\text{ads}}$	$T(E_f)$	$E_{\text{HOMO}}$	$\gamma_L$	$\gamma_R$
 <b>(bp1)</b>	<b>-2.695 eV</b>	<b>0.016 <math>G_0</math></b>	<b>-0.24 eV</b>	<b>0.057 eV</b>	<b>0.057 eV</b>
	<b>-2.631 eV</b>	<b>0.007 <math>G_0</math></b>	<b>-0.61 eV</b>	<b>0.078 eV</b>	<b>0.078 eV</b>
 <b>(bp2)</b>	<b>-0.252 eV</b>	<b>0.010 <math>G_0</math></b>	<b>-1.26 eV</b>	<b>0.095 eV</b>	<b>0.095 eV</b>
	<b>-0.303 eV</b>	<b>0.008 <math>G_0</math></b>	<b>-1.47 eV</b>	<b>0.094 eV</b>	<b>0.094 eV</b>

**Table 3.1:** Binding energies ( $E_{\text{ads}}$ ), conductance ( $T(E_f)$ ), HOMO energies ( $E_{\text{HOMO}}$ ,  $E_{\text{HOMO-1}}$ ), and coupling energies ( $\gamma_L$ ,  $\gamma_R$ ) calculated for bp1, and bp2, and their analogs without methoxy groups using DFT-NEGF transport. In all four molecules the HOMO acted as the main conducting orbital.

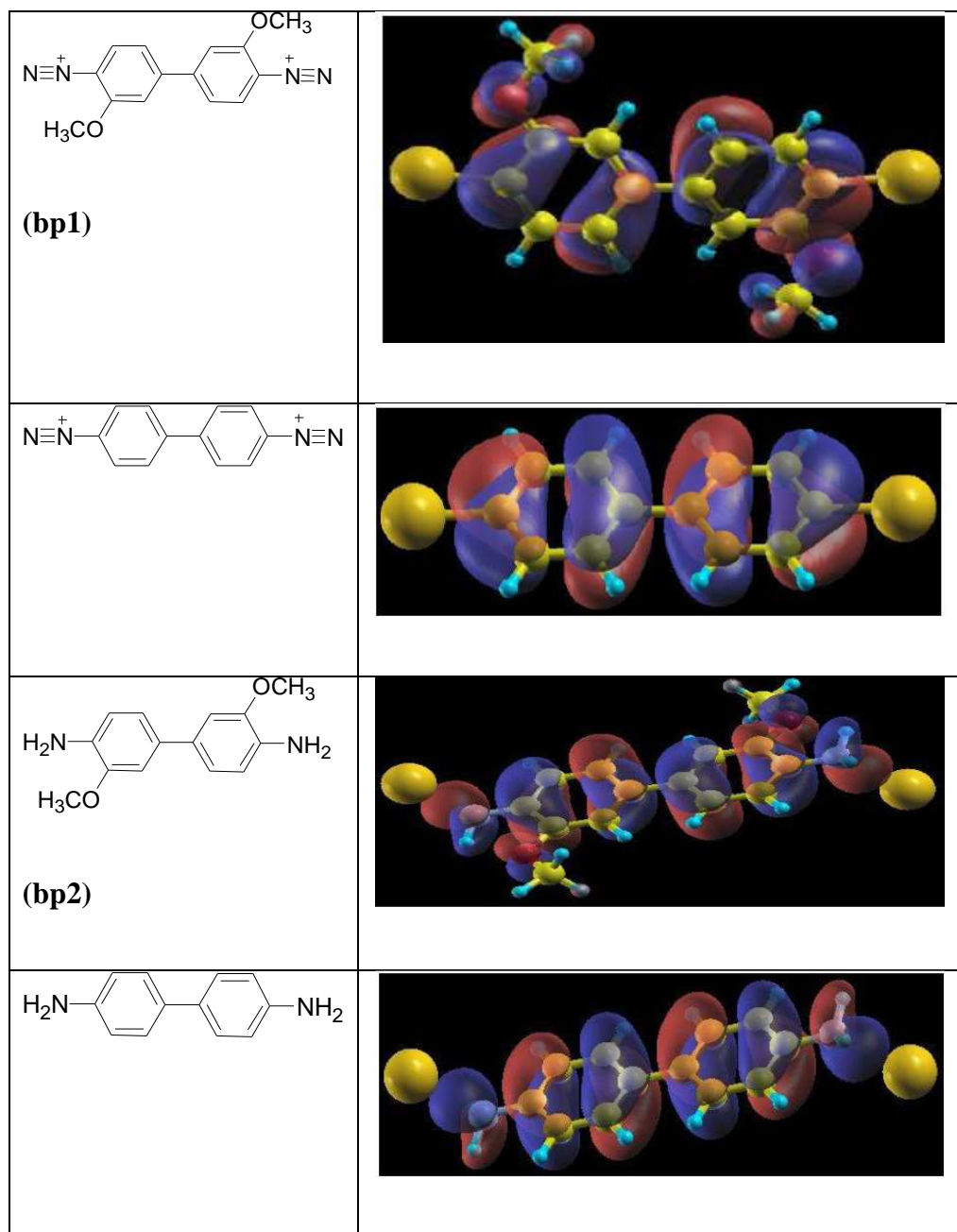


**Table 3.2:** Conducting orbital mappings of **bp1** and **bp2**, and their analogs without methoxy groups. The orbital mappings show greater overlap of the HOMO over the gold

contact for **bp2** compared to **bp1**. This is reflected in the higher orbital-electrode coupling for **bp2** compared to **bp1** given in Table 3.1.

### 3.6 Summary

In summary, we have demonstrated a method of controlling the formation of a single molecule junction by electrochemically reducing diazonium terminal groups to form direct Au-C bonds between the molecule and gold electrodes. The relative yield of junction formation increased as the electrochemical potential was lowered close to the reduction potential of the diazonium groups. Side-by-side comparison of the molecular junction formed by diazonium reduction (**bp1**) with a control junction formed by amine linkers (**bp2**) shows that **bp1** can be stretched significantly farther than **bp2**; but only has marginally higher conductance. This is explained in light of the fact that while **bp1** creates a stronger bond with the electrode, it has relatively weak coupling between the conducting orbital and electrodes compared to that seen in **bp2**.

## 4. THERMALLY INDUCED CONFORMATION CHANGES IN OLIGOTHIOPHENE SINGLE MOLECULE JUNCTIONS

### 4.1 Introduction

A paramount goal in molecular electronics is to understand the mechanism by which charge transport occurs through a single molecule covalently bonded to metal electrodes.<sup>(1, 2)</sup> In small molecules of a few nanometers or less, charge transport occurs via a non-resonant tunneling mechanism, whereby conductance varies exponentially with the length of the junction according to

$$G = G_0 \exp(-\beta L) \quad (4.1)$$

Here the decay constant  $\beta$  scales with the square root of the effective energy barrier created by the lowest lying frontier orbital in the junction. Most reports cite that the tunneling mechanism is temperature independent, because any change in temperature does not have an appreciable effect on the alignment of the frontier orbital relative to the electrodes.

Oligothiophene structures are well known for displaying thermochromic and solvatochromic affects.<sup>(181, 182)</sup> While the specific mechanism behind this property has been widely debated, it is generally claimed that the effect is due to conformational changes in the planar form of the backbone of the molecule.<sup>(183)</sup> A shift towards a more planar conformer increases the conjugation length, which then results in a red shift in the UV-Vis absorption peak, while a shift away from planarity results in a blue shift in the



peak. This mechanism is made possible by the relatively small energy barrier for rotation in oligo and polythiophene systems.(184-187)

Numerous studies on thermochromism in thiophene systems have been reported in the literature. The structures of these systems vary widely and can vary in length from two unit oligomers in solution phase to very long polymers in thin films. Additionally, many reports cite different substituted side groups, which can vary in structure, length and regioregularity. Many reports cite a blue shift with temperature, whereby the backbone shifts away from planarity with increasing temperature.(183, 188-191) However, reports of red shift with increasing temperature have been reported as well. For example, Kurokawa et al. reported a small red shift with increasing temperature in poly(substituted thiophene) nanoparticles.(192) Additionally, Wang et al. reported a small red shift in some polythiophenes at temperatures between about 25 and 90 Celsius,(193) with a blue shift occurring subsequently after the red shift. And finally, Lukes et al. predicted a slight red shift with temperature in unsubstituted bithiophenes.(194) Also noteworthy is that Elmaci et al. report nearly no thermal affect on UV-vis energy gap by performing DFT on various oligothiophene structures.(195)

Here we report modulating the conductance through alkyl substituted oligothiophene single-molecule junctions by thermally shifting the planarity of the molecule. The result is that the energy gap of the junction red shifts with increasing temperature. We support our argument with fixed bias measurements of conductance at temperature intervals of 10° C for oligomers with 1 to 6 thiophene units. We show that the oligomer with a single thiophene unit shows no temperature dependence, whereas

oligomers with between 2 and 6 thiophene units show various degrees of increasing conductance with temperature. We also measure the energy barrier of junctions created with the 1, 3, and 5-mer, and show that for the 3 and 5-mer there is a decrease in energy barrier with temperature which coincides with the conformational shift towards planarity. Finally, we supplement our measurements with density functional theory calculations, which confirm the shift towards planarity at higher temperature.

## **4.2 Methods**

### *4.2.1 Chemicals.*

The oligothiophene molecules used in this study were synthesized at the Laboratory of Advanced Materials at Fudan University.

### *4.2.2 Sample Preparation.*

Gold substrates were prepared in a home-built thermal evaporation chamber. Mica slides were cleaved and placed into the chamber. When the vacuum level reached  $5 \times 10^{-8}$  torr, 130 nm of 99.9995% Alfa Aesar gold was evaporated onto the mica and allowed to anneal at 360 degrees Centigrade for 3 hours. The annealing process ensured that a flat (111) surface was present on the substrates. Before preparing the STM cell, the substrate was flame annealed for approximately 45 seconds using a hydrogen flame to ensure a clean surface. The cell was then assembled and filled with pure mesitylene without any molecules. Mesitylene was chosen as a solvent due to its relatively low vapor pressure which allows it to withstand elevated temperatures without evaporating. STM tips were prepared by cutting 0.25mm 99.998% gold wire from Alfa Aesar. Before

adding molecules to the STM cell, the substrate was imaged to ensure that the gold surface was clean and that there were well defined ledges indicative of a sharp tip. Molecules were added to the STM cell by adding one to two drops of approximately 1  $\mu\text{M}$  solution of the molecules in mesitylene to the STM cell. The iodine terminal groups were immediately cleaved from the backbone of the molecule creating a direct Au-C bond between the molecules and the substrate. This is supported by the fact that steps appeared immediately after commencing the STM break junction cycle.

#### *4.2.3 Electrical Measurements.*

The STM break junction process was used to repeatedly form single molecule junctions between gold electrodes.<sup>(58)</sup> A custom written LabVIEW program modulated the tip into and out of the surface at a speed of 40 nanometers per second using a two setpoint feedback system. In this setup, the two setpoints were separated by four orders of magnitude (the exact setpoints depended on the gain of the current amplifier used for each experiment). To extend the modulation range of the tip, the piezo was instructed to engage an additional 0.3 nm after the high current setpoint had been reached. When molecules bridged the gap between tip and substrate, a molecular bridge would occasionally form manifesting itself as a plateau in the recorded current transient. Under fixed bias measurements, the tip continued to pull until the molecular junction was broken so that the break junction cycle could be repeated. However if current-voltage statistics were being recorded, the LabVIEW program would build a histogram of the current transient in real time in order to detect steps before they broke. If a step was detected, the piezo modulation was paused and the bias was swept over a range of +/- 1.2

Volts. Once the bias sweep was completed, the peizo continued to ramp away from the substrate and the break junction cycle was repeated.

Our STM break junction system consisted of a Molecular Imaging STM head and a Digital Instruments Nanoscope E controller. Homebuilt amplifiers with gains ranging from 1  $\mu\text{A}/\text{V}$  volt to 10 nA/V were used depending on the conductance of the molecule and the bias range used for each particular measurement. The temperature was controlled using a resistive heating stage controlled by a Lakeshore 331 temperature controller. For each temperature measurement, the stage was allowed to stabilize for approximately fifteen minutes before measurements were recorded to reduce thermally induced drift.

#### *4.2.4 Data Processing.*

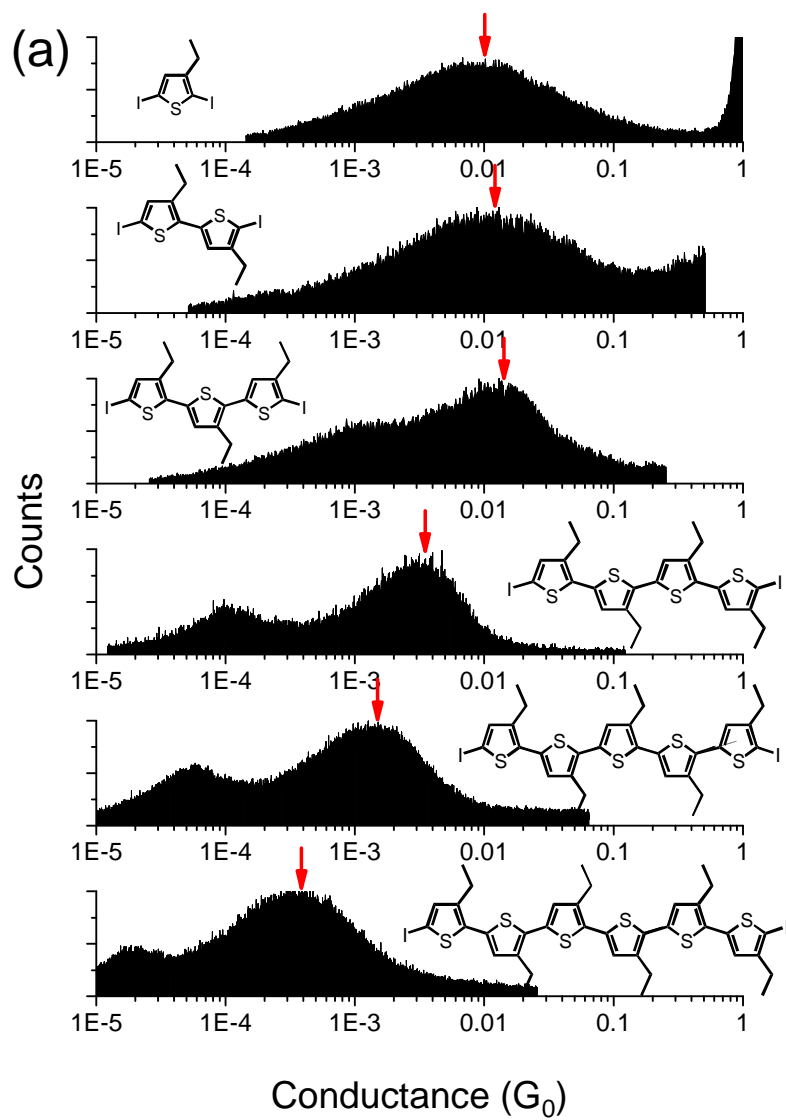
Conductance histograms were constructed by collecting approximately 5000 current traces for each molecule and temperature setting and processing them using a custom written LabVIEW program. The LabVIEW program used an automated process whereby current traces of molecular junctions were identified by looking for a plateau in the trace, and a clean break in the plateau corresponding to rupture of the junction. In this fashion, approximately 10-15% off all current traces recorded showed plateaus corresponding to formation of a molecular junction.

Transition Voltage Spectroscopy statistics were acquired using the same method pioneered by Guo et al. In this method, approximately 2000 current-voltage curves were measured for each molecule and temperature setting. They were then processed using a custom written LabView program that rejected IV curves by comparing the consistency

of the forward and backward sweep, and the antisymmetry of the positive and negative bias sweep. In this manner, approximately two thirds of the recorded current voltage curves were rejected due to drift, or dropped junctions, whereas the remaining one third corresponded to current voltage characteristics through a molecular junction.

### 4.3 Conductance vs. Length.

Figure 4.1a shows the structure of the oligothiophenes measured in this study, along with its accompanying conductance histograms measured at 25° C. The thiophenes range from between 1 and 6 repeat units and length and contain ethyl substituted groups on each thiophene ring arranged in a head to tail manner. Red arrows are included with the conductance histograms to indicate the peak associated with the conductance of the molecule. Each peak was fitted to a Gaussian distribution in order to extract the median conductance and standard deviation of conductance. These values are plotted in Figure 4.1b and Figure 4.1c respectively. The most apparent aspect of figure 1b is that the conductance values for all six oligomers at 25° C do not fit an exponential decay that is expected for a non-resonant tunneling mechanism. Instead, the conductance values increase slightly between oligomers 1 to 3, and subsequently decay exponentially for oligomers 3-6. While unusual, conductance has been reported to increase with length in other thiophene systems.<sup>(196, 197)</sup> This phenomenon will be discussed in greater detail in section 4.6. A least squares fit of the exponential decay in oligomers 3 to 6 shows a beta decay constant of 3.3 nm<sup>-1</sup>, which is slightly higher than other reported values, which typically range between 1 and 2 nm<sup>-1</sup>.<sup>(159, 198)</sup>



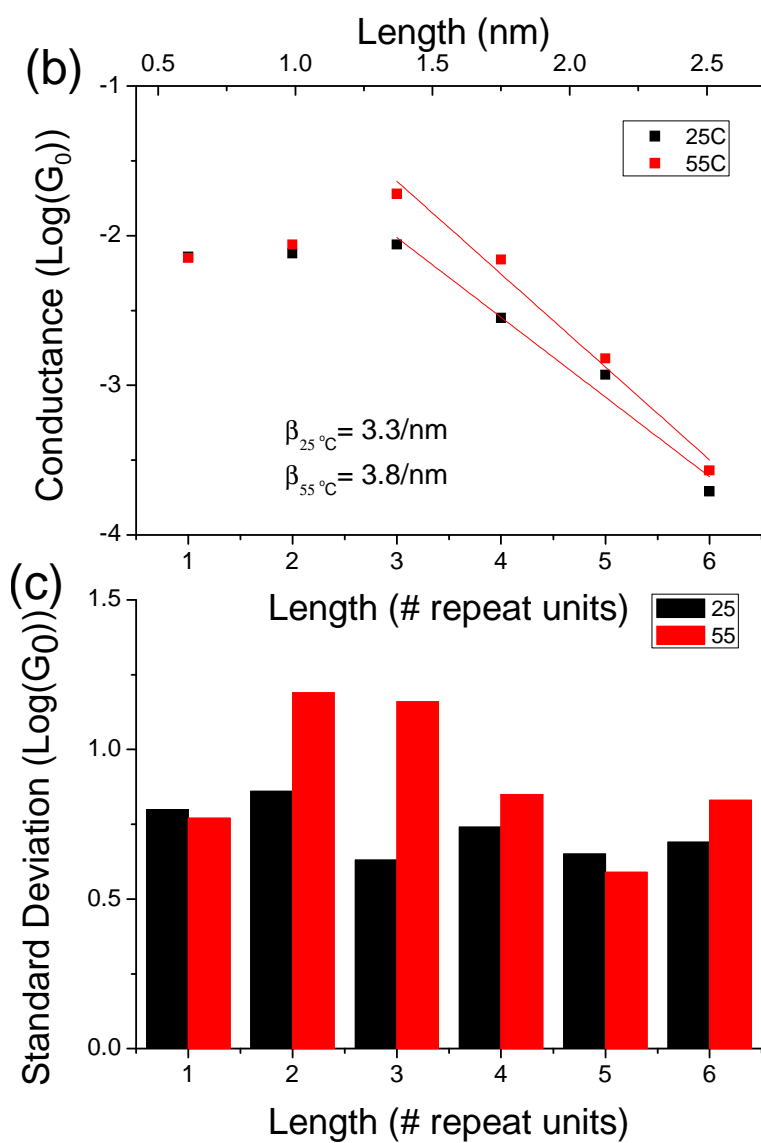


**Figure 4.1:** (a) Conductance histograms for oligomers 1 through 6 at 25° C with accompanying insets of the molecular structures. (b) Median conductance values of each molecule at 25° C and 55° C extracted by Gaussian fitting. (c) Standard deviation of conductance histogram fittings.

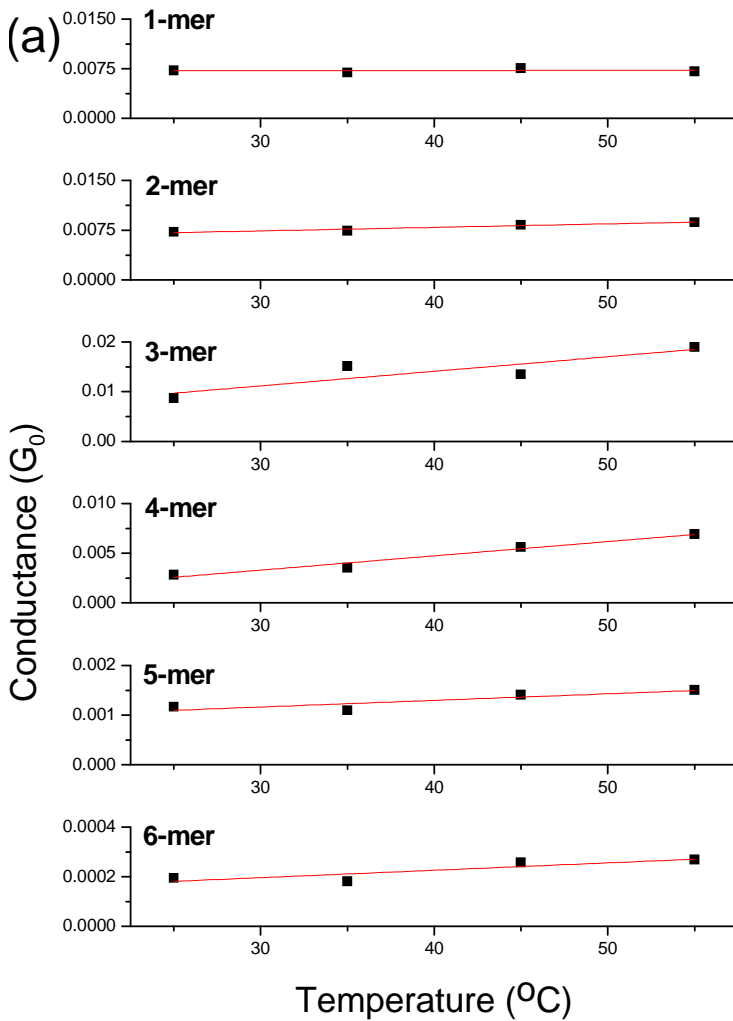
#### 4.4 Conductance vs. Temperature.

In order to gain insight into the peculiar conductance vs. length behavior measured in Figure 1, the conductance of each oligomer was also measured as a function of temperature. Measurements were taken at 25°, 35°, 45° and 55° C. This data is presented in Figure 4.2a. One can see that oligomer 1 shows temperature invariant behavior, whereas oligomers 2 to 6 all show some degree of increase in conductance with temperature. Normally, temperature dependence is associated with a hopping mechanism; however the thiophenes used in this study range between 0.61 and 2.51 nm, which is far shorter than is necessary for hopping to play a significant role in charge transport. For example, Lee et al. measured tunneling in thiophenes up to 14 thiophenes in length at temperatures of 77 C°. (196)

The relative affect of temperature, which is measured as the ratio of conductance at 55° C to conductance at 25° C and plotted in Figure 4.2b, is highest for oligomers 3 and 4. Temperature data measured at 55° C has also been plotted on Figure 4.1b and Figure 4.1c to illustrate the relative increase in temperature as function of length. One aspect that becomes noticeable when the data is plotted in this manner is that a least squares fit of oligomers 3 to 6 produces a different slope at 55° C than the fit at 25° C. Specifically, the extracted beta value at 55 Celsius is 3.8 /nm compared to 3.3 /nm at 25° C. If one were to extrapolate this temperature dependent behavior observed in Figure 1b to lower temperatures, one can see that there may be a temperature in which the



conductance values of all the oligomers align in an exponential decay with a beta value of less than  $3.3 \text{ nm}^{-1}$ . Moreover, the two different beta values measured at  $25^\circ$  and  $55^\circ \text{ C}$  suggests that the energy barrier of the junction is changing with temperature. However, in order to confirm this, transition voltage spectroscopy is needed.



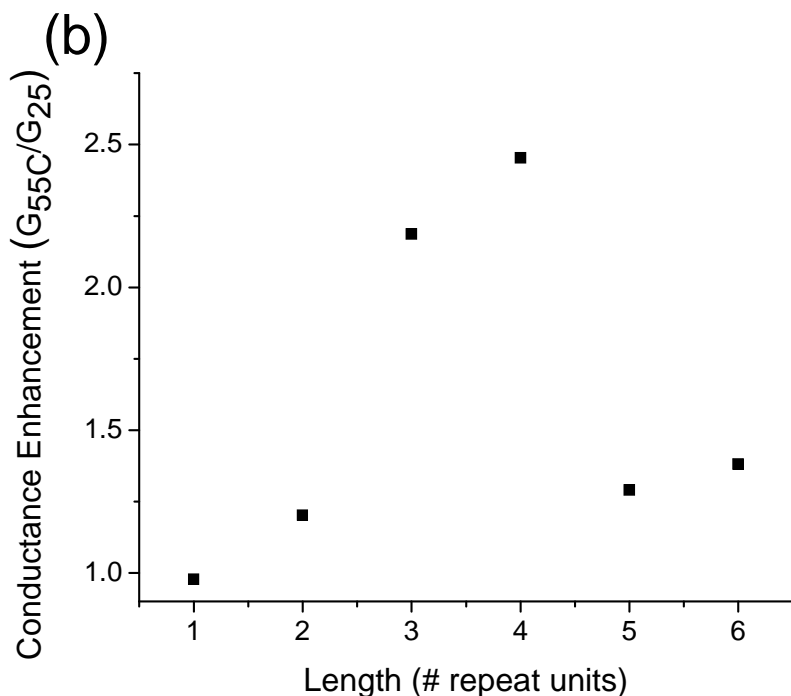
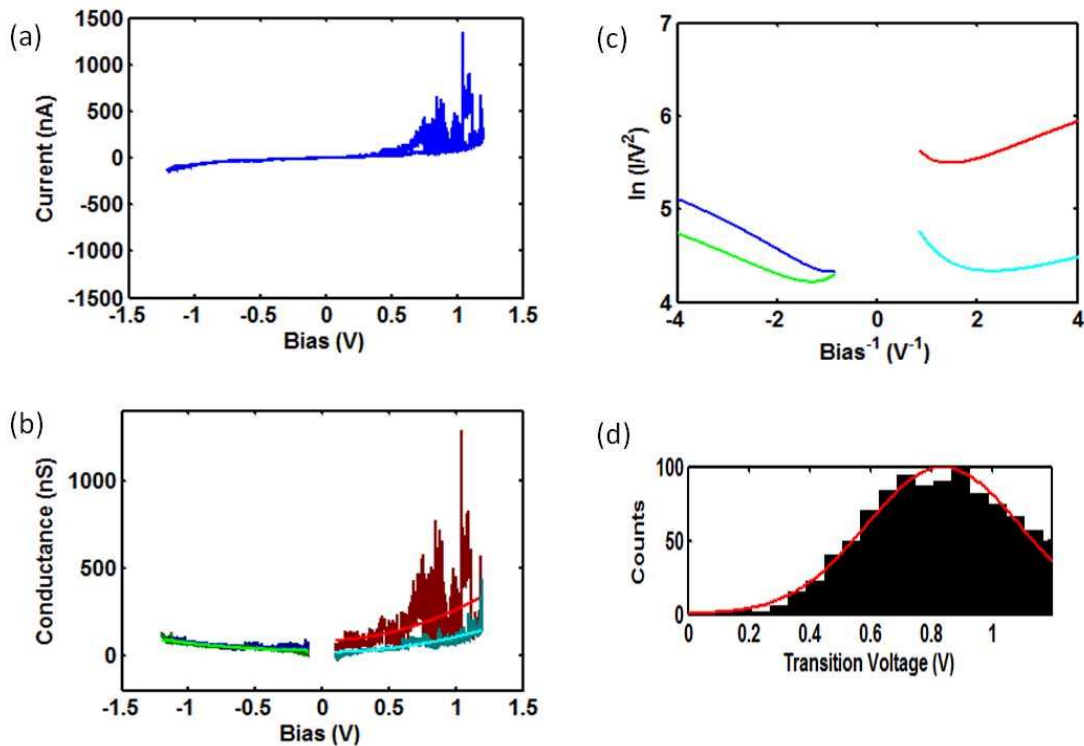


**Figure 4.2:** (a) Conductance vs. temperature for oligomers 1 through 6. (b) Relative increase in conductance as measured by the ratio ( $G_{T=55\text{ C}} / G_{T=25\text{ C}}$ )

#### 4.5 TVS Statistics.

TVS statistics were compiled by rapid measurement of current voltage characteristics using the method first reported by Guo et al. Figure 4.3a shows a representative IV curve collected using this method. Each measured IV curve was subsequently replotted as a GV curve (where G is defined as the total conductance,  $I/V$ ), broken into four regions (corresponding to forward/backward sweep and positive/negative bias) and each region was fitted to a second order polynomial. This is shown in figure 4.3b. The fitted polynomials of each GV curve were then mapped onto a

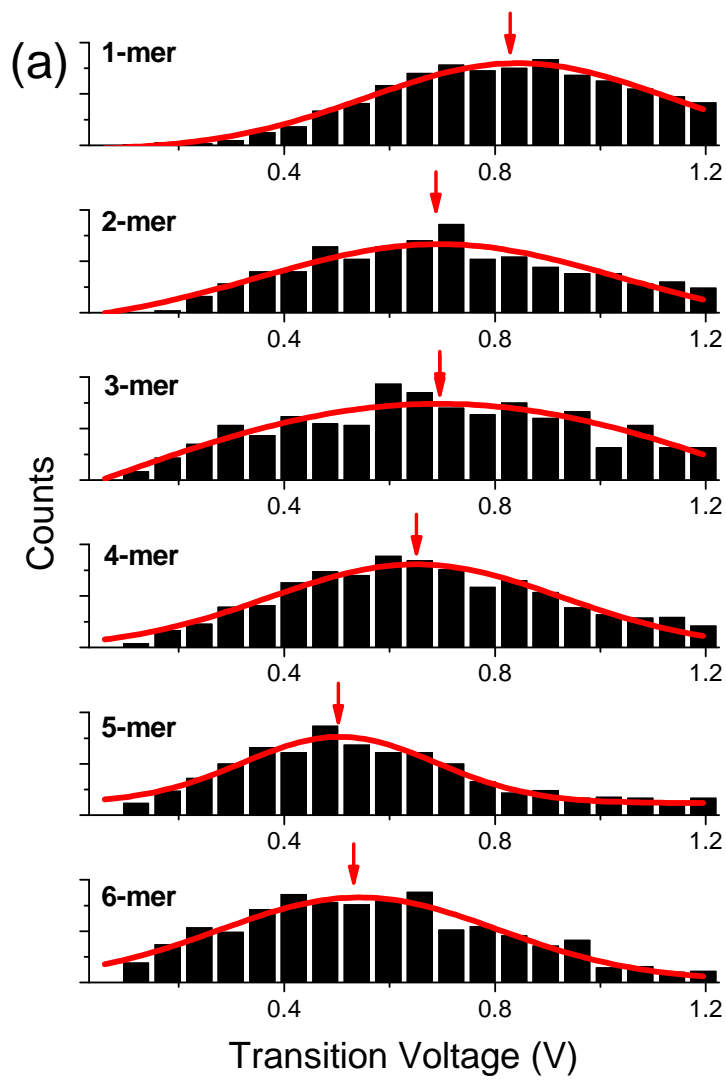
Fowler-Nordheim plot ( $\ln(G/V)$  vs.  $1/V$ ) where the minima represent the transition voltages of the junction, which is a relative measure of the energy barrier of the molecular junction. This is shown in Figure 4.3c. The GV fitting process was used because it provided an effective means of removing fluctuations from recorded measurements and therefore provided a better estimate of the transition voltage. The transition voltages for each junction were then compiled into a histogram shown in figure 4.3d. The analysis presented in Figure 4.3 represents data for only the 1-mer at 25C.

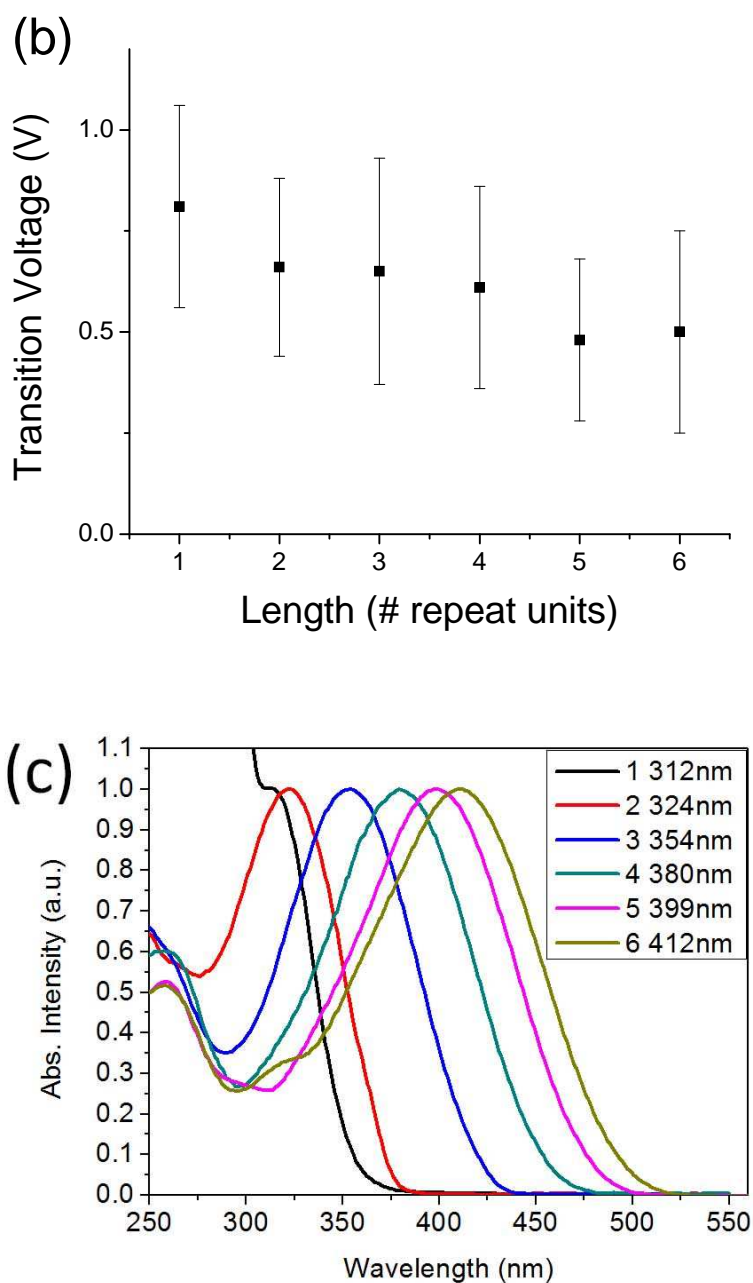


**Figure 4.3:** Illustration of how transition voltage statistics are compiled. A current-voltage trace is recorded when a step is detected in real time (a). The IV sweep is then replotted as a GV sweep ( $G=I/V$ ) and fitted to a second order polynomial (b). The

polynomial fit is then plotted in a Fowler Nordheim plot ( $\ln(G/V)$  vs.  $1/V$ ) (c). Finally, a histogram of transition voltages from all IV sweeps is compiled (d).

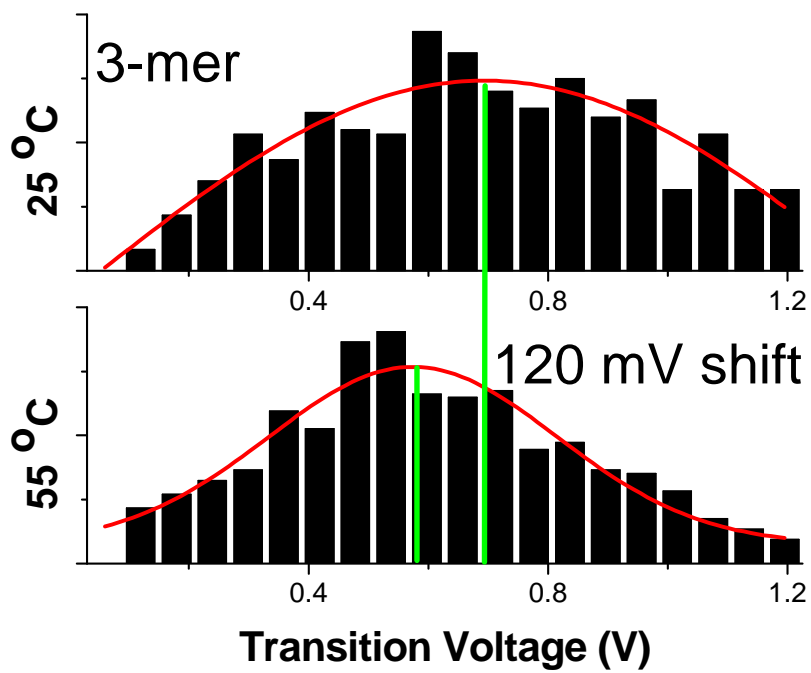
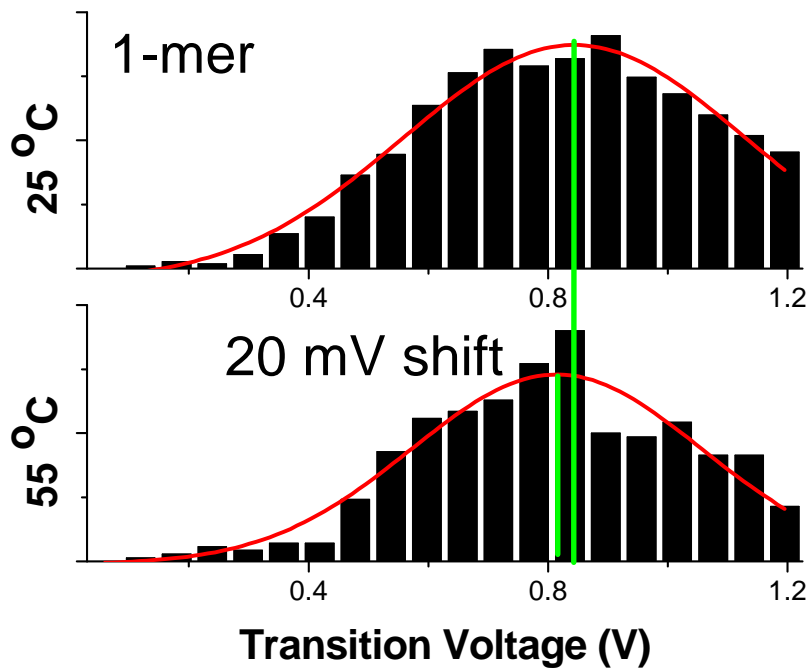
Figure 4.4a shows TVS histograms for oligomers 1 through 6 at 25° C. Each of the histograms shown in Figure 4.4a was fitted to a Gaussian distribution in order to extract the median and standard deviation of the transition voltage. These values are plotted in Figure 4.4b. One can see that the transition voltage decreases from 0.81 V for oligomer 1 to 0.50 V for oligomer 6 in a roughly steady manner. This is expected due to the increasing degree of  $\pi$ -conjugation along the backbone of the molecule, which effectively lowers the energy gap of the molecule (Figure 4.4c) and in turn the energy barrier of the molecular junction.





**Figure 4.4:** (a) Transition voltage histograms for oligomers 1 through 6 at 25° C. (b) Median transition voltage values and standard deviations for oligomers 1 through 6 at 25° C. (c) UV-Vis absorption spectra measured at approximately 25° C for oligomers 1 through 6.

Recall however that the conductance data presented in Figure 4.1b showed temperature dependences for oligomers 2 through 6, suggesting that the energy barrier may be changing with temperature. In order to test this hypothesis, we performed TVS measurements for oligomers 1, 3 and 5 at 55° C. We chose to perform measurements on only three molecules due to the difficult nature of acquiring current-voltage statistics at higher temperatures where drift and telegraphic switching play a more prominent role in the junction. A side-by-side comparison of TVS histograms for oligomers 1, 3 and 5 at both 25° C and 55° C is presented in Figure 4.5. It should be noted that the histograms in Figure 4.5 at 25° C are the same histograms also presented in Figure 4.4a. The TVS histograms in Figure 4.5 show that the transition voltage shifts by 20mV, 120 mV and 40 mV for the 1, 3 and 5-mer respectively when raising the temperature from 25° C to 55° C. The 120 mV in the 3-mer and the 40 mV shift in the 5-mer confirm that the energy barrier decreases with increasing temperature. While there is a small 20 mV shift in transition voltage for the 1-mer, we believe that this is due to statistical variance in the measurement.





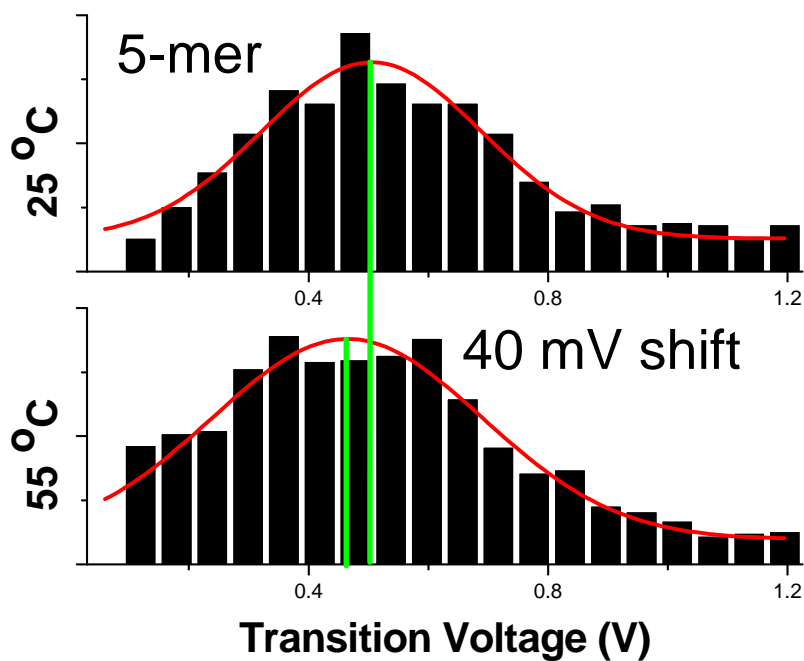


**Figure 4.5:** Comparison of transition voltage histograms for the 1, 3 and 5-mer at 25° and 55° C (top and bottom). The shift in transition voltage is 20 mV, 120 mV, and 40 mV for the 1, 3, and 5-mer respectively. The 20 mV shift for the 1-mer is due to statistical variance.

#### 4.6 Discussion of Experimental Results

Thus far we have shown that conductance increases and transition voltage decreases at elevated temperatures for our oligothiophenes. These two observations suggest that the energy barrier of the junction decreases at higher temperatures. We explain this effect by a temperature induced conformation shift in the molecular junction towards planarity. As the molecule becomes more planar, the degree of  $\pi$ -conjugation

throughout the molecule increases, and the energy gap subsequently decreases. This so called red shift in energy gap has been reported in other oligo and polythiophene systems as well.(192-194) We believe that the approximately 2X to 2.5X increase in conductance found for oligomers 3 and 4 is reasonable under this model, given that the conductance through biphenyl metal-molecule-metal junctions can vary by over one order of magnitude depending on the conformational planarity of the phenyl rings.(199, 200)

It now becomes relevant to consider why the temperature dependence of both change in conductance and change in transition voltage increases and subsequently decreases across the set of oligomers measured. First, we consider that the 1-mer has a fixed energy barrier due to its fixed planarity, and thus shows no significant change in conductance or transition voltage. Next, consider that for molecules such as the 2-mer and 3-mer, there are a limited number of rotational angles between thiophene rings which can affect the degree of  $\pi$ -conjugation throughout the molecule. As a result, by increasing temperature it is fairly likely that the rings will align in a planar conformation, thereby reducing the tunneling barrier and affecting the measured conductance and transition voltage. However when we consider molecules such as the 4, 5, and 6-mer, there are an increasing number of rotational angles that must be properly aligned in order to achieve a planar conformation throughout the molecule. Stochastic processes are therefore more likely to break the conjugation, and as a result there is diminishing temperature dependence for measured conductance and transition voltage as the length of the molecule increases. As a result, we see a trend whereby the change in conductance and change in transition voltage is highest for oligomers with 3 and 4 units. This effect

explains the length dependence in Figure 1b, whereby conductance initially increases, and subsequently decreases with length.

#### 4.7 Comparing Change in Conductance with Change in Transition Voltage

At this point, it is useful to consider whether the amount of shift in transition voltage as measured in Figure 5 is what one would expect based on the amount of change in conductance measured in Figure 2. For this analysis, we consider two simple models. First is the non-resonant tunneling model which describes conductance as an exponential function of length.

$$G = G_0 \exp(-\beta L) \quad (4.1)$$

Second, we consider that beta scales as the square root of the transition voltage, which is an outcome of the Simmons Model. In principle,  $\beta$  and the transition voltage can be related using the constant  $4\pi\sqrt{2m_e}/h$ ; however this relation becomes invalid when we consider that the voltage does not drop evenly across the junction, and as a result we relate  $\beta$  and transition voltage by a constant  $C$ .

$$\beta = C\sqrt{V_t} \quad (4.2)$$

By simple substitution we can say that

$$G = G_0 \exp(-C\sqrt{V_t}L) \quad (4.3)$$

Consider that we have an estimate of the beta decay constant at 25° C based on the results presented in Figure 1b. Using simple arithmetic, we can solve for  $C$  in equation 4.2 for each oligomer. Using this constant, and assuming the contact resistance  $G_0$  does not change with temperature, we can then solve for the expected transition voltage at 55° C according to the following.

$$\frac{G_{T=25}}{G_{T=55}} = \frac{G_0 \exp(-C\sqrt{V_{t(T=25)}}L)}{G_0 \exp(-C\sqrt{V_{t(T=55)}}L)} \quad (4.4)$$

Values used in this calculation are summarized in Table 4.1 below.

	<b>3-mer</b>	<b>5-mer</b>
$G_{T=25}^{\circ C}$	$8.71 \times 10^{-3} G_0$	$1.17 \times 10^{-3} G_0$
$G_{T=25}^{\circ C}$	$1.91 \times 10^{-2} G_0$	$1.51 \times 10^{-3} G_0$
$\beta$	$3.3 \text{ nm}^{-1}$	$3.3 \text{ nm}^{-1}$
$C$	$3.97 \text{ nm}^{-1} \text{V}^{-0.5}$	$4.62 \text{ nm}^{-1} \text{V}^{-0.5}$
$L$	$1.37 \text{ nm}$	$2.13 \text{ nm}$
$V_{t(T=25}^{\circ C)}$	$0.65 \text{ V}$	$0.48 \text{ V}$

**Table 4.1:** Values used in Equation 4.4

And the calculated transition voltages are given in Table 4.2

	<b>3-mer</b>	<b>5-mer</b>
$V_{t(T=55}^{\circ C})$ <b>calculated</b>	$0.45 \text{ V}$	$0.44 \text{ V}$
$V_{t(T=55}^{\circ C})$ <b>measured</b>	$0.53 \text{ V}$	$0.44 \text{ V}$

**Table 4.2:** Comparison of calculated transition voltages using Eq 4.4, and measured transition voltages.

Carrying out this analysis results in expected transition voltages of 0.45 V and 0.44 V for the 3-mer and 5-mer respectively at 55° C. Comparing these values to the measured values, we see that the measured shift in transition voltage is less than expected for the 3-mer and exactly what is expected for the 5-mer. Overall, we believe these results are quite reasonable. Some discrepancy between predicted and measured values is expected, given the spread in transition voltages measured at both temperatures; however the results of this simple model show that the temperature dependence of conductance and transition voltage can be explained by a temperature dependent modulation in the energy barrier of the molecular junction.

#### **4.8 Density Functional Theory and Statistical Mechanics Calculations**

To further support our argument that increasing temperature induces a red shift in our thiophene oligomers, we performed density functional theory (DFT) and molecular dynamics (MD) calculations for the 3-mer. We chose this molecule because it shows one of the highest degrees of temperature dependence. Figure 6 shows the energy barrier for rotation of a single thiophene ring in this molecule. In the figure, zero degrees corresponds to cis-rotamer in which the thiophene rings lie in a planar orientation with adjacent ethyl chains side by side. Steric hindrance caused by neighboring ethyl chains and conjugated  $\pi$ -orbitals causes local and absolute maxima that lie at orientations of approximately -90, 0, 90, and 180 degrees. Likewise, local and absolute minima lie at orientations approximately halfway between the maxima. The absolute minimum in the energy diagram, corresponding to the optimized dihedral angle between thiophene rings is calculated to be -135°. One can see that each of the four minima lie below  $kT$  (26

meV), which is illustrated by the horizontal red line in the figure. Additionally, conformations close to  $\pm 135$  degrees contain a significant range of angles below  $kT$ , spanning from approximately  $\pm 100$  to  $\pm 160$  degrees. Thus we see that the energy barrier for rotation is sufficiently low for an individual thiophene ring to have a considerable range of motion about its dihedral axis at room temperature.

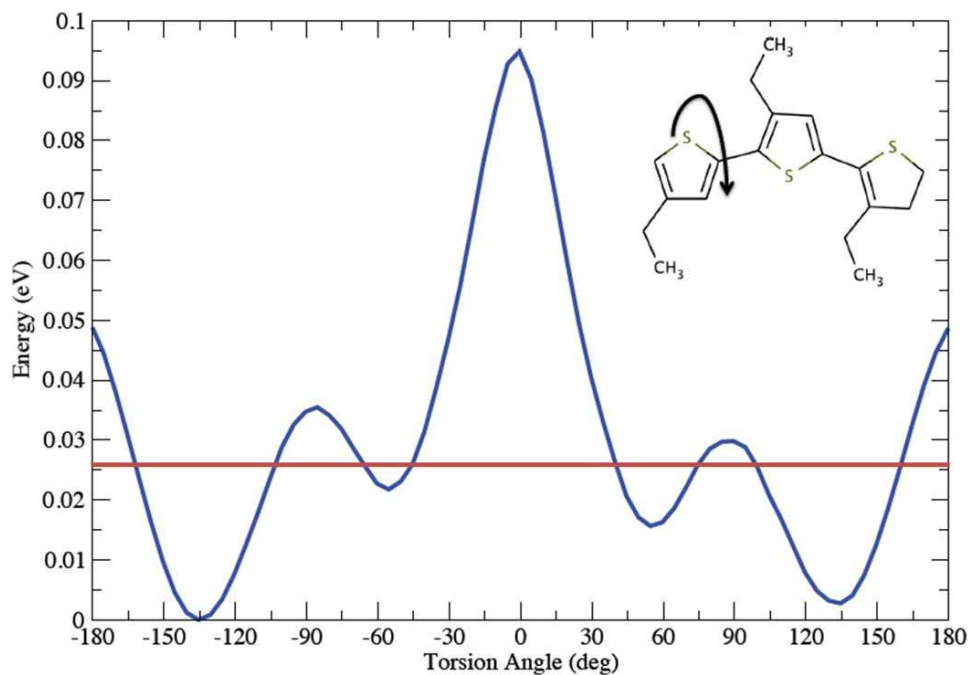


**Figure 4.6:** Torsion angle energy profile for the 3-mer thiophene. Zero degrees is defined as the planar cis formation. The optimized angle between thiophene rings is  $-135^\circ$ . The red horizontal line represents  $k_B T$  at  $25^\circ \text{C}$ .

The energy diagram presented in Figure 4.6 is useful in illustrating the conformations of the 3-mer available at room temperature; however in order to obtain a quantitative description of population densities, the partition function was calculated. For our analysis, we considered three conformers of the 3-mer and calculated the relative population densities of each with respect to temperature. First, the optimized geometric structure with rotational angles of  $-135^\circ$  between thiophenes was considered. Second, the optimized geometry was modified so that one thiophene ring was completely planar in a trans formation with the middle thiophene unit, while the remaining thiophene ring retained the optimized angle of  $-135^\circ$  with the middle thiophene unit. Finally, we considered a conformer in which all thiophene rings lie in a completely planar trans formation. These structures are illustrated in Figure 4.7, and will be referred to as the optimized structure, conformer 1, and conformer 2 from this point forward. As one would expect, the increasing degree of conjugation results in a decreasing energy gap, which falls from 4.36 eV for the optimized structure, to 3.85 eV for conformer 1, and finally to 3.42 eV for conformer 2. Relative population densities of the three conformers at  $25^\circ\text{C}$  and  $55^\circ\text{C}$  were also calculated and are provided in Table 4.3. The population densities at both temperatures were normalized relative to the population density of the optimized structure. The results show that at both  $25^\circ\text{C}$  and  $55^\circ\text{C}$  the optimized structure is the most common conformer of the three. However, when the temperature is increased from  $25^\circ\text{C}$  to  $55^\circ\text{C}$  the relative population densities of both conformer 1 and conformer 2 increase, meaning that conformers 1 and 2 are statistically more likely to occur at higher temperatures. We believe that the higher relative population densities

of conformers 1 and 2 explains the resulting temperature dependence of both conductance and transition voltage of the thiophene oligomers that we measured.

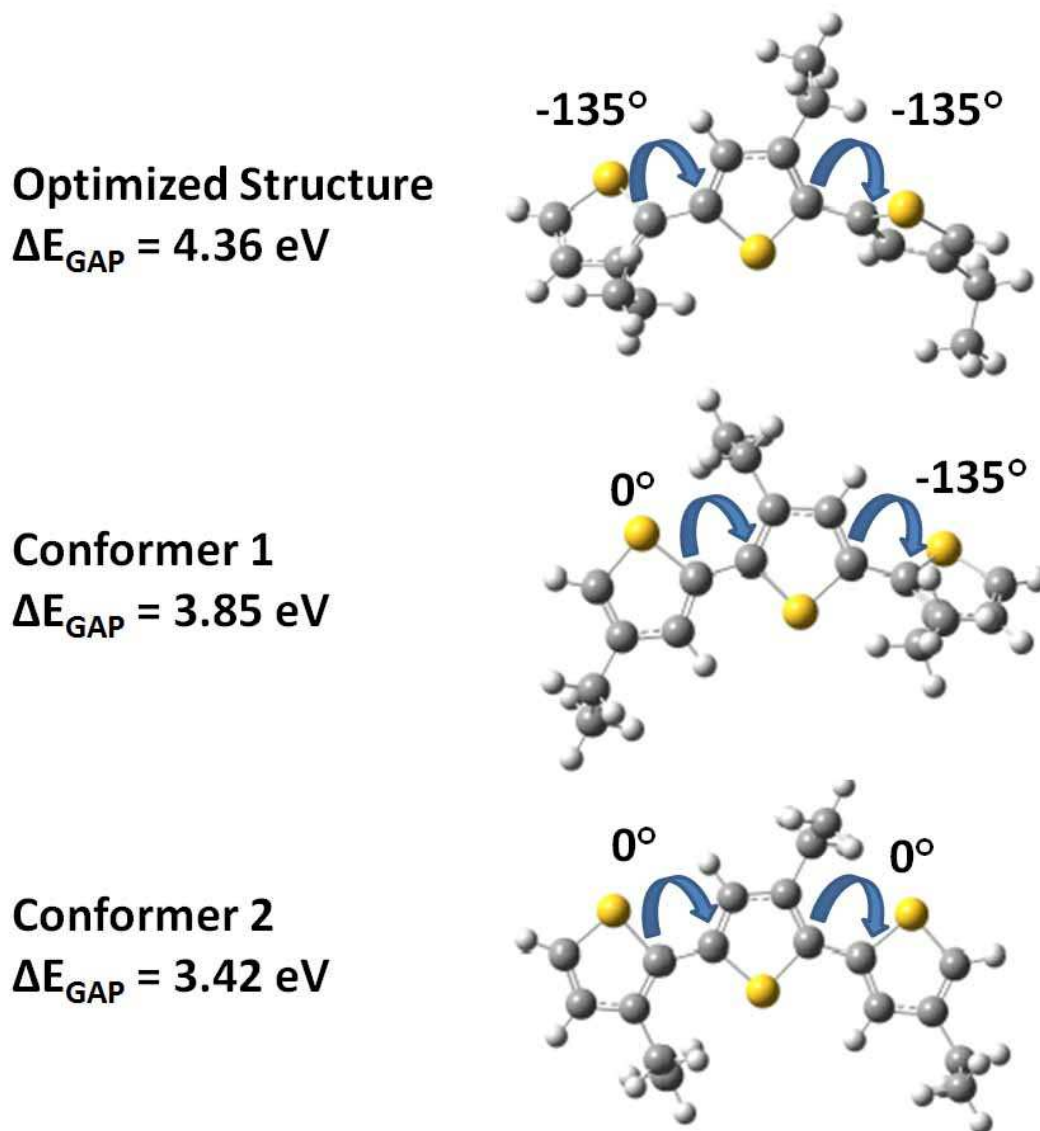


**Figure 4.7:** Illustration of 3 different conformations of the 3-mer analyzed with DFT: the optimized structure (top), conformer 1 with left angle fixed at 0 degrees and the other optimized (middle), and conformer 2 with both angles fixed at 0 degrees (bottom).



	<b>Optimized</b>	<b>Conformer 1</b>	<b>Conformer 2</b>
<b>Relative Population (T = 25° C)</b>	1 P <sub>opt</sub>	0.27 P <sub>opt</sub>	0.17 P <sub>opt</sub>
<b>Relative Population (T = 55° C)</b>	1 P <sub>opt</sub>	0.33 P <sub>opt</sub>	0.19 P <sub>opt</sub>

**Table 4.3:** Relative population of each conformer compared to the population of the optimized structure at 25° and 55° C. One can see that the relative populations of both conformers increase with temperature.

#### 4.9 Summary

Here we have demonstrated a unique temperature dependent tunneling mechanism in a set of oligothiophenes whereby increasing temperature induces a conformational shift towards planarity which increases the conjugation length and decreases the energy barrier of the junction. This effect is measured for oligomers with 2 to 6 thiophene units and is supported by temperature dependent fixed bias measurements of conductance, and temperature dependent current-voltage measurements to extract the transition voltage of the junction. Temperature dependence is seen to increase from oligomers 1 through 3, and decrease for oligomers 4 through 6. We attribute this phenomenon to the increasing difficulty of aligning all thiophene rings in the molecule as the number of thiophene rings increases.

## 5. CONCLUSION AND OUTLOOK

The field of molecular electronics still needs to make considerable advances before single molecules can be used as functional components in electronic devices. However the steady advancement of knowledge and insight gained by performing measurements on the single-molecule level is key to achieving that end. Measurements taken can provide a framework for advancing the theoretical understanding of charge transport phenomena from a first principles perspective. In that spirit, three research projects exploring interesting contact and length dependent effects in single molecule electronics have been the subject of this thesis.

In the first, the transition between charge tunneling and charge hopping is documented in a set of long conjugated molecular wires. This transition process is in general poorly understood from a first principles perspective, and thus experimental measurements provide valuable insight. Measurements show that the transition occurs between 5.2 and 7.3 nm and thus the charge carrier is able to maintain coherency over a considerable length in the junction. Furthermore, measurements show that at elevated temperatures the longer molecules that conduct by hopping can be more conductive than shorter molecules that conduct by tunneling. This effect provides valuable insight into the nature of the hopping mechanism.

In the second project, the formation of a single-molecule junction by electrochemical reduction of diazonium terminal groups is reported. This is interesting in that it not only allows one to control the energetics of formation by an applied

electrochemical potential, but it also creates a junction in which the carbon backbone is covalently bonded to the electrodes without any intermediate linker group. In this case, there is weak coupling between the electrodes and  $\pi$ -orbital system of the junction, and the conductance is not significantly increased compared to the same junction created by amine-gold bonds. This effect has also been reported for benzene junctions created with gold-carbon bonds;<sup>(133)</sup> however many other publications in the literature report that gold carbon bonds produce higher conductance values resulting from stronger coupling. Gold-carbon bonds are thus a hot topic for debate in the field of molecular electronics and future work should explore other systems until a greater consensus is reached.

Finally, in the third project modulation of the energy barrier in molecular junctions is reported by thermally changing the planar form of oligothiophenes. Upon increasing temperature, oligomers with multiple thiophene rings assume a more planar form, which induces a red shift in the energy gap, and makes the molecular junction more conductive and have a lower transition voltage. This shift is not observed for the molecule with a single thiophene ring, due to the fixed planar form of the molecule. The measured shift in conductance values are in good agreement with the measured shifts in transition voltage. It would be interesting to explore the electron-vibronic coupling between charge carriers and the rotational mode of the thiophene ring by inelastic electron tunneling spectroscopy. However certain practical considerations such as the low energy of the mode, and the fact that it would not be activated at low temperatures where IETS measurements are traditionally performed would make this measurement difficult.

## REFERENCES

1. A. Nitzan, M. A. Ratner, Electron transport in molecular wire junctions. *Science* **300**, 1384-1389 (2003); published online EpubMay (
2. N. J. Tao, Electron transport in molecular junctions. *Nature Nanotechnology* **1**, 173-181 (2006); published online EpubDec (10.1038/nnano.2006.130).
3. D. Goldhaber-Gordon, M. S. Montemerlo, J. C. Love, G. J. Opiteck, J. C. Ellenbogen, Overview of nanoelectronic devices. *Proceedings of the Ieee* **85**, 521-540 (1997); published online EpubApr (10.1109/5.573739).
4. N. S. Hush, An overview of the first half-century of molecular electronics. *Molecular Electronics Iii* **1006**, 1-20 (2003)10.1196/annals.1292.016).
5. S. Lindsay, J. He, O. Sankey, P. Hapala, P. Jelinek, P. M. Zhang, S. A. Chang, S. O. Huang, Recognition tunneling. *Nanotechnology* **21**, (2010); published online EpubJul (10.1088/0957-4484/21/26/262001).
6. J. Hihath, B. Q. Xu, P. M. Zhang, N. J. Tao, Study of single-nucleotide polymorphisms by means of electrical conductance measurements. *Proceedings of the National Academy of Sciences of the United States of America* **102**, 16979-16983 (2005); published online EpubNov (10.1073/pnas.0505175102).
7. X. Y. Xiao, B. Q. Xu, N. J. Tao, Changes in the conductance of single peptide molecules upon metal-ion binding. *Angewandte Chemie-International Edition* **43**, 6148-6152 (2004)10.1002/anie.200460886).
8. J. Hihath, C. R. Arroyo, G. Rubio-Bollinger, N. J. Tao, N. Agrait, Study of electron-phonon interactions in a single molecule covalently connected to two electrodes. *Nano Letters* **8**, 1673-1678 (2008); published online EpubJun (10.1021/nl080580e).
9. M. Bixon, B. Giese, S. Wessely, T. Langenbacher, M. E. Michel-Beyerle, J. Jortner, Long-range charge hopping in DNA. *Proceedings of the National Academy of Sciences of the United States of America* **96**, 11713-11716 (1999); published online EpubOct (
10. A. Aviram, M. A. Ratner, MOLECULAR RECTIFIERS. *Chemical Physics Letters* **29**, 277-283 (1974)10.1016/0009-2614(74)85031-1).

11. K. Moth-Poulsen, T. Bjornholm, Molecular electronics with single molecules in solid-state devices. *Nature Nanotechnology* **4**, 551-556 (2009); published online EpubSep (10.1038/nnano.2009.176).
12. C. Joachim, M. A. Ratner, Molecular electronics: Some views on transport junctions and beyond. *Proceedings of the National Academy of Sciences of the United States of America* **102**, 8801-8808 (2005); published online EpubJun (10.1073/pnas.0500075102).
13. Y. Selzer, D. L. Allara, Single-molecule electrical junctions. *Annual Review of Physical Chemistry* **57**, 593-623 (2006)10.1146/annurev.physchem.57.032905.104709).
14. F. Chen, J. Hihath, Z. F. Huang, X. L. Li, N. J. Tao, Measurement of single-molecule conductance. *Annual Review of Physical Chemistry* **58**, 535-564 (2007)10.1146/annurev.physchem.58.032806.104523).
15. M. Buttiker, Y. Imry, R. Landauer, S. Pinhas, GENERALIZED MANY-CHANNEL CONDUCTANCE FORMULA WITH APPLICATION TO SMALL RINGS. *Physical Review B* **31**, 6207-6215 (1985)10.1103/PhysRevB.31.6207).
16. V. Mujica, M. Kemp, M. A. Ratner, ELECTRON CONDUCTION IN MOLECULAR WIRES .1. A SCATTERING FORMALISM. *Journal of Chemical Physics* **101**, 6849-6855 (1994); published online EpubOct (10.1063/1.468314).
17. A. Vilan, D. Cahen, E. Kraissler, Rethinking Transition Voltage Spectroscopy within a Generic Taylor Expansion View. *Acs Nano* **7**, 695-706 (2013); published online EpubJan (10.1021/nn3049686).
18. V. Mujica, M. Kemp, M. A. Ratner, ELECTRON CONDUCTION IN MOLECULAR WIRES .2. APPLICATION TO SCANNING-TUNNELING-MICROSCOPY. *Journal of Chemical Physics* **101**, 6856-6864 (1994); published online EpubOct (10.1063/1.468315).
19. R. Landauer, CONDUCTANCE DETERMINED BY TRANSMISSION - PROBES AND QUANTIZED CONSTRICTION RESISTANCE. *Journal of Physics-Condensed Matter* **1**, 8099-8110 (1989); published online EpubOct (10.1088/0953-8984/1/43/011).

20. D. Segal, A. Nitzan, M. Ratner, W. B. Davis, Activated conduction in microscopic molecular junctions. *Journal of Physical Chemistry B* **104**, 2790-2793 (2000); published online EpubApr (
21. D. Segal, A. Nitzan, W. B. Davis, M. R. Wasielewski, M. A. Ratner, Electron transfer rates in bridged molecular systems 2. A steady-state analysis of coherent tunneling and thermal transitions. *Journal of Physical Chemistry B* **104**, 3817-3829 (2000); published online EpubApr (10.1021/jp993260f).
22. A. Nitzan, A relationship between electron-transfer rates and molecular conduction. *Journal of Physical Chemistry A* **105**, 2677-2679 (2001); published online EpubMar (10.1021/jp003884h).
23. W. B. Davis, M. R. Wasielewski, M. A. Ratner, V. Mujica, A. Nitzan, Electron transfer rates in bridged molecular systems: A phenomenological approach to relaxation. *Journal of Physical Chemistry A* **101**, 6158-6164 (1997); published online EpubAug (
24. A. Nitzan, The relationship between electron transfer rate and molecular conduction. 2. The sequential hopping case. *Israel Journal of Chemistry* **42**, 163-166 (2002)10.1560/yibd-yf7y-4j4e-epqe).
25. S. H. Ke, H. U. Baranger, W. T. Yang, Electron transport through molecules: Self-consistent and non-self-consistent approaches. *Physical Review B* **70**, (2004); published online EpubAug (10.1103/PhysRevB.70.085410).
26. T. N. Todorov, Spatial distribution of the electric current and field in atomic-scale conductors. *Philosophical Magazine B-Physics of Condensed Matter Statistical Mechanics Electronic Optical and Magnetic Properties* **79**, 1577-1590 (1999); published online EpubOct (10.1080/014186399256411).
27. P. L. Pernas, A. Martinrodero, F. Flores, ELECTROCHEMICAL-POTENTIAL VARIATIONS ACROSS A CONSTRICTION. *Physical Review B* **41**, 8553-8556 (1990); published online EpubApr (10.1103/PhysRevB.41.8553).
28. M. Brandbyge, J. L. Mozos, P. Ordejon, J. Taylor, K. Stokbro, Density-functional method for nonequilibrium electron transport. *Physical Review B* **65**, (2002); published online EpubApr (10.1103/PhysRevB.65.165401).
29. Y. A. Berlin, M. A. Ratner, Intra-molecular electron transfer and electric conductance via sequential hopping: Unified theoretical description. *Radiation*

- Physics and Chemistry* **74**, 124-131 (2005); published online EpubOct-Nov (10.1016/j.radphyschem.2005.04.004).
30. D. R. Strachan, D. E. Smith, D. E. Johnston, T. H. Park, M. J. Therien, D. A. Bonnell, A. T. Johnson, Controlled fabrication of nanogaps in ambient environment for molecular electronics. *Applied Physics Letters* **86**, (2005); published online EpubJan (10.1063/1.1857095).
  31. T. Taychatanapat, K. I. Bolotin, F. Kuemmeth, D. C. Ralph, Imaging electromigration during the formation of break junctions. *Nano Letters* **7**, 652-656 (2007); published online EpubMar (10.1021/nl062631i).
  32. A. K. Mahapatro, S. Ghosh, D. B. Janes, Nanometer scale electrode separation (nanogap) using electromigration at room temperature. *Ieee Transactions on Nanotechnology* **5**, 232-236 (2006); published online EpubMay (10.1109/tnano.2006.874053).
  33. M. L. Chabinyc, X. X. Chen, R. E. Holmlin, H. Jacobs, H. Skulason, C. D. Frisbie, V. Mujica, M. A. Ratner, M. A. Rampi, G. M. Whitesides, Molecular rectification in a metal-insulator-metal junction based on self-assembled monolayers. *Journal of the American Chemical Society* **124**, 11730-11736 (2002); published online EpubOct (10.1021/ja020506c).
  34. R. E. Holmlin, R. Haag, M. L. Chabinyc, R. F. Ismagilov, A. E. Cohen, A. Terfort, M. A. Rampi, G. M. Whitesides, Electron transport through thin organic films in metal-insulator-metal junctions based on self-assembled monolayers. *Journal of the American Chemical Society* **123**, 5075-5085 (2001); published online EpubMay (10.1021/ja004055c).
  35. K. Slowinski, H. K. Y. Fong, M. Majda, Mercury-mercury tunneling junctions. 1. Electron tunneling across symmetric and asymmetric alkanethiolate bilayers. *Journal of the American Chemical Society* **121**, 7257-7261 (1999); published online EpubAug (10.1021/ja991613i).
  36. K. Slowinski, M. Majda, Mercury-mercury tunneling junctions - Part II. Structure and stability of symmetric alkanethiolate bilayers and their effect on the rate of electron tunneling. *Journal of Electroanalytical Chemistry* **491**, 139-147 (2000); published online EpubSep (10.1016/s0022-0728(00)00305-3).
  37. J. G. Kushmerick, D. B. Holt, S. K. Pollack, M. A. Ratner, J. C. Yang, T. L. Schull, J. Naciri, M. H. Moore, R. Shashidhar, Effect of bond-length alternation in

- molecular wires. *Journal of the American Chemical Society* **124**, 10654-10655 (2002); published online EpubSep (10.1021/ja027090n).
38. J. G. Kushmerick, A. S. Blum, D. P. Long, Metrology for molecular electronics. *Analytica Chimica Acta* **568**, 20-27 (2006); published online EpubMay (10.1016/j.aca.2005.12.033).
  39. A. Troisi, M. A. Ratner, Molecular transport junctions: Propensity rules for inelastic electron tunneling spectra. *Nano Letters* **6**, 1784-1788 (2006); published online EpubAug (10.1021/nl0609394).
  40. J. G. Kushmerick, J. Naciri, J. C. Yang, R. Shashidhar, Conductance scaling of molecular wires in parallel. *Nano Letters* **3**, 897-900 (2003); published online EpubJul (10.1021/nl034201n).
  41. D. J. Wold, C. D. Frisbie, Formation of metal-molecule-metal tunnel junctions: Microcontacts to alkanethiol monolayers with a conducting AFM tip. *Journal of the American Chemical Society* **122**, 2970-2971 (2000); published online EpubMar (10.1021/ja994468h).
  42. D. J. Wold, C. D. Frisbie, Fabrication and characterization of metal-molecule-metal junctions by conducting probe atomic force microscopy. *Journal of the American Chemical Society* **123**, 5549-5556 (2001); published online EpubJun (10.1021/ja0101532).
  43. D. J. Wold, R. Haag, M. A. Rampi, C. D. Frisbie, Distance dependence of electron tunneling through self-assembled monolayers measured by conducting probe atomic force microscopy: Unsaturated versus saturated molecular junctions. *Journal of Physical Chemistry B* **106**, 2813-2816 (2002); published online EpubMar (10.1021/jp013476t).
  44. V. B. Engelkes, J. M. Beebe, C. D. Frisbie, Analysis of the causes of variance in resistance measurements on metal-molecule-metal junctions formed by conducting-probe atomic force microscopy. *Journal of Physical Chemistry B* **109**, 16801-16810 (2005); published online EpubSep (10.1021/jp052348s).
  45. L. A. Bumm, J. J. Arnold, M. T. Cygan, T. D. Dunbar, T. P. Burgin, L. Jones, D. L. Allara, J. M. Tour, P. S. Weiss, Are single molecular wires conducting? *Science* **271**, 1705-1707 (1996); published online EpubMar (10.1126/science.271.5256.1705).



46. W. Haiss, H. van Zalinge, D. Bethell, J. Ulstrup, D. J. Schiffrin, R. J. Nichols, Thermal gating of the single molecule conductance of alkanedithiols. *Faraday Discussions* **131**, 253-264 (2006)10.1039/b507520n).
47. X. Lu, K. W. Hipps, Scanning tunneling microscopy of metal phthalocyanines: d(6) and d(8) cases. *Journal of Physical Chemistry B* **101**, 5391-5396 (1997); published online EpubJul (10.1021/jp9707448).
48. G. V. Nazin, X. H. Qiu, W. Ho, Visualization and spectroscopy of a metal-molecule-metal bridge. *Science* **302**, 77-81 (2003); published online EpubOct (10.1126/science.1088971).
49. W. Haiss, R. J. Nichols, H. van Zalinge, S. J. Higgins, D. Bethell, D. J. Schiffrin, Measurement of single molecule conductivity using the spontaneous formation of molecular wires. *Physical Chemistry Chemical Physics* **6**, 4330-4337 (2004)10.1039/b404929b).
50. J. Chen, M. A. Reed, A. M. Rawlett, J. M. Tour, Large on-off ratios and negative differential resistance in a molecular electronic device. *Science* **286**, 1550-1552 (1999); published online EpubNov (10.1126/science.286.5444.1550).
51. J. Chen, W. Wang, M. A. Reed, A. M. Rawlett, D. W. Price, J. M. Tour, Room-temperature negative differential resistance in nanoscale molecular junctions. *Applied Physics Letters* **77**, 1224-1226 (2000); published online EpubAug (10.1063/1.1289650).
52. W. Y. Wang, T. Lee, M. A. Reed, Elastic and inelastic electron tunneling in alkane self-assembled monolayers. *Journal of Physical Chemistry B* **108**, 18398-18407 (2004); published online EpubDec (10.1021/jp048904k).
53. M. W. Holman, R. C. Liu, L. Zang, P. Yan, S. A. DiBenedetto, R. D. Bowers, D. M. Adams, Studying and switching electron transfer: From the ensemble to the single molecule. *Journal of the American Chemical Society* **126**, 16126-16133 (2004); published online EpubDec (10.1021/ja047386o).
54. Y. Selzer, L. T. Cai, M. A. Cabassi, Y. X. Yao, J. M. Tour, T. S. Mayer, D. L. Allara, Effect of local environment on molecular conduction: Isolated molecule versus self-assembled monolayer. *Nano Letters* **5**, 61-65 (2005); published online EpubJan (10.1021/nl048372j).
55. M. A. Reed, C. Zhou, C. J. Muller, T. P. Burgin, J. M. Tour, Conductance of a molecular junction. *Science* **278**, 252-254 (1997); published online EpubOct (

56. R. H. M. Smit, Y. Noat, C. Untiedt, N. D. Lang, M. C. van Hemert, J. M. van Ruitenbeek, Measurement of the conductance of a hydrogen molecule. *Nature* **419**, 906-909 (2002); published online EpubOct (10.1038/nature01103).
57. H. B. Weber, J. Reichert, R. Ochs, D. Beckmann, M. Mayor, H. von Lohneysen, Conductance properties of single-molecule junctions. *Physica E-Low-Dimensional Systems & Nanostructures* **18**, 231-232 (2003); published online EpubMay (10.1016/s1386-9477(02)00986-4).
58. B. Q. Xu, N. J. J. Tao, Measurement of single-molecule resistance by repeated formation of molecular junctions. *Science* **301**, 1221-1223 (2003); published online EpubAug (
59. J. He, F. Chen, J. Li, O. F. Sankey, Y. Terazono, C. Herrero, D. Gust, T. A. Moore, A. L. Moore, S. M. Lindsay, Electronic decay constant of carotenoid polyenes from single-molecule measurements. *Journal of the American Chemical Society* **127**, 1384-1385 (2005); published online EpubFeb (10.1021/ja0432791).
60. K. Ishizuka, M. Suzuki, S. Fujii, Y. Takayama, F. Sato, M. Fujihira, Effect of molecule-electrode contacts on single-molecule conductivity of mu-conjugated system measured by scanning tunneling microscopy under ultrahigh vacuum. *Japanese Journal of Applied Physics Part 1-Regular Papers Brief Communications & Review Papers* **45**, 2037-2040 (2006); published online EpubMar (10.1143/jjap.45.20371).
61. L. Venkataraman, J. E. Klare, I. W. Tam, C. Nuckolls, M. S. Hybertsen, M. L. Steigerwald, Single-molecule circuits with well-defined molecular conductance. *Nano Letters* **6**, 458-462 (2006); published online EpubMar (10.1021/nl052373+).
62. Z. H. Li, I. Pobelov, B. Han, T. Wandlowski, A. Blaszczyk, M. Mayor, Conductance of redox-active single molecular junctions: an electrochemical approach. *Nanotechnology* **18**, (2007); published online EpubJan (10.1088/0957-4484/18/4/044018).
63. K. H. Muller, Effect of the atomic configuration of gold electrodes on the electrical conduction of alkanedithiol molecules. *Physical Review B* **73**, (2006); published online EpubJan (045403  
10.1103/PhysRevB.73.045403).
64. K. Burke, Perspective on density functional theory. *Journal of Chemical Physics* **136**, (2012); published online EpubApr (10.1063/1.4704546).

65. C. D. Sherrill, Frontiers in electronic structure theory. *Journal of Chemical Physics* **132**, (2010); published online EpubMar (10.1063/1.3369628).
66. J. A. Pople, Nobel Lecture: Quantum chemical models. *Reviews of Modern Physics* **71**, 1267-1274 (1999); published online EpubOct (10.1103/RevModPhys.71.1267).
67. T. Hines, I. Diez-Perez, H. Nakamura, T. Shimazaki, Y. Asai, N. J. Tao, Controlling Formation of Single-Molecule Junctions by Electrochemical Reduction of Diazonium Terminal Groups. *Journal of the American Chemical Society* **135**, 3319-3322 (2013); published online EpubMar (10.1021/ja3106434).
68. S. Y. Quek, L. Venkataraman, H. J. Choi, S. G. Louie, M. S. Hybertsen, J. B. Neaton, Amine-gold linked single-molecule circuits: Experiment and theory. *Nano Letters* **7**, 3477-3482 (2007); published online EpubNov (10.1021/n10720581).
69. S. M. Lindsay, M. A. Ratner, Molecular transport junctions: Clearing mists. *Advanced Materials* **19**, 23-31 (2007); published online EpubJan (10.1002/adma.200601140).
70. P. Darancet, J. R. Widawsky, H. J. Choi, L. Venkataraman, J. B. Neaton, Quantitative Current-Voltage Characteristics in Molecular Junctions from First Principles. *Nano Letters* **12**, 6250-6254 (2012); published online EpubDec (10.1021/nl3033137).
71. V. M. Garcia-Suarez, J. Ferrer, Nonequilibrium transport response from equilibrium transport theory. *Physical Review B* **86**, (2012); published online EpubSep (10.1103/PhysRevB.86.125446).
72. D. Vuillaume, S. Lenfant, D. Guerin, C. Delerue, C. Petit, G. Salace, Electronic properties of organic, monolayers and molecular devices. *Pramana-Journal of Physics* **67**, 17-32 (2006); published online EpubJul (10.1007/s12043-006-0033-x).
73. M. Kula, J. Jiang, Y. Luo, A molecular view on electron transport in molecular electronic devices. *Journal of Computational and Theoretical Nanoscience* **5**, 401-421 (2008); published online EpubApr (
74. A. J. Bergren, R. L. McCreery, Analytical Chemistry in Molecular Electronics. *Annual Review of Analytical Chemistry, Vol 4* **4**, 173-195 (2011)10.1146/annurev-anchem-061010-113847).

75. X. Y. Zhu, Electronic structure and electron dynamics at molecule-metal interfaces: implications for molecule-based electronics. *Surface Science Reports* **56**, 1-83 (2004); published online EpubNov (10.1016/j.surfrep.2004.09.002).
76. T. Hines, I. Diez-Perez, J. Hihath, H. M. Liu, Z. S. Wang, J. W. Zhao, G. Zhou, K. Muellen, N. J. Tao, Transition from Tunneling to Hopping in Single Molecular Junctions by Measuring Length and Temperature Dependence. *Journal of the American Chemical Society* **132**, 11658-11664 (2010); published online EpubAug (10.1021/ja1040946).
77. S. H. Choi, B. Kim, C. D. Frisbie, Electrical resistance of long conjugated molecular wires. *Science* **320**, 1482-1486 (2008); published online EpubJun (10.1126/science.1156538).
78. S. H. Choi, C. D. Frisbie, Enhanced Hopping Conductivity in Low Band Gap Donor-Acceptor Molecular Wires Up to 20 nm in Length. *Journal of the American Chemical Society* **132**, 16191-16201 (2010); published online EpubNov (10.1021/ja1060142).
79. J. G. Kushmerick, J. Lazorcik, C. H. Patterson, R. Shashidhar, D. S. Seferos, G. C. Bazan, Vibronic contributions to charge transport across molecular junctions. *Nano Letters* **4**, 639-642 (2004); published online EpubApr (10.1021/nl049871n).
80. A. A. Voityuk, Charge transfer in DNA: Hole charge is confined to a single base pair due to solvation effects. *Journal of Chemical Physics* **122**, (2005); published online EpubMay (10.1063/1.1924551).
81. N. Darwish, I. Diez-Perez, P. Da Silva, N. J. Tao, J. J. Gooding, M. N. Paddon-Row, Observation of Electrochemically Controlled Quantum Interference in a Single Anthraquinone-Based Norbornylogous Bridge Molecule. *Angewandte Chemie-International Edition* **51**, 3203-3206 (2012)10.1002/anie.201107765).
82. X. Y. Xiao, B. Q. Xu, N. J. Tao, Conductance titration of single-peptide molecules. *Journal of the American Chemical Society* **126**, 5370-5371 (2004); published online EpubMay (10.1021/ja049469a).
83. F. Chen, J. He, C. Nuckolls, T. Roberts, J. E. Klare, S. Lindsay, A molecular switch based on potential-induced changes of oxidation state. *Nano Letters* **5**, 503-506 (2005); published online EpubMar (10.1021/nl0478474).

84. B. Mann, H. Kuhn, TUNNELING THROUGH FATTY ACID SALT MONOLAYERS. *Journal of Applied Physics* **42**, 4398-& (1971)10.1063/1.1659785).
85. G. Binnig, H. Rohrer, C. Gerber, E. Weibel, VACUUM TUNNELING. *Physica B & C* **109**, 2075-2077 (1982)10.1016/0378-4363(82)90241-8).
86. G. Binnig, H. Rohrer, SCANNING TUNNELING MICROSCOPY. *Surface Science* **126**, 236-244 (1983)10.1016/0039-6028(83)90716-1).
87. M. Fujihira, K. Nishiyama, H. Yamada, PHOTOELECTROCHEMICAL RESPONSES OF OPTICALLY TRANSPARENT ELECTRODES MODIFIED WITH LANGMUIR-BLODGETT-FILMS CONSISTING OF SURFACTANT DERIVATIVES OF ELECTRON-DONOR, ACCEPTOR AND SENSITIZER MOLECULES. *Thin Solid Films* **132**, 77-82 (1985); published online EpubOct (10.1016/0040-6090(85)90459-6).
88. R. M. Metzger, B. Chen, U. Hopfner, M. V. Lakshmikantham, D. Vuillaume, T. Kawai, X. L. Wu, H. Tachibana, T. V. Hughes, H. Sakurai, J. W. Baldwin, C. Hosch, M. P. Cava, L. Brehmer, G. J. Ashwell, Unimolecular electrical rectification in hexadecylquinolinium tricyanoquinodimethanide. *Journal of the American Chemical Society* **119**, 10455-10466 (1997); published online EpubOct (10.1021/ja971811e).
89. H. B. Akkerman, B. de Boer, Electrical conduction through single molecules and self-assembled monolayers. *Journal of Physics-Condensed Matter* **20**, (2008); published online EpubJan (10.1088/0953-8984/20/01/013001).
90. M. Paulsson, C. Krag, T. Frederiksen, M. Brandbyge, Conductance of Alkanedithiol Single-Molecule Junctions: A Molecular Dynamics Study. *Nano Letters* **9**, 117-121 (2009); published online EpubJan (10.1021/nl802643h).
91. I. Diez-Perez, J. Hihath, T. Hines, Z.-S. Wang, G. Zhou, K. Mullen, N. Tao, *Controlling single-molecule conductance through lateral coupling of [pi] orbitals*.
92. C. Bruot, J. Hihath, N. J. Tao, Mechanically controlled molecular orbital alignment in single molecule junctions. *Nature Nanotechnology* **7**, 35-40 (2012); published online EpubJan (10.1038/nnano.2011.212).
93. C. P. Collier, G. Mattersteig, E. W. Wong, Y. Luo, K. Beverly, J. Sampaio, F. M. Raymo, J. F. Stoddart, J. R. Heath, A 2 catenane-based solid state electronically

- reconfigurable switch. *Science* **289**, 1172-1175 (2000); published online EpubAug (10.1126/science.289.5482.1172).
94. A. S. Blum, J. G. Kushmerick, D. P. Long, C. H. Patterson, J. C. Yang, J. C. Henderson, Y. X. Yao, J. M. Tour, R. Shashidhar, B. R. Ratna, Molecularly inherent voltage-controlled conductance switching. *Nature Materials* **4**, 167-172 (2005); published online EpubFeb (10.1038/nmat1309).
95. J. Chen, W. Wang, J. Klemic, M. A. Reed, B. W. Axelrod, D. M. Kaschak, A. M. Rawlett, D. W. Price, S. M. Dirk, J. M. Tour, D. S. Grubisha, D. W. Bennett, Molecular wires, switches, and memories. *Molecular Electronics II* **960**, 69-99 (2002).
96. I. Diez-Perez, J. Hihath, Y. Lee, L. P. Yu, L. Adamska, M. A. Kozhushner, Oleynik, II, N. J. Tao, Rectification and stability of a single molecular diode with controlled orientation. *Nature Chemistry* **1**, 635-641 (2009)10.1038/nchem.392).
97. P. Jiang, G. M. Morales, W. You, L. P. Yu, Synthesis of diode molecules and their sequential assembly to control electron transport. *Angewandte Chemie-International Edition* **43**, 4471-4475 (2004)10.1002/anie.200460110).
98. A. Salomon, R. Arad-Yellin, A. Shanzer, A. Karton, D. Cahen, Stable room-temperature molecular negative differential resistance based on molecule-electrode interface chemistry. *Journal of the American Chemical Society* **126**, 11648-11657 (2004); published online EpubSep (10.1021/ja0495841).
99. R. A. Kiehl, J. D. Le, P. Candra, R. C. Hoye, T. R. Hoye, Charge storage model for hysteretic negative-differential resistance in metal-molecule-metal junctions. *Applied Physics Letters* **88**, (2006); published online EpubApr (10.1063/1.2195696).
100. H. Song, Y. Kim, Y. H. Jang, H. Jeong, M. A. Reed, T. Lee, Observation of molecular orbital gating. *Nature* **462**, 1039-1043 (2009); published online EpubDec (10.1038/nature08639).
101. X. L. Li, B. Q. Xu, X. Y. Xiao, X. M. Yang, L. Zang, N. J. Tao, Controlling charge transport in single molecules using electrochemical gate. *Faraday Discussions* **131**, 111-120 (2006)10.1039/b505666g).
102. Y. Selzer, M. A. Cabassi, T. S. Mayer, D. L. Allara, Thermally activated conduction in molecular junctions. *Journal of the American Chemical Society* **126**, 4052-4053 (2004); published online EpubApr (10.1021/ja039015y).

103. C. M. Guedon, H. Valkenier, T. Markussen, K. S. Thygesen, J. C. Hummelen, S. J. van der Molen, Observation of quantum interference in molecular charge transport. *Nature Nanotechnology* **7**, 304-308 (2012); published online EpubMay (10.1038/nnano.2012.37).
104. J. R. Widawsky, P. Darancet, J. B. Neaton, L. Venkataraman, Simultaneous Determination of Conductance and Thermopower of Single Molecule Junctions. *Nano Letters* **12**, 354-358 (2012); published online EpubJan (10.1021/nl203634m).
105. J. Hihath, C. Bruot, N. J. Tao, Electron-Phonon Interactions in Single Octanedithiol Molecular Junctions. *Acs Nano* **4**, 3823-3830 (2010); published online EpubJul (10.1021/nn100470s).
106. J. Hihath, C. Bruot, H. Nakamura, Y. Asai, I. Diez-Perez, Y. Lee, L. P. Yu, N. J. Tao, Inelastic Transport and Low-Bias Rectification in a Single-Molecule Diode. *Acs Nano* **5**, 8331-8339 (2011); published online EpubOct (10.1021/nn2030644).
107. A. M. Scott, M. R. Wasielewski, Temperature Dependence of Spin-Selective Charge Transfer Pathways in Donor-Bridge-Acceptor Molecules with Oligomeric Fluorenone and p-Phenylethynylene Bridges. *Journal of the American Chemical Society* **133**, 3005-3013 (2011); published online EpubMar (10.1021/ja1095649).
108. R. Landauer, SPATIAL VARIATION OF CURRENTS AND FIELDS DUE TO LOCALIZED SCATTERERS IN METALLIC CONDUCTION. *Ibm Journal of Research and Development* **1**, 223-231 (1957).
109. H. Klein, T. Leoni, R. Zoubkoff, P. Dumas, A. Saul, Conductance fluctuations in gold point contacts: an atomistic picture. *Nanotechnology* **23**, (2012); published online EpubJun (10.1088/0957-4484/23/23/235707).
110. T. Hansen, V. Mujica, M. A. Ratner, Cotunneling Model for Current-induced Events in Molecular Wires. *Nano Letters* **8**, 3525-3531 (2008); published online EpubOct (10.1021/nl801001q).
111. D. V. Averin, Y. V. Nazarov, VIRTUAL ELECTRON-DIFFUSION DURING QUANTUM TUNNELING OF THE ELECTRIC CHARGE. *Physical Review Letters* **65**, 2446-2449 (1990); published online EpubNov (10.1103/PhysRevLett.65.2446).

112. L. J. Lauhon, W. Ho, Control and characterization of a multistep unimolecular reaction. *Physical Review Letters* **84**, 1527-1530 (2000); published online EpubFeb (10.1103/PhysRevLett.84.1527).
113. J. Simmons. (American Institute of Physics, 1963), vol. 34, pp. 1793-1803.
114. S. H. Choi, C. Risko, M. C. R. Delgado, B. Kim, J. L. Bredas, C. D. Frisbie, Transition from Tunneling to Hopping Transport in Long, Conjugated Oligo-imine Wires Connected to Metals. *Journal of the American Chemical Society* **132**, 4358-4368 (2010); published online EpubMar (10.1021/ja910547c).
115. J. M. Beebe, B. Kim, J. W. Gadzuk, C. D. Frisbie, J. G. Kushmerick, Transition from direct tunneling to field emission in metal-molecule-metal junctions. *Physical Review Letters* **97**, (2006); published online EpubJul (026801 10.1103/PhysRevLett.97.026801).
116. F. Chen, X. L. Li, J. Hihath, Z. F. Huang, N. J. Tao, Effect of anchoring groups on single-molecule conductance: Comparative study of thiol-, amine-, and carboxylic-acid-terminated molecules. *Journal of the American Chemical Society* **128**, 15874-15881 (2006); published online EpubDec (10.1021/ja065864k).
117. C. Li, I. Pobelov, T. Wandlowski, A. Bagrets, A. Arnold, F. Evers, Charge transport in single Au vertical bar alkanedithiol vertical bar Au junctions: Coordination geometries and conformational degrees of freedom. *Journal of the American Chemical Society* **130**, 318-326 (2008); published online EpubJan (10.1021/ja0762386).
118. M. S. Hybertsen, L. Venkataraman, J. E. Klare, A. Cwhalley, M. L. Steigerwald, C. Nuckolls, Amine-linked single-molecule circuits: systematic trends across molecular families. *Journal of Physics-Condensed Matter* **20**, (2008); published online EpubSep (10.1088/0953-8984/20/37/374115).
119. S. Y. Quek, M. Kamenetska, M. L. Steigerwald, H. J. Choi, S. G. Louie, M. S. Hybertsen, J. B. Neaton, L. Venkataraman, Mechanically controlled binary conductance switching of a single-molecule junction. *Nature Nanotechnology* **4**, 230-234 (2009); published online EpubApr (10.1038/nano.2009.10).
120. W. J. Hong, D. Z. Manrique, P. Moreno-Garcia, M. Gulcur, A. Mishchenko, C. J. Lambert, M. R. Bryce, T. Wandlowski, Single Molecular Conductance of Tolanes: Experimental and Theoretical Study on the Junction Evolution Dependent on the Anchoring Group. *Journal of the American Chemical Society* **134**, 2292-2304 (2012); published online EpubFeb (10.1021/ja209844r1).



121. B. Kim, J. M. Beebe, Y. Jun, X. Y. Zhu, C. D. Frisbie, Correlation between HOMO alignment and contact resistance in molecular junctions: Aromatic thiols versus aromatic isocyanides. *Journal of the American Chemical Society* **128**, 4970-4971 (2006); published online EpubApr (10.1021/ja0607990).
122. A. Mishchenko, L. A. Zotti, D. Vonlanthen, M. Burkle, F. Pauly, J. C. Cuevas, M. Mayor, T. Wandlowski, Single-Molecule Junctions Based on Nitrile-Terminated Biphenyls: A Promising New Anchoring Group. *Journal of the American Chemical Society* **133**, 184-187 (2011); published online EpubJan (10.1021/ja107340t).
123. L. A. Zotti, T. Kirchner, J. C. Cuevas, F. Pauly, T. Huhn, E. Scheer, A. Erbe, Revealing the Role of Anchoring Groups in the Electrical Conduction Through Single-Molecule Junctions. *Small* **6**, 1529-1535 (2010); published online EpubJul (10.1002/sml.200902227).
124. C. H. Ko, M. J. Huang, M. D. Fu, C. H. Chen, Superior Contact for Single-Molecule Conductance: Electronic Coupling of Thiolate and Isothiocyanate on Pt, Pd, and Au. *Journal of the American Chemical Society* **132**, 756-764 (2010); published online EpubJan (10.1021/ja9084012).
125. Y. S. Park, A. C. Whalley, M. Kamenetska, M. L. Steigerwald, M. S. Hybertsen, C. Nuckolls, L. Venkataraman, Contact chemistry and single-molecule conductance: A comparison of phosphines, methyl sulfides, and amines. *Journal of the American Chemical Society* **129**, 15768-+ (2007); published online EpubDec (10.1021/ja0773857).
126. Y. J. Xing, T. H. Park, R. Venkatramani, S. Keinan, D. N. Beratan, M. J. Therien, E. Borguet, Optimizing Single-Molecule Conductivity of Conjugated Organic Oligomers with Carbodithioate Linkers. *Journal of the American Chemical Society* **132**, 7946-7956 (2010); published online EpubJun (10.1021/ja909559m).
127. C. A. Martin, D. Ding, J. K. Sorensen, T. Bjornholm, J. M. van Ruitenbeek, H. S. J. van der Zant, Fullerene-based anchoring groups for molecular electronics. *Journal of the American Chemical Society* **130**, 13198-13199 (2008); published online EpubOct (10.1021/ja804699a).
128. M. Kiguchi, Electrical conductance of single C-60 and benzene molecules bridging between Pt electrode. *Applied Physics Letters* **95**, (2009); published online EpubAug (10.1063/1.3204466).

129. J. Fock, J. K. Sorensen, E. Lortscher, T. Vosch, C. A. Martin, H. Riel, K. Kilsa, T. Bjornholm, H. van der Zant, A statistical approach to inelastic electron tunneling spectroscopy on fullerene-terminated molecules. *Physical Chemistry Chemical Physics* **13**, 14325-14332 (2011)10.1039/c1cp20861f).
130. E. Leary, M. T. Gonzalez, C. van der Pol, M. R. Bryce, S. Filippone, N. Martin, G. Rubio-Bollinger, N. Agrait, Unambiguous One-Molecule Conductance Measurements under Ambient Conditions. *Nano Letters* **11**, 2236-2241 (2011); published online EpubJun (10.1021/nl200294s).
131. X. L. Li, J. He, J. Hihath, B. Q. Xu, S. M. Lindsay, N. J. Tao, Conductance of single alkanedithiols: Conduction mechanism and effect of molecule-electrode contacts. *Journal of the American Chemical Society* **128**, 2135-2141 (2006); published online EpubFeb (10.1021/ja057316x).
132. V. B. Engelkes, J. M. Beebe, C. D. Frisbie, Length-dependent transport in molecular junctions based on SAMs of alkanethiols and alkanedithiols: Effect of metal work function and applied bias on tunneling efficiency and contact resistance. *Journal of the American Chemical Society* **126**, 14287-14296 (2004); published online EpubNov (10.1021/ja046274u).
133. Z. L. Cheng, R. Skouta, H. Vazquez, J. R. Widawsky, S. Schneebeli, W. Chen, M. S. Hybertsen, R. Breslow, L. Venkataraman, In situ formation of highly conducting covalent Au-C contacts for single-molecule junctions. *Nature Nanotechnology* **6**, 353-357 (2011); published online EpubJun (10.1038/nnano.2011.66).
134. W. Hong, H. Li, S.-X. Liu, Y. Fu, J. Li, V. Kaliginedi, S. Decurtins, T. Wandlowski, Trimethylsilyl-Terminated Oligo(phenylene ethynylene)s: An Approach to Single-Molecule Junctions with Covalent Au-C  $\sigma$ -Bonds. *Journal of the American Chemical Society* **134**, 19425-19431 (2012); published online Epub2012/12/17 (10.1021/ja307544w).
135. W. B. Chen, J. R. Widawsky, H. Vazquez, S. T. Schneebeli, M. S. Hybertsen, R. Breslow, L. Venkataraman, Highly Conducting pi-Conjugated Molecular Junctions Covalently Bonded to Gold Electrodes. *Journal of the American Chemical Society* **133**, 17160-17163 (2011); published online EpubNov (10.1021/ja208020j).
136. S. Chen, Z. Zhao, H. Liu, Charge Transport at the Metal-Organic Interface. *Annual Review of Physical Chemistry* **64**, 221-245 (2013)doi:10.1146/annurev-physchem-040412-110035).

137. M. Magoga, C. Joachim, Minimal attenuation for tunneling through a molecular wire. *Physical Review B* **57**, 1820-1823 (1998); published online EpubJan (
138. W. B. Davis, W. A. Svec, M. A. Ratner, M. R. Wasielewski, Molecular-wire behaviour in p-phenylenevinylene oligomers. *Nature* **396**, 60-63 (1998); published online EpubNov (
139. B. Giese, J. Amaudrut, A. K. Kohler, M. Spormann, S. Wessely, Direct observation of hole transfer through DNA by hopping between adenine bases and by tunnelling. *Nature* **412**, 318-320 (2001); published online EpubJul (
140. A. Nitzan, Electron transmission through molecules and molecular interfaces. *Annual Review of Physical Chemistry* **52**, 681-750 (2001).
141. E. G. Petrov, Y. V. Shevchenko, V. I. Teslenko, V. May, Nonadiabatic donor-acceptor electron transfer mediated by a molecular bridge: A unified theoretical description of the superexchange and hopping mechanism. *Journal of Chemical Physics* **115**, 7107-7122 (2001); published online EpubOct (
142. A. K. Felts, W. T. Pollard, R. A. Friesner, MULTILEVEL REDFIELD TREATMENT OF BRIDGE-MEDIATED LONG-RANGE ELECTRON-TRANSFER - A MECHANISM FOR ANOMALOUS DISTANCE DEPENDENCE. *Journal of Physical Chemistry* **99**, 2929-2940 (1995); published online EpubMar (
143. A. Okada, V. Chernyak, S. Mukamel, Solvent reorganization in long-range electron transfer: Density matrix approach. *Journal of Physical Chemistry A* **102**, 1241-1251 (1998); published online EpubFeb (
144. B. Q. Xu, P. M. Zhang, X. L. Li, N. J. Tao, Direct conductance measurement of single DNA molecules in aqueous solution. *Nano Letters* **4**, 1105-1108 (2004); published online EpubJun (10.1021/nl0494295).
145. J. Hihath, F. Chen, P. M. Zhang, N. J. Tao, Thermal and electrochemical gate effects on DNA conductance. *Journal of Physics-Condensed Matter* **19**, (2007); published online EpubMay (215202 10.1088/0953-8984/19/21/215202).
146. A. Landau, L. Kronik, A. Nitzan, Cooperative effects in molecular conduction. *Journal of Computational and Theoretical Nanoscience* **5**, 535-544 (2008); published online EpubApr (

147. Q. Lu, K. Liu, H. M. Zhang, Z. B. Du, X. H. Wang, F. S. Wang, From Tunneling to Hopping: A Comprehensive Investigation of Charge Transport Mechanism in Molecular Junctions Based on Oligo(p-phenylene ethynylene)s. *Acs Nano* **3**, 3861-3868 (2009)10.1021/nn9012687).
148. R. H. Goldsmith, O. DeLeon, T. M. Wilson, D. Finkelstein-Shapiro, M. A. Ratner, M. R. Wasielewski, Challenges in distinguishing superexchange and hopping mechanisms of intramolecular charge transfer through fluorene ligomers. *Journal of Physical Chemistry A* **112**, 4410-4414 (2008); published online EpubMay (10.1021/jp801084v).
149. M. Tsutsui, K. Shoji, K. Morimoto, M. Taniguchi, T. Kawai, Thermodynamic stability of single molecule junctions. *Applied Physics Letters* **92**, (2008); published online EpubJun (223110 10.1063/1.2939219).
150. H. Basch, R. Cohen, M. A. Ratner, Interface geometry and molecular junction conductance: Geometric fluctuation and stochastic switching. *Nano Letters* **5**, 1668-1675 (2005); published online EpubSep (10.1021/nl050702s).
151. Y. B. Hu, Y. Zhu, H. J. Gao, H. Guo, Conductance of an ensemble of molecular wires: A statistical analysis. *Physical Review Letters* **95**, (2005); published online EpubOct (156803 10.1103/PhysRevLett.95.156803).
152. J. M. Beebe, B. Kim, C. D. Frisbie, J. G. Kushmerick, Measuring relative barrier heights in molecular electronic junctions with transition voltage spectroscopy. *Acs Nano* **2**, 827-832 (2008); published online EpubMay (10.1021/nn700424u).
153. R. Yamada, H. Kumazawa, S. Tanaka, H. Tada, Electrical Resistance of Long Oligothiophene Molecules. *Applied Physics Express* **2**, (2009)10.1143/apex.2.025002).
154. A. Salomon, D. Cahen, S. Lindsay, J. Tomfohr, V. B. Engelkes, C. D. Frisbie, Comparison of electronic transport measurements on organic molecules. *Advanced Materials* **15**, 1881-1890 (2003); published online EpubNov (10.1002/adma.200306091).
155. Y. Arikuma, H. Nakayama, T. Morita, S. Kimura, Electron Hopping over 100 angstrom Along an alpha Helix. *Angewandte Chemie-International Edition* **49**, 1800-1804 (2010)10.1002/anie.200905621).

156. W. B. Davis, M. A. Ratner, M. R. Wasielewski, Conformational gating of long distance electron transfer through wire-like bridges in donor-bridge-acceptor molecules. *Journal of the American Chemical Society* **123**, 7877-7886 (2001); published online EpubAug (10.1021/ja010330z).
157. Z. F. Huang, F. Chen, P. A. Bennett, N. J. Tao, Single molecule junctions formed via au-thiol contact: Stability and breakdown mechanism. *Journal of the American Chemical Society* **129**, 13225-13231 (2007); published online EpubOct (10.1021/ja074456t).
158. B. Q. Xu, X. Y. Xiao, N. J. Tao, Measurements of single-molecule electromechanical properties. *Journal of the American Chemical Society* **125**, 16164-16165 (2003); published online EpubDec (10.1021/ja038949j).
159. R. Yamada, H. Kumazawa, T. Noutoshi, S. Tanaka, H. Tada, Electrical conductance of oligothiophene molecular wires. *Nano Letters* **8**, 1237-1240 (2008)10.1021/nl0732023).
160. M. Kamenetska, M. Koentopp, A. C. Whalley, Y. S. Park, M. L. Steigerwald, C. Nuckolls, M. S. Hybertsen, L. Venkataraman, Formation and Evolution of Single-Molecule Junctions. *Physical Review Letters* **102**, (2009); published online EpubMar (126803 10.1103/PhysRevLett.102.126803).
161. Z. F. Huang, B. Q. Xu, Y. C. Chen, M. Di Ventra, N. J. Tao, Measurement of current-induced local heating in a single molecule junction. *Nano Letters* **6**, 1240-1244 (2006); published online EpubJun (10.1021/nl0608285).
162. M. Kiguchi, S. Miura, K. Hara, M. Sawamura, K. Murakoshi, Conductance of a single molecule anchored by an isocyanide substituent to gold electrodes. *Applied Physics Letters* **89**, (2006); published online EpubNov (213104 10.1063/1.2392816).
163. J. Park, A. N. Pasupathy, J. I. Goldsmith, C. Chang, Y. Yaish, J. R. Petta, M. Rinkoski, J. P. Sethna, H. D. Abruna, P. L. McEuen, D. C. Ralph, Coulomb blockade and the Kondo effect in single-atom transistors. *Nature* **417**, 722-725 (2002); published online EpubJun (10.1038/nature00791).
164. S. Ranganathan, I. Steidel, F. Anariba, R. L. McCreery, Covalently bonded organic monolayers on a carbon substrate: A new paradigm for molecular electronics. *Nano Letters* **1**, 491-494 (2001); published online EpubSep (10.1021/nl015566f).

165. P. Allongue, M. Delamar, B. Desbat, O. Fagebaume, R. Hitmi, J. Pinson, J. M. Saveant, Covalent modification of carbon surfaces by aryl radicals generated from the electrochemical reduction of diazonium salts. *Journal of the American Chemical Society* **119**, 201-207 (1997); published online EpubJan (10.1021/ja963354s).
166. F. Anariba, S. H. DuVall, R. L. McCreery, Mono- and multilayer formation by diazonium reduction on carbon surfaces monitored with atomic force microscopy "scratching". *Analytical Chemistry* **75**, 3837-3844 (2003); published online EpubAug (10.1021/ac034026v).
167. J. Lehr, B. E. Williamson, B. S. Flavel, A. J. Downard, Reaction of Gold Substrates with Diazonium Salts in Acidic Solution at Open-Circuit Potential. *Langmuir* **25**, 13503-13509 (2009); published online EpubDec (10.1021/la902002n).
168. A. Laforgue, T. Addou, D. Belanger, Characterization of the deposition of organic molecules at the surface of gold by the electrochemical reduction of aryldiazonium cations. *Langmuir* **21**, 6855-6865 (2005); published online EpubJul (10.1021/la047369c).
169. A. Bousquet, M. Ceccato, M. Hinge, S. U. Pedersen, K. Daasbjerg, Redox Grafting of Diazotated Anthraquinone as a Means of Forming Thick Conducting Organic Films. *Langmuir* **28**, 1267-1275 (2011); published online Epub2012/01/17 (10.1021/la203657n).
170. V. Stockhausen, J. Ghilane, P. Martin, G. Trippe-Allard, H. Randriamahazaka, J. C. Lacroix, Grafting Oligothiophenes on Surfaces by Diazonium Electroreduction: A Step toward Ultrathin Junction with Well-Defined Metal/Oligomer Interface. *Journal of the American Chemical Society* **131**, 14920-14927 (2009); published online EpubOct (10.1021/ja9047009).
171. A. M. Nowak, R. L. McCreery, Characterization of carbon/nitroazobenzene/titanium molecular electronic junctions with photoelectron and Raman spectroscopy. *Analytical Chemistry* **76**, 1089-1097 (2004); published online EpubFeb (10.1021/ac034807w).
172. A. M. Nowak, R. L. McCreery, In situ Raman spectroscopy of bias-induced structural changes in nitroazobenzene molecular electronic junctions. *Journal of the American Chemical Society* **126**, 16621-16631 (2004); published online EpubDec (10.1021/ja045763r).

173. A. M. Mahmoud, A. J. Bergren, R. L. McCreery, Derivatization of Optically Transparent Materials with Diazonium Reagents for Spectroscopy of Buried Interfaces. *Analytical Chemistry* **81**, 6972-6980 (2009); published online EpubAug (10.1021/ac901052v).
174. R. L. McCreery, J. Wu, R. P. Kalakodimi, Electron transport and redox reactions in carbon-based molecular electronic junctions. *Physical Chemistry Chemical Physics* **8**, 2572-2590 (2006); published online EpubJun (10.1039/b601163m).
175. J. Ru, B. Szeto, A. Bonifas, R. L. McCreery, Microfabrication and Integration of Diazonium-Based Aromatic Molecular Junctions. *Acs Applied Materials & Interfaces* **2**, 3693-3701 (2010); published online EpubDec (10.1021/am100833e).
176. A. J. Bergren, K. D. Harris, F. J. Deng, R. L. McCreery, Molecular electronics using diazonium-derived adlayers on carbon with Cu top contacts: critical analysis of metal oxides and filaments. *Journal of Physics-Condensed Matter* **20**, (2008); published online EpubSep (10.1088/0953-8984/20/37/374117).
177. A. P. Bonifas, R. L. McCreery, 'Soft' Au, Pt and Cu contacts for molecular junctions through surface-diffusion-mediated deposition. *Nature Nanotechnology* **5**, 612-617 (2010); published online EpubAug (10.1038/nnano.2010.115).
178. P. Martin, M. L. Della Rocca, A. Anthore, P. Lafarge, J. C. Lacroix, Organic Electrodes Based on Grafted Oligothiophene Units in Ultrathin, Large-Area Molecular Junctions. *Journal of the American Chemical Society* **134**, 154-157 (2012); published online EpubJan (10.1021/ja209914d).
179. J. M. Soler, E. Artacho, J. D. Gale, A. Garcia, J. Junquera, P. Ordejon, D. Sanchez-Portal, The SIESTA method for ab initio order-N materials simulation. *J Phys-Condens Mat* **14**, 2745-2779 (2002); published online EpubMar 25 (
180. H. Nakamura, K. Yamashita, A. R. Rocha, S. Sanvito, Efficient ab initio method for inelastic transport in nanoscale devices: Analysis of inelastic electron tunneling spectroscopy. *Phys Rev B* **78**, 235420 (2008); published online EpubDec (
181. K. Yoshino, S. Nakajima, H. B. Gu, R. Sugimoto, OPTICAL-PROPERTIES OF SOLUTION OF POLYTHIOPHENE DERIVATIVES AS FUNCTIONS OF ALKYL CHAIN-LENGTH, CONCENTRATION AND TEMPERATURE. *Japanese Journal of Applied Physics Part 2-Letters* **26**, L1371-L1373 (1987); published online EpubAug (

182. K. Yoshino, S. Nakajima, H. B. Gu, R. Sugimoto, ABSORPTION AND EMISSION SPECTRAL CHANGES IN A POLY(3-ALKYLTHIOPHENE) SOLUTION WITH SOLVENT AND TEMPERATURE. *Japanese Journal of Applied Physics Part 2-Letters* **26**, L2046-L2048 (1987); published online EpubDec (
183. K. Yoshino, S. Nakajima, D. H. Park, R. Sugimoto, THERMOCHROMISM, PHOTOCROMISM AND ANOMALOUS TEMPERATURE-DEPENDENCE OF LUMINESCENCE IN POLY(3-ALKYLTHIOPHENE) FILM. *Japanese Journal of Applied Physics Part 2-Letters* **27**, L716-L718 (1988); published online EpubApr (10.1143/jjap.27.1716).
184. C. Aleman, L. Julia, pi conjugation in 2,2'-bithiophene and its dimethyl derivatives: Model compounds of organic conducting polymers based on thiophene rings. *Journal of Physical Chemistry* **100**, 1524-1529 (1996); published online EpubFeb (10.1021/jp951592o).
185. E. Orti, P. M. Viruela, J. Sanchezmarin, F. Tomas, AB-INITIO DETERMINATION OF THE GEOMETRIC STRUCTURE AND INTERNAL-ROTATION POTENTIAL OF 2,2'-BITHIOPHENE. *Journal of Physical Chemistry* **99**, 4955-4963 (1995); published online EpubApr (10.1021/j100014a014).
186. D. A. Dossantos, D. S. Galvao, B. Laks, M. C. Dossantos, CONFORMATIONAL STUDY ON ALKYL-SUBSTITUTED THIOPHENE OLIGOMERS. *Chemical Physics Letters* **184**, 579-583 (1991); published online EpubOct (10.1016/0009-2614(91)80037-x).
187. N. Di Cesare, M. Belletete, M. Leclerc, G. Durocher, A conformational study of ethyl-substituted bithiophenes. Semi-empirical versus ab initio methods. *Synthetic Metals* **94**, 291-298 (1998); published online EpubMay (10.1016/s0379-6779(98)00024-1).
188. W. R. Salaneck, O. Inganas, B. Themans, J. O. Nilsson, B. Sjogren, J. E. Osterholm, J. L. Bredas, S. Svensson, THERMOCHROMISM IN POLY(3-HEXYLTHIOPHENE) IN THE SOLID-STATE - A SPECTROSCOPIC STUDY OF TEMPERATURE-DEPENDENT CONFORMATIONAL DEFECTS. *Journal of Chemical Physics* **89**, 4613-4619 (1988); published online EpubOct (10.1063/1.454802).
189. G. Zerbi, B. Chierichetti, O. Inganas, THERMOCHROMISM IN POLYALKYLTHIOPHENES - MOLECULAR ASPECTS FROM



- VIBRATIONAL SPECTROSCOPY. *Journal of Chemical Physics* **94**, 4646-4658 (1991); published online EpubMar (10.1063/1.460593).
190. F. Raymond, N. Di Cesare, M. Belletete, G. Durocher, M. Leclerc, Molecular design of a thermochromic polythiophene derivative. *Advanced Materials* **10**, 599-+ (1998); published online EpubJun (10.1002/(sici)1521-4095(199805)10:8<599::aid-adma599>3.0.co;2-m).
  191. C. Yang, F. P. Orfino, S. Holdcroft, A phenomenological model for predicting thermochromism of regioregular and nonregioregular poly(3-alkylthiophenes). *Macromolecules* **29**, 6510-6517 (1996); published online EpubSep (10.1021/ma9604799).
  192. N. Kurokawa, H. Yoshikawa, N. Hirota, K. Hyodo, H. Masuhara, Size-dependent spectroscopic properties and thermochromic behavior in poly(substituted thiophene) nanoparticles. *Chemphyschem* **5**, 1609-1615 (2004); published online EpubOct (10.1002/cphc.200400117).
  193. Y. Wang, N. Archambault, A. Marold, L. Weng, B. L. Lucht, W. B. Euler, Observation of two-step thermochromism in poly(3-docosylthiophene): DSC and reflection spectroscopy. *Macromolecules* **37**, 5415-5422 (2004); published online EpubJul (10.1021/ma0494277).
  194. V. Lukes, M. Breza, Thermochromism of bithiophenes and internal aromatic chain rotation. *Journal of Molecular Structure-Theochem* **820**, 35-39 (2007); published online EpubOct (10.1016/j.theochem.2007.06.003).
  195. N. Elmaci, E. Yurtsever, Thermochromism in oligothiophenes: The role of the internal rotation. *Journal of Physical Chemistry A* **106**, 11981-11986 (2002); published online EpubDec (10.1021/jp026768i).
  196. S. K. Lee, R. Yamada, S. Tanaka, G. S. Chang, Y. Asai, H. Tada, Universal Temperature Crossover Behavior of Electrical Conductance in a Single Oligothiophene Molecular Wire. *Acs Nano* **6**, 5078-5082 (2012); published online EpubJun (10.1021/nn3006976).
  197. B. Q. Q. Xu, X. L. L. Li, X. Y. Y. Xiao, H. Sakaguchi, N. J. J. Tao, Electromechanical and conductance switching properties of single oligothiophene molecules. *Nano Letters* **5**, 1491-1495 (2005); published online EpubJul (10.1021/nl050860j).

198. Y. Le, M. Endou, S. K. Lee, R. Yamada, H. Tada, Y. Aso, Completely Encapsulated Oligothiophenes: Synthesis, Properties, and Single-Molecule Conductance. *Angewandte Chemie-International Edition* **50**, 11980-11984 (2011)10.1002/anie.201104700).
199. L. Venkataraman, J. E. Klare, C. Nuckolls, M. S. Hybertsen, M. L. Steigerwald, Dependence of single-molecule junction conductance on molecular conformation. *Nature* **442**, 904-907 (2006); published online EpubAug (10.1038/nature05037).
200. D. Vonlanthen, A. Mishchenko, M. Elbing, M. Neuberger, T. Wandlowski, M. Mayor, Chemically Controlled Conductivity: Torsion-Angle Dependence in a Single-Molecule Biphenyldithiol Junction. *Angewandte Chemie-International Edition* **48**, 8886-8890 (2009)10.1002/anie.200903946).